# UNIVERSITA' DEGLI STUDI DI PADOVA

---


**SCUOLA DI DOTTORATO DI RICERCA IN**

**SCIENZE DELLE PRODUZIONI VEGETALI**

INDIRIZZO AGRONOMIA AMBIENTALE – CICLO XXIV

Dipartimento di Agronomia Ambientale e Produzioni Vegetali


## *Investigating the effects of SOC on soil structure: three-dimensional visualisation and modelling*


**Direttore della Scuola:** Ch.mo Prof. Andrea Battisti

**Supervisore**: Ch.mo Prof. Francesco Morari

**Dottorando**: Nicola Dal Ferro



DATA CONSEGNA TESI

31 gennaio 2012

**Declaration**

I hereby declare that this submission is my own work and that, to the best of my knowledge and belief, it contains no material previously published or written by another person nor material which to a substantial extent has been accepted for the award of any other degree or diploma of the university or other institute of higher learning, except where due acknowledgment has been made in the text.

Nicola Dal Ferro, January 31st 2012

A copy of the thesis will be available at *http://paduaresearch.cab.unipd.it/*

**Dichiarazione**

Con la presente affermo che questa tesi è frutto del mio lavoro e che, per quanto io ne sia a conoscenza, non contiene materiale precedentemente pubblicato o scritto da un'altra persona né materiale che è stato utilizzato per l'ottenimento di qualunque altro titolo o diploma dell'università o altro istituto di apprendimento, a eccezione del caso in cui ciò venga riconosciuto nel testo.

Nicola Dal Ferro, 31 gennaio 2012

Una copia della tesi sarà disponibile presso *http://paduaresearch.cab.unipd.it/*

## *Table of contents*

## *Riassunto*

La quantificazione della struttura del suolo è di primaria importanza per determinare gli effetti di diverse pratiche colturali sul terreno. La struttura è influenzata dal contenuto di carbonio organico (SOC), il quale è ampiamente identificato come il principale indicatore della fertilità del suolo, anche grazie alle sua attitudine di migliorarne la struttura fisica. Le interazioni che legano la struttura al SOC sono complesse e principalmente legate alla capacità di agire come agente aggregante tra le particelle che compongono la matrice del suolo.

Molti studi si sono concentrati sulle dinamiche che legano il SOC e la microporosità degli aggregati (che è riconosciuta come un surrogato della complessa struttura del suolo) trascurando, in questo modo, la macroporosità, la quale non è individuabile in campioni di piccole dimensioni. Le misure fatte a scala di aggregato, perciò, ricoprono solo una parte delle importanti e complesse proprietà di un suolo. Di conseguenza è importante valutare l'effetto che esercita il SOC sia in piccoli aggregati che in campioni indisturbati.

L'obiettivo generale di questo lavoro è valutare gli effetti di diversi regimi di fertilizzazione (organica, minerale e mista) in una prova di lungo periodo, iniziata nel 1962, gestita secondo una monosuccessione di mais. Sono stati analizzati sia aggregati di piccole dimensioni (pochi mm), che campioni indisturbati (5 cm di diametro, 6 cm di altezza), con innovative tecniche tridimensionali. La tesi è strutturata in cinque capitoli: il primo è una *review* sulle interazioni struttura del suolo-SOC e sulle tecniche tridimensionali utilizzate per la quantificazione della struttura. Il secondo capitolo analizza gli effetti del SOC e delle frazioni umiche sulla stabilità di struttura degli aggregati, individuando inoltre un nuovo meccanismo, legato alla diversa distribuzione della porosità, finora non considerato. Il terzo capitolo confronta e combina la porosimetria a intrusione di mercurio e la microtomografia a raggi X per la caratterizzazione della struttura. Il quarto capitolo analizza tridimensionalmente la struttura di campioni indisturbati e gli effetti del SOC sulla struttura stessa. Infine, l'ultimo capitolo riporta le conclusioni generali del lavoro.

## *Summary*

The quantification of soil structure is primordial to determine the effects of management practices on soil environment. Soil structure is influenced by soil organic carbon content (SOC), which is usually recognised as one of the main indicator of soil fertility as it improves structure stability. Complex interactions link the soil structure and SOC that acts as a binding agent promoting aggregation.

Several studies focussed on SOC dynamics and the relationship with soil aggregate microporosity, which is usually considered as a surrogate of the soil matrix complexity, neglecting the soil macropores outside aggregates. Therefore, the measures made at aggregate scale form only a small part of the important and complex properties of soil. Accordingly, it is important to quantify the effects that SOC exerts both is soil aggregates and undisturbed cores.

The general aim of this work is to study the effects of different fertilisations (organic, mineral and mixed) applied to continuous maize by means of a long-term experiment established in 1962 in north-eastern Italy, analysing both small aggregates (few mm) and undisturbed soil cores (5 cm diameter, 6 cm length) with innovative three-dimensional techniques. The thesis is structured in five chapters. The first one is a review of the soil structure-SOC interactions and innovative three-dimensional methods involved in soil structure quantification. The second chapter analyses the effects of SOC and its humic fraction on the mechanisms of aggregate breakdown and improves upon the knowledge of aggregate structural properties. The third chapter compares and combines mercury intrusion porosimetry (MIP) and X-ray computer assisted microtomography (micro-CT) for characterising the soil structure. The fourth chapter analyses the 3D soil structure of undisturbed soil cores and the effects of SOC. The final chapter presents the general conclusions of the work.

# Chapter I

# General Introduction

## *Structure and organic matter*

"Soil structure refers to the size, shape and arrangement of solids and voids, continuity of pores and voids, their capacity to retain and transmit fluids and organic and inorganic substances, and ability to support vigorous root growth and development" (Bronick and Lal, 2005). This definition announces the pivotal role of soil structure for both agriculture and the environment since it aids good soil quality; a well-structured soil also avoids phenomena of degradation such as surface crusting, erosion and compaction (Horn et al., 1994).

Soil degradation is a major environmental problem worldwide and many studies reported a strong relationship between loss of soil fertility and management practices (Pagliai et al., 2004; Papadopoulos et al., 2009; Williams and Petticrew, 2009). Minimum or zero tillage, soil application of biosolids (manure, crop residues, compost), cover and deep-rooting crops, conversion to grassland and woodland and improved rotations are considered recommended management practices (RMPs) with the aim of reducing the environmental impact of agricultural activities and controlling soil degradation. The quantification of soil structure is therefore essential to aim at good land management and sustainability.

A complex feedback links the soil organic carbon (SOC) content and soil structure: SOC acts as a binding agent promoting structure stability and aggregation (Tisdall and Oades, 1982). In turn, the soil matrix affects the organic carbon availability according to its spatial location (Bachmann et al., 2008) and stabilises SOC by three main mechanisms (Figure 1.1): a) chemical stabilisation as a result of chemical binding between SOC compounds and mineral particles; b) physical protection by aggregates as they form barriers between microbes and enzymes and their substrates; c) biochemical stabilisation due to SOC chemical composition and complexing processing (Six et al., 2002).

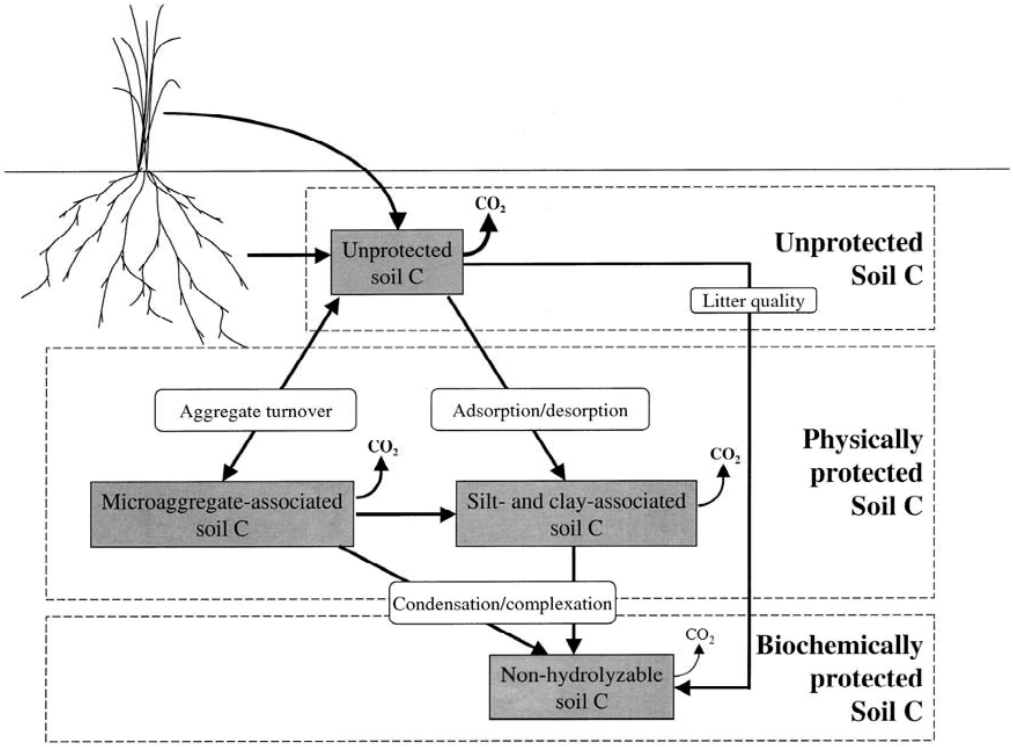


**Figure 1.1 -** Conceptual model of SOC dynamics of stabilisation and mineralization in the soil (Six et al., 2002).

Therefore, studying the strong relationship which combines SOC and soil structure dynamics is considered a key issue to monitor the soil quality because intensive agriculture might cause soil degradation due to a reduction of organic matter (Six et al., 2004).

In the early fifties it was already clear that different organic (and inorganic) compounds influenced the soil aggregation and structure: soil fauna, soil microorganisms, roots, inorganic binding agents and environmental variables. Monnier (1965) studied the temporal properties of organic compounds on soil structure and proposed that the short-term effects of organic matter on aggregate stability were due to the turnover of microbial products and cells while the long-term effects were due to humified compounds. Since then a large range of organic products have been studied, from different crop residues (Martens, 2000) to manures (Paré et al., 1999), composts (Celik et al., 2004) and miscellaneous wastes (Metzger et al., 1987; N'Dayegamiye and Angers, 1993), in order to evaluate their effects on structural stability. Finally Williams and Petticrew (2009) studied SOC effects to evaluate the sustainability of different

management practices and found that, among the types of farming system and fertilisers, organic matter content was determined as being the primary control on aggregate stability.

At aggregate scale, the most significant aggregate-SOC conceptual model was proposed by Tisdall and Oades (1982). The different binding agents act at different hierarchical stages of aggregation. Free primary particles and silt-sized aggregates (< 20 μm) are bound together into microaggregates (20-250 μm) by persistent binding agents (e.g. humic fractions and metal cation complexes), oxides and highly disordered aluminosilicates. In turn, these microaggregates are bound together into macroaggregates (> 250 μm) by temporary and transient binding agents (fungal hyphae, microbial and plant-derived polysaccharides, roots etc.) (Six et al., 2004).

Recent studies identified pore size distribution as a significant factor influencing soil structure, especially the aggregate stability: for Six et al. (2004), the effectiveness of different binding agents would depend on their dimensions relative to the size of the pores, while Papadopoulos et al. (2009), studying organic and conventional farming systems, found that macroporosity would favour aggregation by allowing entrapped air to escape, reducing pressure build-up. Lastly, the higher volume of large-pores of aggregates could allow a rapid entry of water that causes a build-up of internal air pressure and consequent disruption of the aggregates (Lugato et al., 2010).

Even at macroscale, SOC has recently been considered a key issue for soil structure dynamics: it is increasingly being recognised that measures make at aggregate scale form only a small part of the important properties of soil. The undisturbed 3D macropore structure is a key property of the soil structure. Macropores are important for several soil processes and functions. For example, they can trigger preferential flow, with the fast direct transfer of contaminants such as herbicides from the soil surface to the groundwater (Jarvis, 2007). The macropore structure governs the gas exchange between the soil and the atmosphere as a consequence of different moisture conditions and connections between macropores (Deurer et al., 2009).

Recently, increasing attention has been paid to the soil system as a potential medium to adsorb $CO_2$ fluxes from the atmosphere. Carbon sequestration in agricultural soils might affect global warming by reducing atmospheric $CO_2$ concentrations, as recognised in

Article 3.4 of the Kyoto Protocol of the United Nations Framework Convention on Climate Change (UNFCCC). The soil C pool is 3.3 times the size of the atmospheric pool and 4.5 times the size of the biotic pool (Lal, 2004). Several strategies exist to prevent the loss of SOC, to enhance soil C sequestration, and thus restore degraded soils and increase soil quality (Silver et al., 2000). For example, reduced or zero tillage, soil application of biosolids (manure, crop residues, compost), cover and deep-rooting crops, conversion to grassland and woodland, improved rotations, fertilisation and irrigation, are known to increase SOC content. Many studies focussed on soil quality and SOC turnover mediated by diverse factors such as biota, ionic bridging, clay, carbonates and SOC that determine, in the end, the soil structure (Bronick and Lal, 2005).

Although it is difficult to measure the carbon sequestration sinks and the effects of agricultural policies, Freibauer et al. (2004) reported that encouragement of organic farming and the introduction of set-aside have probably helped to maintain carbon stocks in agricultural soils in Europe. Smith (2004) estimated the potential biological sequestration in European (EU 15) arable land, with the adoption of recommended management practices, as 90-120 Mt C $year^{-1}$. However, due to socio-economic constraints, the realistic achievable potential is only 20% of the biological one. Italy approved the Kyoto protocol in 2002 in order to diminish C emission by 6.5% in the period 2008-2012, compared to the carbon-emission reference value measured in 1990.

Long-term field experiments, which manage OC addition, are excellent systems to study soils under controlled conditions in order to enhance the soil physical quality as well as mitigate carbon dioxide emissions (e.g. Schjonning et al., 2002; Schjonning et al., 2005; Morari et al., 2006; Lugato et al., 2009; Chakraborty et al., 2010).

Schjonning et al. (2002) quantified the structure of soils that have been managed for 50 years as part of an organic dairy farm and compared them with conventionally managed neighbouring soil. They showed that the pore system of the dairy farm soil with applications of animal manure was more tortuous and complex than the conventional one, with positive implications for aeration and microbial biomass. Morari et al. (2006), studying the effects of recommended management practices in two long-term trials underway in north-eastern Italy, found a general decrease in SOC content (1.1 t C $ha^{-1}$ $year^{-1}$), after the introduction of intensive soil tillage, and a fall in soil quality. Vice

versa, permanent grassland and use of organic manures were the most promising management practices. Deurer et al. (2009) showed that a sustainable C management enhanced the soil structure by stabilising the macropores and increasing the aggregate stability. They also observed that the long-term C input possibly combats climate change in two ways: first, it leads to C sequestration; second, it might create more and better connected macropores near the soil surface which favour less favourable conditions for $N_2O$ production and emission. Finally Lugato et al. (2009), studying the aggregate pore size distribution in contrasting soils, showed a direct influence of SOC on pore size distribution as it increased the ultramicropores (30-5 μm). In turn this soil structure change would slow down the C turnover allowing the accumulation of C even in the more labile forms and. Therefore soil porosity distribution could be a valuable indicator of the soil capacity to sequester organic carbon.

## *Techniques to quantify soil structure*

Several studies have focussed on pore network at micropore (< 50 µm) and macropore (> 50 µm) scale to quantify soil structure characteristics. Both water retention (Schjonning et al., 2005; Holtham et al., 2007) and mercury intrusion curves (Lugato et al., 2009) are traditional and widespread techniques to estimate pore size distribution in soils. The classical method of analysing mercury intrusion pressure-volume curves is based on the model of parallel cylindrical non-intersecting pores of differing radii (Gregg and Sing, 1982). However, these techniques have some important disadvantages: they cannot provide an estimation of the pore shape and total porosity is calculated as the sum of accessible pores from the intrusion of the liquid (mercury or water) so that unconnected pores are not detected. Pores are detected only below 900 µm and their dimensions do not reflect the real pore size distribution since the liquid reveals the diameter of the throat entrance instead of the true pore diameter (Cnudde et al., 2009). Pore size distribution curves have been successfully parameterised with many models to estimate different parameters such as pore connectivity, tortuosity, anisotropy, hydraulic properties, etc. (Bartoli et al., 1999; Johnson et al., 2003; Boulin et al., 2008). Recently a three-dimensionally interconnected model of pore structure, called Pore-Cor, has been developed to study subtle structural changes in porous media such as sandstones (Matthews et al., 2006), filters (Gribble et al., 2011) and soils (Matthews et al., 2010). The pore network model can generate a simple 3D stochastic representation of a porous structure and then quantify pore network characteristics and associated dynamic processes. The importance of this approach is that a realistic estimate is made of the effect of large pores shielded (from intrusion by mercury or water) by narrow surrounding throats. More advanced methods of pore morphology characterisation are based on thin sectioning and image analysis (Ringrose-Voase, 1996; Hubert et al., 2007). These techniques are time consuming and usually performed on only a few images, although they allow the quantification of soil micromorphology. However accurate interpretations of the 3D organisation of soil from 2D thin-sections are impossible (Taina et al., 2008).

X-ray computer assisted microtomography (micro-CT), combined with image processing techniques, has been put forward as a non-destructive method to study the three-

dimensional soil structure as it allows the quantification of pore size distribution and total porosity (Hainsworth and Aylmore, 1983). It can reveal both individual pores and pore shape depending on the spatial resolution of the instrument, but only analyses of small samples can provide detailed information on high resolution images (Mees et al., 2003). Given the strong contrast in X-ray attenuation of soil pores and solid matrix, a rough discrimination of the pore network is relatively easy, while the precise interpretation of grey levels of pixels belonging to different objects (and pores) is much more difficult (Baveye et al., 2010). However if the micro-CT scanners are used to generate three-dimensional data with the same settings related to attenuation and contrast, the resulting 2D or 3D images can be much more easily compared. Structural analyses by micro-CT were performed both on a) undisturbed soil cores, to investigate the effects of simulated rainfall (Lee et al., 2008), sodium content (Jassogne et al., 2007) and root growth (Mooney et al., 2006; Sander et al., 2008); and b) on soil aggregates, to study the soil particles and related structural properties (Macedo et al., 1999), the importance of soil treatments on microbial micro-habitat structure (Nunan et al., 2006) and the pore-space related to fungal growth (Pajor et al., 2010).

Recently, X-ray micro-CT was used to study the effects of organic compounds on soil structure. The relationship between organic carbon, pore size distribution and morphology were assessed in small incubated, newly formed and field aggregates to which fresh residue was added (De Gryze, 2006). Papadopoulos et al. (2009) observed cracks and elongated pores connected to the surface of stable soil aggregates that can provide an escape route for entrapped air. Deurer et al. (2009), studying the effects of long-term OC addition on apple orchards using X-ray micro-CT, evidenced larger simulated gas diffusion and less $N_2O$ emissions in organic orchards than in conventional ones, due to more and better connected macropores. Finally, for Schlüter et al. (2011) the higher OC content and nutrient supply trigger an enhanced biological activity including root growth with implications for macropore-space reallocation.

## *Objectives*

The general aims of this work are:

1. To evaluate the effects of SOC and its humic fractions on soil structure at micro- and macropore scale, analysing both small aggregates and undisturbed soil cores. Soils came from a long-term experiment and allowed the soil physical quality to be studied under controlled conditions. The trial, which considers different fertilisation levels with maize as a main crop, was established in 1962 at the experimental farm of the University of Padova (IT) and is the oldest running rotation experiment in Italy.
2. To evaluate the long-term effects of the adoption of recommended management practices (RMPs), in particular the application of organic fertilisers (e.g. farmyard manure), to improve the soil structure.
3. To improve upon the conceptual aspects that link soil stability and structural properties, identifying the quantitative and qualitative characteristics of SOC and its humic fraction that affect the mechanisms of structure breakdown. In order to evaluate this, a multidisciplinary approach is essential. For this purpose structure analyses were supported by a detailed chemical characterisation of SOC and its humic constituents by means of thermal and spectroscopic analyses (TG-DTA, DRIFT and $^{1}$H HR MAS NMR).
4. To test the effectiveness of innovative three-dimensional methods as tools that provide a parameterisation of the soil structure and related properties (pore connectivity, tortuosity, hydraulic conductivity), in comparison with more traditional techniques such as mercury intrusion porosimetry or water retention curves. A network model called Pore-Cor was used to reconstruct the soil structure (from mercury intrusion curves), parameterise its characteristics and simulate hydraulic properties. In addition, X-ray computed assisted microtomography (micro-CT) allowed non-destructive analyses in order to visualise and quantify the real pore morphology of soil samples. X-ray micro-CT was also compared and combined with traditional mercury intrusion porosimetry (MIP) analyses to better evaluate limitations and opportunities provided by new three-dimensional techniques.

## *References*


Bachmann, J., Guggenberger, G., Baumgartl, T., Ellerbrock, R.H., Urbanek, E., Goebel, M.O., Kaiser, K., Horn, R., Fischer, W.R., 2008. Physical carbon-sequestration mechanisms under special consideration of soil wettability. J. Plant Nutr. Soil Sci. 171, 14-26.

Bartoli, F., Bird, N.R.A., Gomendy, V., Vivier, H., Niquet, S., 1999. The relation between silty soil structures and their mercury porosimetry curve counterparts: fractals and percolation. Eur. J. Soil Sci. 50, 9-22.

Baveye, P.C., Laba, M., Otten, W., Bouckaert, L., Dello Sterpaio, P., Goswami, R.R., Grinev, D., Houston, A., Hu, Y.P., Liu, J.L., Mooney, S., Pajor, R., Sleutel, S., Tarquis, A., Wang, W., Wei, Q., Sezgin, M., 2010. Observer-dependent variability of the thresholding step in the quantitative analysis of soil images and X-ray microtomography data. Geoderma 157, 51-63.

Boulin, P.F., Angulo-Jaramillo, R., Daian, J.F., Talandier, J., Berne, P., 2008. Pore gas connectivity analysis in Callovo-Oxfordian argillite. Appl. Clay. Sci. 42, 276-283.

Bronick, C.J., Lal, R., 2005. Soil structure and management: a review. Geoderma 124, 3-22.

Celik, I., Ortas, I., Kilic, S., 2004. Effects of compost, mycorrhiza, manure and fertilizer on some physical properties of a Chromoxerert soil. Soil Till. Res. 78, 59-67.

Chakraborty, D., Garg, R.N., Tomar, R.K., Dwivedi, B.S., Aggarwal, P., Singh, R., Behera, U.K., Thangasamy, A., Singh, D., 2010. Soil physical quality as influenced by long-term application of fertilizers and manure under maize-wheat system. Soil Sci. 175, 128-136.

Cnudde, V., Cwirzen, A., Masschaele, B., Jacobs, P.J.S., 2009. Porosity and microstructure characterization of building stones and concretes. Eng. Geol. 103, 76-83.

De Gryze, S., Jassogne, L., Six, J., Bossuyt, H., Wevers, M. Merckx, R., 2006. Pore structure changes during decomposition of fresh residue: X-ray tomography analyses. Geoderma 134, 82-96.

Deurer, M., Grinev, D., Young, I., Clothier, B.E., Müller, K., 2009. The impact of soil carbon management on soil macropore structure: a comparison of two apple orchard systems in New Zealand. Eur. J. Soil Sci. 60, 945-955.

Freibauer, A., Rounsevell, M.D.A., Smith, P., Verhagen, J., 2004. Carbon sequestration in the agricultural soils of Europe. Geoderma 122, 1-23.

Gregg, S J., Sing, K.S.W., 1982. Adsorption, surface and porosity. Academic Press, New York.

Gribble, C.M., Matthews, G.P., Laudone, G.M., Turner, A., Ridgway, C.J., Schoelkopf, J., Gane, P.A.C., 2011. Porometry, porosimetry, image analysis and void network modelling in the study of the pore-level properties of filters. Chem. Eng. Sci. 66, 3701-3709.

Hainsworth, J.M., Aylmore, L.A.G., 1983. The use of computer assisted tomography to determine spatial distribution of soil water content. Aust. J. Soil Res. 21, 435-443.

Holtham, D.A.L., Matthews, G.P., Scholefield, D.S., 2007. Measurement and simulation of void structure and hydraulic changes caused by root-induced soil structuring under white clover compared to ryegrass. Geoderma 142, 142-151.

Horn, R., Taubner, H., Wuttke, M., Baumgartl, T., 1994. Soil physical properties related to soil structure. Soil Till. Res. 30, 187-216.

Hubert, F., Hallaire, V., Sardini, P., Caner, L., Heddadj, D., 2007. Pore morphology changes under tillage and no-tillage practices. Geoderma 142, 226-236.

Jarvis, N.J., 2007. A review of non-equilibrium water flow and solute transport in soil macropores: principles, controlling factors and consequences for water quality. Eur. J. Soil Sci. 58, 523-546.

Jassogne, L.T.P., McNeill, A.M., Chittleborough, D.J., 2007. 3D-visualization and analysis of macro-and meso-porosity of the upper horizons of a sodic, texture-contrast soil. Eur. J. Soil Sci. 58, 589-598.

Johnson, A., Roy, I.M., Matthews, G.P., Patel, D., 2003. An improved simulation of void structure, water retention and hydraulic conductivity in soil with the Pore-Cor three-dimensional network. Eur. J. Soil Sci. 54, 477-489.

Lal, R., 2004. Soil carbon sequestration impacts on global climate change and food security. Science 304, 1623-1627.

Lee, S.S., Gantzer, C.J., Thompson, A.L., Anderson, S.H., Ketcham, R.A., 2008. Using high-resolution computed tomography analysis to characterize soil-surface seals. Soil Sci. Soc. Am. J. 72, 1478-1485.

Lugato, E., Morari, F., Nardi, S., Berti, A., Giardini, L., 2009. Relationship between aggregate pore size distribution and organic-humic carbon in contrasting soils. Soil Till. Res. 103, 153-157.

Lugato, E., Simonetti, G., Morari, F., Nardi, S., Berti, A., Giardini, L., 2010. Distribution of organic and humic carbon in wet-sieved aggregates of different soils under long-term fertilization experiment. Geoderma 157, 80-85.

Macedo, A., Vaz, C.M.P., Naime, J.M., Cruvinel, P.E., Crestana, S., 1999. X-ray microtomography to characterize the physical properties of soil and particulate systems. Powder Technol. 101, 178-182.

Martens, D.A., 2000. Plant residue biochemistry regulates soil carbon cycling and carbon sequestration. Soil Biol Biochem. 32, 361-369.

Matthews, G.P., Canonville, C.F., Moss, A.K., 2006. Use of a void network model to correlate porosity, mercury porosimetry, thin section, absolute permeability, and NMR relaxation time data for sandstone rocks. Phys. Rev. E. 73, 031307-1-031307-9.

Matthews, G.P., Laudone, G.M., Gregory, A.S., Bird, N.R.A., Matthews, A.G.G., Whalley, W.R., 2010. Measurement and simulation of the effect of compaction on the pore structure and saturated hydraulic conductivity of grassland and arable soil. Water Resour. Res. 46, W05501-1-13.

Mees, F., Swennen, R., Geet, M.V., Jacobs, P., 2003. Applications of X-ray computed tomography in the geosciences. Geological Society, London, Special Publications. 215, 1-6.

Metzger, L., Levanon, D., Mingelgrin, U., 1987. The effect of sewage sludge on soil structural stability: Microbiological aspects. Soil Sci. Soc. Am. J. 51, 346-351.

Monnier, G., 1965. Action des matières organiques sur la stabilité structurale des sols, 140

Mooney, S.J., Morris, C., Berry, P.M., 2006. Visualization and quantification of the effects of cereal root lodging on three-dimensional soil macrostructure using X-ray computed tomography. Soil Sci. 171, 706.

Morari, F., Lugato, E., Berti, A., Giardini, L., 2006. Long-term effects of recommended management practices on soil carbon changes and sequestration in north-eastern Italy. Soil Use Manage. 22, 71-81.

N'Dayegamiye, A., Angers, D.A., 1993. Organic matter characteristics and water stable aggregation of a sandy loam soil after 9 years of wood-residue applications. Can. J. Soil Sci. 73, 115-122.

Nunan, N., Ritz, K., Rivers, M., Feeney, D.S., Young, I.M., 2006. Investigating microbial micro-habitat structure using X-ray computed tomograph. Geoderma 133, 398-407.

Pagliai, M., Vignozzi, N., Pellegrini, S., 2004. Soil structure and the effect of management practices. Soil Till Res. 79, 131-143.

Pajor, R., Falconer, R., Hapca, S., Otten, W., 2010. Modelling and quantifying the effect of heterogeneity in soil physical conditions on fungal growth. Biogeosciences 7, 3731-3740.

Papadopoulos, A., Bird, N.R.A., Whitmore, A.P., Mooney, S.J., 2009. Investigating the effects of organic and conventional management on soil aggregate stability using X-ray computed tomography. Eur. J. Soil Sci. 60, 360-368.

Paré, T., Dinel, H., Moulin, A.P., Townley-Smith, L., 1999. Organic matter quality and structural stability of a Black Chernozemic soil under different manure and tillage practices. Geoderma 91, 311-326.

Ringrose-Voase, A.J., 1996. Measurement of soil macropore geometry by image analysis of sections through impregnated soil. Plant Soil 183, 27-47.

Sander, T., Gerke, H.H., Rogasik, H., 2008. Assessment of Chinese paddy-soil structure using X-ray computed tomography. Geoderma 145, 303-314.

Schjonning, P., Iversen, B.V., Munkholm, L.J., Labouriau, R., Jacobsen, O.H., 2005. Pore characteristics and hydraulic properties of a sandy loam supplied for a century with either animal manure or mineral fertilizers. Soil Use Manage. 21, 265-275.

Schjonning, P., Munkholm, L.J., Moldrup, P., Jacobsen, O.H., 2002. Modelling soil pore characteristics from measurements of air exchange: the long-term effects of fertilization and crop rotation. Eur. J. Soil Sci. 53, 331-339.

Schlüter, S., Weller, U., Vogel, H.J., 2011. Soil-structure development including seasonal dynamics in a long-term fertilization experiment. J. Plant Nutr. Soil Sci. 174, 395-403.

Silver, W.L., Ostertag, R., Lugo, A.E., 2000. The potential for carbon sequestration through reforestation of abandoned tropical agricultural and pasture. Lands. Restor. Ecol. 8, 394-407.

Six, J., Bossuyt, H., De Gryze, S., Denef, K., 2004. A history of research on the link between (micro)aggregates, soil biota, and soil organic matter dynamics. Soil Till. Res. 79, 7-31.

Six, J., Conant, R.T., Paul, E.A., Paustian, K., 2002. Stabilization mechanisms of soil organic matter: Implications for C-saturation of soils. Plant Soil 241, 155-176.

Smith, P., 2004. Carbon sequestration in croplands: the potential in Europe and the global context. Eur. J. Agron. 20, 229-236.

Taina, I.A., Heck, R.J., Elliot, T.R., 2008. Application of X-ray computed tomography to soil science: A literature review. Can. J. Soil Sci. 88, 1-20.

Tisdall, J.M., Oades, J.M., 1982. Organic matter and water-stable aggregates in soils. J. Soil Sci. 33, 141-163.

Williams, N.D., Petticrew, E.L., 2009. Aggregate stability in organically and conventionally farmed soils. Soil Use Manage. 25, 284-292.

# Chapter II

# Investigating the effects of wettability and pore size distribution on aggregate stability. The role of soil organic matter and its humic fraction

## *Introduction*

Interest in aggregate breakdown mechanisms has recently been intensified because of the complex feedback existing between soil structure dynamics, soil organic carbon (SOC) turnover and SOC sequestration (Six et al., 2004; Papadopoulos et al., 2009).

Compression of entrapped air during wetting (i.e. slaking) and physico-chemical dispersion of colloidal cements are two main mechanisms causing aggregate breakdown (Le Bissonnais, 1996). Soil organic matter (SOM) plays a pivotal role in the process since it increases both the inter-particle cohesion of aggregates (Bachmann et al., 2008) and soil hydrophobicity (Chenu et al., 2000), to an extent which depends on chemical composition of SOM (Abiven et al., 2009). Carbohydrates and polysaccharides improve the structural stability by binding inorganic soil particles into stable aggregates (Piccolo and Mbagwu, 1999). Hydrophobic substances, such as lipids and waxes (mainly composed of aliphatic constituents), can diminish breakdown effects by reducing soil wettability (Bachmann et al., 2008). Humic compounds are mainly hydrophobic and they may coat soil particles, particularly clays and aggregates, rendering them much more hydrophobic (Bartoli and Dousset, 2011). Thus products rich in humic compounds, such as manures or composts, would be expected to improve aggregate stability by increasing hydrophobicity (Abiven et al., 2009). Piccolo and Mbagwu (1990) found that high molecular weight humic fractions enhanced aggregate stability due to the presence of aliphatic and aromatic components that formed hydrophobic humic-clay complexes. Besides hydrophobic substances (stearic acid) and humic acids were likely to be more effective and long-lasting aggregate binding agents than hydrophilic compounds (Piccolo and Mbagwu, 1999).

Recent studies highlighted that SOM can also enhance aggregate stability by modifying aggregate pore space (e.g. Zaher et al., 2005; Hafida et al., 2007; Papadopoulos et al., 2009). Zaher et al. (2005) observed that SOM reduced the internal air pressure evolution during aggregate wetting and consequently slaking as a result of a lower near-saturated hydraulic conductivity. These authors hypothesised that the aggregate hydraulic conductivity was reduced by an increased occlusion of pore network by SOM. Hafida et al. (2007) demonstrated that the mechanism of action was nonspecific for hydrophobic lipids and hydrophilic carbohydrates (e.g. uronic acid sugar). Conversely, data obtained

by Papadopoulos et al. (2009) by X-ray µCT suggested that intra-aggregate porosity did not significantly affect aggregate stability. In aggregates of organically managed soils they observed a considerable number of cracks and elongated pores connected to the edges. They proposed that these types of pores provided a positive effect allowing entrapped air to escape during wetting and therefore reducing pressure build-up. By contrast, Lugato et al. (2010) compared long-term effects of organic and mineral fertilisations in three contrasting soils and hypothesised that a higher volume of large-pores could allow a rapid entry of water that would cause a build-up of internal air pressure and consequent disruption of the aggregates.

Among methods used to measure aggregate stability, only a few have attempted to separate the underlying mechanisms of breakdown (Abiven et al., 2009) and the role of SOM on these, especially in long-term experiments. Hence, it could be hypothesised that the effects of hydrophobicity on aggregate stability have been overestimated in past studies and confused with those associated with the aggregate structure and hydraulic properties.

A multidisciplinary approach is therefore essential to investigate the subtle structural properties and chemical aspects affecting aggregate stability. This paper aims to: a) improve upon the knowledge of aggregate structural properties, using a pore network model; b) identify the effect of SOM and its humic fraction on the mechanisms of aggregate breakdown in a long-term cropping systems established in the early 1960s in north-eastern Italy.

## *Materials and methods*

### The long-term experiment

The long-term experiment is located at the experimental farm of the University of Padua (Legnaro, Veneto Region, Italy 45°21' N; 11°58' E, 6 m a.s.l.). The local climate is sub-humid with annual rainfall of about 850 mm distributed uniformly throughout the year. The mean annual temperature is 12 °C. The soil is a fluvi-calcaric cambisol (CMcf), silty or sandy loam (FAO-UNESCO, 1990) with a mean pH of 8.1 (Table 2.1). The soil contains predominantly dolomite (35%), quartz (28%), feldspar (15 %) and mica (13%).

**Table 2.1 -** Mean, minimum and maximum values of physical and chemical properties of the top soil (0-20 cm).

| | Mean | Min | Max |
|---|---|---|---|
| Sand (2000-50 μm) (%) | 37.8 | 29.2 | 47.3 |
| Silt (50-2 μm) (%) | 49.5 | 40.8 | 56.6 |
| Clay (< 2 μm) (% ) | 12.7 | 8.8 | 15.9 |
| Bulk Density (g $cm^{-3}$) | 1.4 | 1.3 | 1.5 |
| pH | 8.1 | 7.7 | 8.4 |
| $EC_e$ (μS $cm^{-1}$) | 358.9 | 106.0 | 715.0 |
| Organic carbon (g $kg^{-1}$) | 8.1 | 4.9 | 13.9 |
| Total Nitrogen (g $kg^{-1}$) | 1.1 | 0.7 | 1.9 |
| C/N | 7.2 | 4.6 | 9.1 |
| CEC (meq 100 $g^{-1}$) | 12.5 | 7.8 | 15.4 |

Rotations with different fertilisation rates have been used to compare high and low input cropping systems (Giardini, 2004). The experimental layout is a split plot with three replicates on plots of 7.8 m × 6 m. All the rotations end their cycle simultaneously every 12 years. At the end of each rotation cycle, the type of intensification was modified to keep the experiment up-to-date, but always maintaining the same type of rotations and fertilisation levels. The first rotation cycle compared irrigated and non-irrigated crops;

the second compared inter-annual successions and growing with just a main crop; while crop residue burial was compared with removal in the third cycle.

This work considered eight fertilisation treatments with maize as a main crop for a total of 24 plots. In the last rotation cycle these have allowed a comparison of fertilisation with organic fertilisers only ($F_2$, high farmyard manure input; $L_2$, high liquid manure input), with mineral only ($NPK_2$, high inorganic input), mixed fertilisation ($F_1NPK_1$, farmyard manure + inorganic; $L_1NPK_1$, liquid manure + inorganic) and with no inputs (O). Half of the treatments also included crop residues (Table 2.2). Soil tillage is homogeneous in all treatments with autumn ploughing at 30-35 cm. Organic inputs are distributed just before ploughing.

Sampling was done in the last year of the third cycle (September 2000) at the end of the maize growing season in the first 25 cm layer. The samples were taken from five different points in the plot and bulked to obtain a sample of about 1 kg. Sampling involved the central area of 16 $m^2$ to avoid soil movement effects (Sibbesen et al., 2000).

**Table 2.2 -** Experimental treatments in the continuous maize of the last rotation cycle.

| | | Treatments[a] | | | | | | | |
|---|---|---|---|---|---|---|---|---|---|
| Rotation cycle | | $F_2$ | $F_1NPK_1$ | $NPK_2$ | O | $L_2$+r | $L_1NPK_1$+r | $NPK_2$+r | O+r |
| (1990-2001) | Residue incorporation | no | no | No | no | yes | yes | yes | yes |
| Inorganic inputs: | N (kg $ha^{-1}$) | - | 150 | 300 | - | - | 150 | 300 | - |
| | P (kg $ha^{-1}$ $y^{-1}$) | - | 33 | 66 | - | - | 33 | 66 | - |
| | K (kg $ha^{-1}$) | - | 174 | 348 | - | - | 174 | 348 | - |
| Organic inputs: | L (t C $ha^{-1}$) | - | - | - | - | 5.58 | 2.79 | - | - |
| | F (t C $ha^{-1}$) | 5.58 | 2.79 | - | - | - | - | - | - |

[a]F, farmyard manure; L, liquid manure; NPK, inorganic fertilisation; O, control (no fertilisation); r, residue incorporation. Subscripts 1 and 2 refer to low and high input fertilisation.

## Aggregate stability measurement

Samples were air dried. During the drying operation the bulk soil was broken along natural fissures into small pieces by gentle hand manipulation (Douglas and Goss, 1982). Once dried, 1-2 mm aggregate fraction was separated and subjected to 200-µm wet sieving, applying a vertical shaking for 30 minutes with a frequency of 30 oscillations min-1 (900 oscillations in total) at a 3-cm amplitude (Bocchi et al., 2008). The material was then carefully transferred to a second beaker by a washing flask and oven-dried at 105°C to constant weight. The coarse sand (200-2000 µm) content was determined by adding 25 ml of a solution (40 g sodium hexametaphosphate and 10 g sodium carbonate in 1000 ml) to each dry sample (about 7 g) allowing to stand for 24 hours, washing (with demineralised water) on a sieve (200 µm) and oven drying the material retained. The wet aggregate stability index (*WASI*) was calculated as follows (Diaz-Zorita et al., 2002),

$$WASI = \frac{WSA - W_{sand}}{W_{agg} - W_{sand}} \quad [2.1]$$

where *WSA* is the dry weight of water stable aggregates > 200 µm, $W_{agg}$ the total dry weight of the sieved aggregates and $W_{sand}$ the dry weight of coarse sand particles measured after dispersion.

Before applying wet sieving, soil aggregates were subjected to slow and fast wetting (Le Bissonnais, 1996). Slow wetting (SW) was carried out by laying 10-g of soil aggregates on a tension table at a matric potential of -0.3 kPa for 30 min. Fast wetting (FW) was performed immersing 10 g of soil aggregates in deionised water for 10 min. The first treatment corresponds to field conditions of wetting under gentle rainfall while the second one simulates the effect of heavy rain storms (Le Bissonnais, 1996). To distinguish the slaking from the physico-chemical dispersion, before fast wetting soil aggregates were subjected to: a) no pre-treatment (fw); b) pre-treatment with benzene (benz), to emphasise the hydrophobic nature of SOM by coating the aggregates with benzene (Henin et al., 1958); c) pre-treatment with ethanol (etoh) to test the wet mechanical cohesion by substituting air with a polar liquid before energy is applied

(Henin et al., 1958). Immersion of ethanol-pretreated soil aggregates in water minimises the slaking of dried soil aggregates and emphasises the resistance of soil aggregates to dissolution and the dispersive action of water.

## Pore-size distribution and Pore-Cor modelling

Around 1-g of soil aggregates was air dried and analysed by mercury porosimetry (e.g. Echeverría et al., 1999) to estimate the pore distribution in the range of 0.0074-100 μm. Pores within the range 0.0074-15 μm were analysed with a Thermo Finnigan Pascal 240 porosimeter, and pores within the range 13.6-100 μm were analysed with Thermo Finnigan Pascal 140 porosimeter. The pore radius into which mercury (Hg) was intruded was estimated as a function of pressure using the Young-Laplace equation:

$$r = \frac{2\gamma \cos\theta}{P} \qquad [2.2]$$

where $r$ is the pore radius, $P$ is the pressure, $\gamma$ is the Hg surface tension (0.47 N $m^{-1}$) and $\theta$ is the contact angle between Hg and soil (140°). In total, six measurements were performed per treatment (3 blocks × 2 sub-replicates). According to Cameron and Buchan (2006), pores were classified as macropores (C100-75 μm, $m^3$ $m^{-3}$), mesopores (C75-30 μm, $m^3$ $m^{-3}$), micropores (C30-5 μm, $m^3$ $m^{-3}$), ultramicropores (C5-0.1 μm, $m^3$ $m^{-3}$) and cryptopores (C0.1-0.0074 μm, $m^3$ $m^{-3}$).

To evaluate the effect of soil structure on aggregate stability, 48 pore distribution curves (8 treatments × 3 blocks × 2 sub-replicates) were analysed with Pore-Cor (Matthews et al., 2010), a pore network model that can generate a simple 3D stochastic representation of soil structure and then quantify soil characteristics and associated dynamic processes (e.g. tortuosity, saturated hydraulic conductivity, fast wetting). The pore structure is represented by cubes that simulate pores, surrounded by cylindrical throats. The unit cell of the model comprises 1000 pores in a 10 × 10 × 10 array, connected by up to 3000 throats. A Boltzmann-annealed simplex is used to adjust model parameters so that the simulated mercury intrusion curve closely matches the experimental one. The importance of this approach is that a realistic estimate is made of the effect of large pores shielded from intrusion by mercury by narrow surrounding throats. The estimates

of the sizes of the shielded pores has been shown to be accurate for sandstones (Matthews et al., 2006) and for filters (Gribble et al., 2011). Soil is a much more complex porous medium, but we infer from these other studies that the void sizes from the network model for soil will be much closer to reality than those traditionally calculated from the slope of the mercury intrusion curve; the latter implies a capillary bundle with no shielded pores.

The shape of the simulated curve is determined by five fitting parameters: pore skew (a scaling factor which bulks up the sizes of the pores to achieve the experimental porosity); throat skew (the asymmetry of the throat distribution); throat spread (defined as twice the standard deviation of the beta distribution: a value > 0.5 indicates a bimodal distribution); connectivity (the average number of connected throats per pore) and correlation level (setting level of local autocorrelation of the features) (Matthews et al., 2010). The reconstructed unit cells can be used to estimate secondary properties (e.g. saturated hydraulic conductivity). Ten fits were conducted per replication, corresponding to different stochastic generation numbers. The average values of the five parameters were used for the comparison. The Pore-Cor saturated hydraulic conductivity was predicted in terms of maximum flow capacity of the whole pore network from the knowledge of the flow capacity of each pore-throat-pore connection, according to Poiseuille's law (Johnson et al., 2003).

To evaluate the influence of the aggregate porosity on the wetting dynamics and consequently on the slaking mechanisms, a simple wetting model was applied to the simulated unit cells. In particular, the model applies the equation of Lucas and Washburn, who equated the capillary wetting pressure to the pressure required for laminar flow as described in Poiseuille's equation. The fast wetting was calculated in each throat in the pore network after every time-step (Bodurtha et al., 2005). An additional approximation was to assume that all the pore features can be represented by a single cylinder of radius *r*, known as the effective hydraulic radius.

Then the distance travelled, *h*, by a liquid front in time, *t*, is given as follows:

$$h^2 = \frac{r\gamma \cos\theta}{2\eta} t \qquad [2.3]$$

where $\eta$ is the dynamic viscosity of liquid and $\theta$ the contact angle between water and soil. The model simulated the wetting of an entirely dry aggregate sample in contact with an infinite reservoir (supersource) of water under no applied pressure and hydrostatic head effect. The incorporation of inertial and viscous forces was excluded due to great heterogeneity of the wetting front simulated when using them (Bodurtha et al., 2005). The situation is hypothetical and simplified and does not consider: a) the inertial and viscous forces which act as a fluid that enters the capillary tube; b) the effect of the pneumatic potential generated at the wetting front due to trapped air; or c) the change of pore size distribution due to slaking, pore clogging and swelling (Zaher et al., 2005). However, the simulation does take into account the very important effect of narrow throats holding up wetting further into the network, though not being able to supply water sufficiently quickly into these subsequent features. There is therefore a successive retardation of wetting through the network. This is particularly evident for void networks such as those in soil where the voids sizes span many orders of magnitude.

Wetting dynamics were simulated considering both the measured apparent contact angle (see paragraph below) and a contact angle of 0° (no water repellency). Calculations were performed on eight selected unit cells (one reconstruction per each treatment) that were representative, on average, of the different soil treatments. Fast wetting was calculated for 900 s and the time step for wetting calculation was 0.01 μs.

## Capillary rise method

Hydrophobicity was measured in terms of the advancing contact angle by the capillary rise method (CRM) (De Bano, 1981). The applied technique is based on the capillary rise of a liquid in columns of packed powder. The contact angle is derived from Washburn's equation [2.3] considering also the effect of the hydrostatic head, $L$ (i.e. the immersion depth of the column) (Siebold et al., 1997):

$$h^2 + 2hL = \frac{r\gamma \cos\theta}{2\eta} t \qquad [2.4]$$

The concept of wetting angle is useful to quantify hydrophobicity (De Bano, 1981). Pure ethanol wets all solids at a zero contact angle while water infiltration is affected by

hydrophobic substances that reduce the attraction between water and soil surface. The heights of rise for both ethanol and water were therefore measured. Then, if the contact angle of ethanol is assumed to equal zero and the capillary radius remains constant, the equation [2.4] both for ethanol and water can be combined to calculate the apparent liquid-solid contact angle. The larger the angle, the greater is the water repellency. Two similar glass tubes averaging 1 cm in internal diameter by 50 cm long were used. Prior to being filled with powdered soil, the tubes were coated with a thin film of paraffin wax to make the glass water repellent. The bottoms of the tubes were covered with plastic fabric. To get nearly identical maximum density, the soil was compacted by tapping the samples with approximately 50 similar impacts while avoiding further compaction of the samples in contact with the testing liquid. The use of powdered soil allowed the effective capillary radius to be standardised among treatments, although precluded the consideration of the effect of small-scale architecture of the pore space and the distribution/position of hydrophobic components inside the matrix (Ramirez-Flores et al., 2008).

## Humic substances analyses

The procedures for determination of SOC, humic carbon (HC) and separation of humic substances (HS) into three molecular weight fractions (HF1-C > 100 kDa, HF2-C 100-10 kDa and HF3-C < 10 kDa) have been described in a previous paper by Nardi et al. (2004). A brief description follows. The humic substances were extracted from the air-dried samples with 0.1 M KOH (1:20 w/v) at room temperature for 16 h in a $N_2$ atmosphere and were freed from the suspended material by centrifuging at 7000 × g for 20 min. Here, the term HS is the fraction soluble in bases and comprehensive of humic and fulvic acids (Dell'Agnola and Ferrari, 1971). Humic extracts (50 ml) were transferred into 18,000 mol. wt cut-off dialysis Visking tubing (Medicell LTD, London, UK) and dialysed against double-distilled water. The water was changed daily until the liquid outside the dialysis tube was colourless. Subsequently the retained solution was desalted by ion exchange on Amberlite IR 120 H.

The separation of HS into the three molecular weight fractions was carried out with gel-permeation chromatography of each humic extract on a Sephadex G-100 gel packed in a 70 × 1.6 cm Pharmacia column (Pharmacia, Uppsala, Sweden). The gel packing solution

and eluent were 0.02 M $Na_2B_4O_7$. Column calibration was based on previously assessed standard proteins (Kit MS-II, Serva, Heidelberg, Germany) (Martin et al., 2006).

The effect of treatments on HS chemical structure was analysed on a composite lyophilised HS samples obtained by mixing the HS extracted in the three replicates (in total eight samples corresponding to the treatments). Thermogravimetric analysis and differential thermal analysis (TG-DTA) of HS were carried out simultaneously using a TG-DTA92 instrument (SETARAM, France); details on this procedure were described by Montecchio et al. (2006). Two strong exothermic reactions at ca. 300 °C (Exo1) and ca. 490 °C (Exo2) were observed in all samples. Each HS was analysed three times and mean values of triplicates of mass loss percentages were estimated. Diffuse reflectance infrared Fourier transform (DRIFT) spectra were recorded with a Bruker TENSOR series FT-IR spectrophotometer (Ettlingen, Germany) equipped with an apparatus for diffuse reflectance (Spectra-Tech. Inc., Stamford, CT) (spectra not shown).

An amount of 2 mg of each lyophilised HS was mixed with 100 mg of KBr in an agate mortar. KBr was used to provide a background reference spectrum. The spectra were collected from 4000 to 400 $cm^{-1}$, averaged over 200 scans (resolution ± 4 $cm^{-1}$) and converted into Kubelka-Munk units. Three spectra from three different replicates were recorded for each sample. The spectra were baseline corrected and then processed for integrated areas at the spectral range between 3000-1400 $cm^{-1}$ by using Grams/386 spectral software (Galactic Industries, Salem, NH). The second-derivative of each spectrum was used for wavenumber determination of overlapped bands. The triplicate values of the integrated area of the peaks of each spectrum (-$CH_3$ at 2960 $cm^{-1}$; -$CH_2$ at 2925 $cm^{-1}$; -CO2R at 1735 $cm^{-1}$; -COOH at 1710 $cm^{-1}$; amide I at 1650 $cm^{-1}$, -COO- and C=C in aromatic ring at 1600 $cm^{-1}$; amide II at 1540 $cm^{-1}$; C=C in aromatic ring from lignin at 1510 $cm^{-1}$) were used for statistical analysis.

Proton High Resolution Magic Angle Spinning Nuclear Magnetic Resonance ($^1$H HR MAS NMR) spectra were recorded with a Bruker FT-NMR Avance 400 Spectrometer at 298K using 8 kHz spinning rate. Samples (~30 mg) were dissolved in 100 µL of DMSO-d6 and analysed in a 90 µL HR-MAS zirconium rotor (4 mm OD). Nominal frequency for $^1$H was 400.13 MHz for $^1$H and 100.61 MHz for 13C. $^1$H NMR spectra were acquired using standard pulse sequence. $^1$H NMR spectra were integrated on the following

regions: A1 (10-6.0 ppm) amide groups in peptides, aromatics, vinyl groups and lignin; A2 (5.7-2.85 ppm) carbohydrates, β protons in peptides, lignin, ethers; A3 (2.3-0 ppm) side chain protons in amino acids; -$CH_2$- chains of lipids, waxes and cuticles, and terminal -$CH_3$ groups. Each integrated area is the average value on three independent calculations, with a standard error < 5%.

## Statistical analysis

Data were analysed with one-way ANOVA and significantly different means were differentiated with the Duncan's test. To estimate a possible linear relationship between physical and chemical parameters the Pearson correlation coefficient was calculated. A stepwise multiple regression analysis ($Y = \beta_0 + \beta_1X_1 + \beta_2X_2 + \ldots + \beta_kX_k$) with forward selection was also carried out in order to identify the stronger physical and chemical predictors (sand, clay, SOC, HF1-C and HF3-C) of aggregate porosity (pore size distribution and Pore-Cor parameters).

The general structure of the interdependences existing between soil organic matter, hydrophobicity, aggregate porosity and stability was finally evaluated performing a joint principal component analysis (PCA) on 12 standardised variables: SOC, HF1-C, HF3-C, $WASI_{fw}$, $WASI_{sw}$, $WASI_{etoh}$, $WASI_{benz}$, contact angle, C30-5, C5-0.1, C0.1-0.0074 and PERM, i.e. Pore-Cor saturated hydraulic conductivity.

Variables were selected according to Kaiser's measure of sampling adequacy (MSA). The overall MSA was 0.72 indicating that PCA was suitable (Kaiser, 1974). Rotated orthogonal components (varimax normalised method of rotation) were extracted and the relative scores were determined. Only principal components with eigenvalues > 1 were considered for the discussion. Statistical analyses were performed with STATISTICA 7.0 (Statsoft Inc., 2004).

## *Results*

### Porosity of aggregates and Pore-Cor modelling

Total porosity was on average 0.37 $m^3$ $m^{-3}$, represented by ultramicropores (C5-0.1) (71% of the total porosity) and to a lesser extent by mesopores (C75-30), micropores (C30-5), circa 3.5%, and macro and (C100-75) cryptopores (C0.1-0.0074), less than 2% ($p < 0.01$) (Figure 2.1). No significant differences were observed between treatments even if an apparent increase in ultramicropores in $F_2$ and $L_2$+r treatments was detected (data not shown).

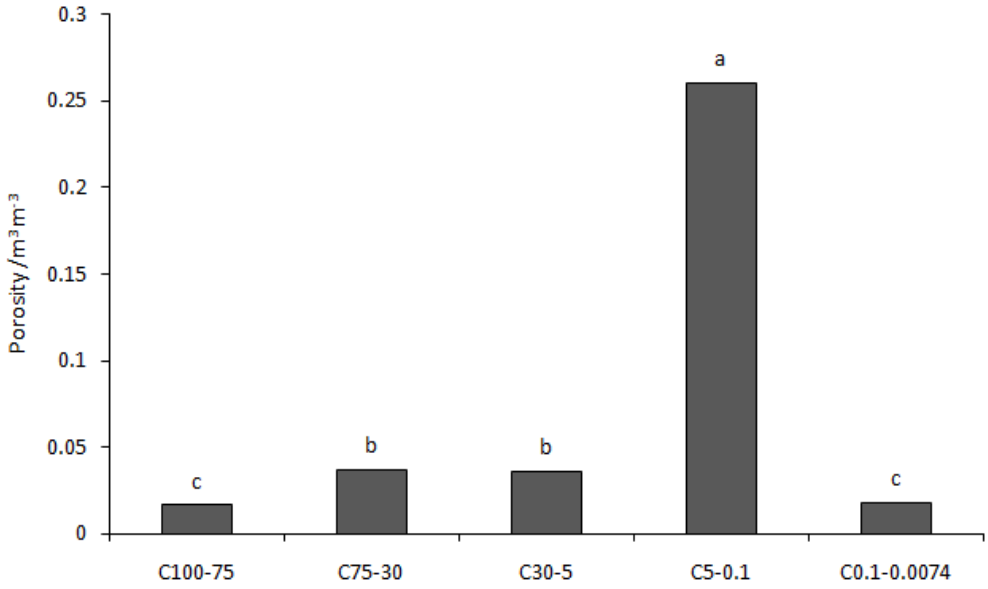


**Figure 2.1** - Pore size distribution ($m^3$ $m^{-3}$) in the range 100-0.0074 μm. C100-75, macropores; C73-30, mesopores; C30-5, micropores; C5-0.1, ultramicropores; C0.1-0.0074, cryptopores. Columns labelled with different letters (a, b and c) are significantly different ($p < 0.01$).

Significant correlations were found by multiple linear regressions between pore size distribution and texture and chemical properties (Table 2.3). SOC content was a significant predictor in the range of porosity 0.1-75 μm. It affected positively C5-0.1 (standardised regression coefficient d = 1.07) and negatively C30-5 (d = -0.95) and C75-30 (d = -0.43). HF1-C content had an opposite effect on C5-0.1 (e = -0.61) and C30-5 (e

= 0.71). Texture influenced only the extreme porosity classes: sand increased the macroporosity whereas clay was associated to intra-particle cryptoporosity. Predictors had, however, a poor capacity to represent the observed variability of dependent variables except for SOC and HF1-C with respect to C5-0.1 (multiple r = 0.63).

**Table 2.3** – Multiple linear regression analysis for pore classes and Pore-Cor modelling parameters: y = a + b × sand + c × clay + d × SOC + e × HF1-C + f × HF3-C. Both standardised and unstandardised (in brackets) regression coefficients are reported.

| | Regression coefficients[a] | | | | | | |
|---|---|---|---|---|---|---|---|
| | Intercept | Sand (%) | Clay (%) | SOC (%) | HF1-C (%) | HF3-C (%) | Multiple r |
| | a | b | c | d | e | f | |
| Pore size distribution (μm) | | | | | | | |
| C100-75 | -0.63 | 0.48 (0.06)[b] | - | - | - | - | 0.47 |
| C75-30 | 2.97[b] | - | - | -0.43 (-3.08)[b] | - | | 0.46 |
| C30-5 | 7.60[b] | - | - | -0.95 (-8.40)[b] | 0.71 (0.22)[a] | - | 0.49 |
| C5-0.1 | 18.43[b] | - | - | 1.07 (13.75)[b] | -0.61 (-0.27)[a] | - | 0.63 |
| C0.1-0.0074 | 0.40 | - | 0.44 (0.11)[b] | - | - | - | 0.44 |
| Pore-Cor parameters | | | | | | | |
| Throat Spread | 0.85[b] | - | - | -1.24 (-0.26)[b] | 0.86 (0.01)[b] | - | 0.65 |
| Connectivity | 4.75[b] | - | -0.55 (-0.08)[b] | - | - | - | 0.55 |

[a]significant for $p < 0.08$;
[b]significant for $p < 0.05$.

The aggregate structure simulated by Pore-Cor (Table 2.4) was characterised by an average connectivity (number of throats per pore) of 3.7 with a low variability for all the treatments but $NPK_2$+r. The throat size distribution was bimodal (mean throat spread of 0.72), with a low correlation level between the sizes of pores and connected throats (mean correlation level of 0.15). As a result, the stochastically generated unit cells did not show any sort of banded structure.

Throat skew and saturated hydraulic conductivity (PERM) evidenced a high variability, with a range from -5.61 to 0.82 and 8.7 10-5 to 1.44 m $s^{-1}$, respectively.

High PERM variability could arise from low accuracy of the unit cell of 1000 pores connected by up to 3000 throats to represent the complexity of the actual pore networks in soil. Treatment effect was not significant for all the parameters, even if on average: a) throat skew assumed positive values (i.e. a greater number of large throats relative to that of those smaller) for control and farmyard manure treatments and negative ones for liquid manure and mineral fertilised treatments, b) saturated hydraulic conductivity had higher values in the mineral treatments ($NPK_2$ and $NPK_2$+r) and lower in $F_2$. Multiple regressions highlighted the influence of both textural and chemical characteristics on Pore-Cor parameters. The number of throats per pore was negatively correlated with the clay content (c = -0.55), while SOC and HF1-C contents were both correlated with throat spread: an increase of SOC reduced the degree of bimodality (d = -1.24), while an increase of HF1-C had an opposite effect.

**Table 2.4** - Mean results of Pore-Cor five parameters and estimated saturated hydraulic conductivity (PERM).

| Treatments[a] | Connectivity (s.e.[b]) | Throat Spread (s.e.) | Correlation Level (s.e.) | Throat Skew (s.e.) | Pore Skew (s.e.) | PERM ($m\ s^{-1}$) (s.e.) |
|---|---|---|---|---|---|---|
| $F_2$ | 3.64 (0.04) | 0.66 (0.037) | 0.15 (0.02) | 0.53 (4.08) | 2536.91 (575.59) | $8.7\ 10^{-5}$ ($3.5\ 10^{-5}$) |
| $L_2$+r | 3.75 (0.04) | 0.70 (0.018) | 0.13 (0.02) | -1.91 (2.19) | 1712.67 (450.28) | $1.5\ 10^{-4}$ ($4.4\ 10^{-5}$) |
| $F_1NPK_1$ | 3.79 (0.07) | 0.71 (0.003) | 0.16 (0.01) | 0.82 (3.51) | 2700.8 (1024.16) | $2.1\ 10^{-3}$ ($1.2\ 10^{-3}$) |
| $L_1NPK_1$+r | 3.63 (0.07) | 0.73 (0.025) | 0.12 (0.01) | -2.16 (4.37) | 1948.53 (342.84) | $3.0\ 10^{-4}$ ($2.0\ 10^{-4}$) |
| $NPK_2$ | 3.54 (0.04) | 0.72 (0.015) | 0.20 (0.01) | -4.23 (1.13) | 946.35 (614.33) | 1.44 (1.44) |
| $NPK_2$+r | 4.00 (0.38) | 0.79 (0.025) | 0.19 (0.05) | -5.61 (7.90) | 530.51 (452.22) | $1.7\ 10^{-2}$ ($1.5\ 10^{-2}$) |
| O | 3.71 (0.15) | 0.72 (0.015) | 0.11 (0.02) | 0.34 (2.47) | 2147.32 (1400.28) | $7.7\ 10^{-4}$ ($7.0\ 10^{-4}$) |
| O+r | 3.60 (0.11) | 0.74 (0.020) | 0.10 (0.02) | 0.81 (1.83) | 1082.03 (821.58) | $1.3\ 10^{-4}$ ($8.3\ 10^{-5}$) |

[a]F, farmyard manure; L, liquid manure; NPK, inorganic fertilisation; O, control (no fertilisation); r, residue incorporation. Subscripts 1 and 2 refer to low and high input fertilisation.

[b]Standard error.

## Hydrophobicity and Wet Aggregate Stability Indices

Treatments influenced the hydrophobicity with contact angles higher than 75° ($p < 0.05$) in $F_2$, $L_2$+r and $F_1NPK_1$, around 74° in $NPK_2$ and $L_1NPK_1$+r, and lower than 73.2° in O, $NPK_2$+r and O+r (Figure 2.2). Hydrophobicity was positively correlated with SOC (r = 0.76), HC (r = 0.63) and HF1-C (r = 0.64) and HF2-C (r = 0.64) contents. On the contrary, a negative relationship was observed with HF3-C (r = -0.75) (data not shown).

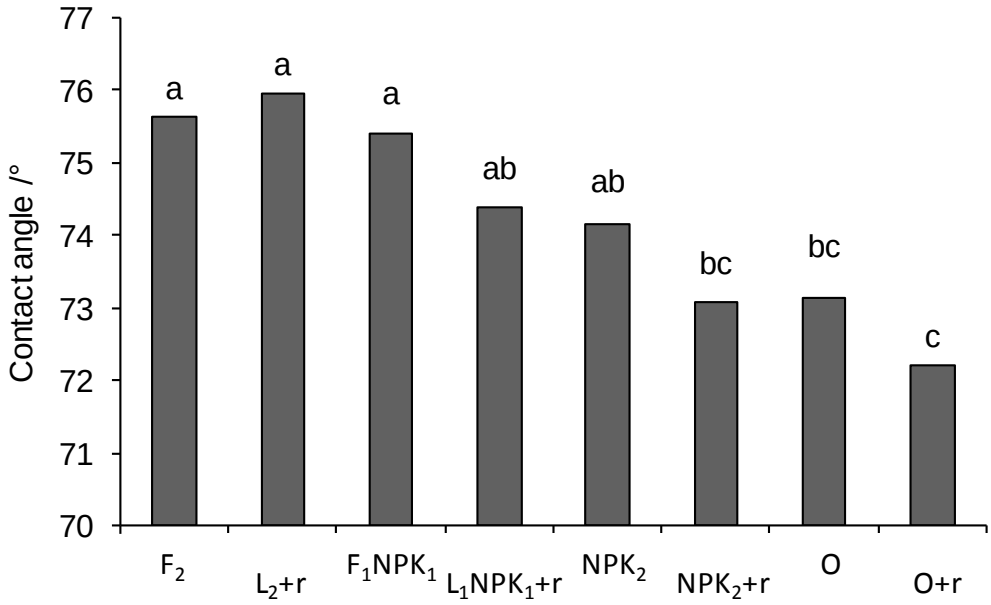


**Figure 2.2** – Apparent contact angle in the different treatments. F, farmyard manure; L, liquid manure; NPK, inorganic fertilisation; O, control (no fertilisation); r, residue incorporation. Subscripts 1 and 2 refer to low and high input fertilisation. Columns labelled with different letters (a, b and c) are significantly different ($p < 0.05$).

Wet Aggregate Stability Indices (WASIs) varied according to the pre-treatments: $WASI_{etoh}$ (65.1%) > $WASI_{sw}$ (17.0%) > $WASI_{fw}$ (8.5%) > $WASI_{benz}$ (6.7%). They also varied for different fertiliser applications (Figure 2.3). Organic fertilisers significantly increased the aggregate stability with an effect that depended on both the type and application dose. $F_2$ showed the highest values of $WASI_{sw}$ (27.85%), $WASI_{etoh}$ (71.9%) and $WASI_{benz}$ (14.8%), while $L_2$+r had the highest values of $WASI_{fw}$ (15.0%). Contrasting effects were observed for the mixed and mineral treatments. In the case of pre-treatment with benzene, $F_1NPK_1$ and $L_1NPK_1$+r had intermediate $WASI_{benz}$ of 6%, with lower

values observed for O and $NPK_2$, of 2.3% and 2.7%. No significant differences were observed between mixed and mineral/control treatments for both the fast and slow wetting indices, except for $NPK_2$ which showed the lowest $WASI_{fw}$ and $WASI_{sw}$ (Figure 2.3). The variability between treatments was slightly detectable by $WASI_{etoh}$ and significant differences were observed only between $F_2$ and mineral input ($NPK_2$ and $NPK_2$+r).

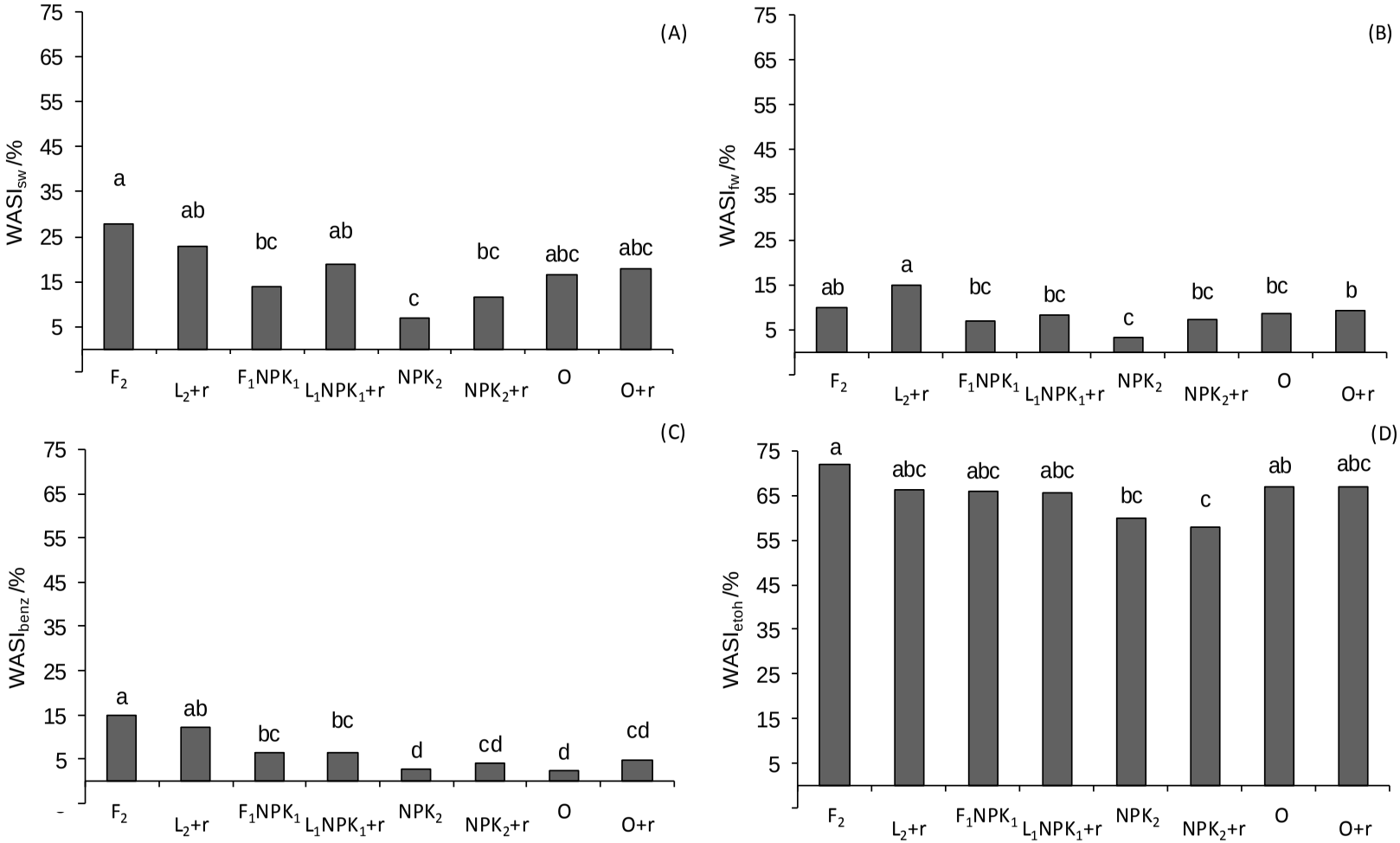


**Figure 2.3** – Aggregate stability indices: slow wetting (A), fast wetting (B), fast wetting after pre-treatment with benzene (C), fast wetting after pre-treatment with ethanol (D). F, farmyard manure; L, liquid manure; NPK, inorganic fertilisation; O, control (no fertilisation); r, residue incorporation. Subscripts 1 and 2 refer to low and high input fertilisation. Columns labelled with different letters (a, b, c and d) are significantly different ($p < 0.05$).

For both the fast and slow wetting indices, no significant differences were observed between mixed and mineral/control treatments, except $NPK_2$ which showed the lowest $WASI_{fw}$ and $WASI_{sw}$ (Figure 2.3). The pre-treatments with ethanol reduced the variability between the treatments and significant differences were observed only between $F_2$ and mineral input ($NPK_2$ and $NPK_2$+r).

The quantity and quality of SOC, as well as the pore size distribution, had a significant effect on WASIs. Stronger correlations were observed between $WASI_{benz}$ and SOC (r = 0.79), HC (r = 0.78) and the humic fractions. In particular, they were positive for HF1-C and HF2-C and negative for HF3-C contents (r = -0.76). Weaker correlations with the same sign were also observed between soil parameters and $WASI_{sw}$ (Table 2.5). The porosity had a contrasting influence according to the pore diameter. Specifically, C5-0.1 was correlated positively with all WASIs (r around 0.6) but WASIetoh, C30-5 had a negative correlation with $WASI_{sw}$ and $WASI_{benz}$, as well as C75-30 with $WASI_{etoh}$. The latter also showed a weak positive relationship with C0.1-0.0074 and the apparent contact angle. A value of r = 0.63 was also found between contact angle and $WASI_{benz}$ (Table 2.5).

**Table 2.5** - Correlation matrix of selected soil parameters and WASIs (values in bold are significantly different at $p < 0.05$).

| WASI indices[a] | Sand | Silt | Clay | Chemical characterisation[b] | | | | | Pore size distribution | | | | | CA[c] |
|---|---|---|---|---|---|---|---|---|---|---|---|---|---|---|
| | | | | SOC | HC | HF1-C | HF2-C | HF3-C | C100-75 | C75-30 | C30-5 | C5-0.1 | C0.1-0.0074 | |
| $WASI_{sw}$ | 0.34 | -0.22 | **-0.51** | **0.50** | **0.58** | **0.45** | 0.24 | **-0.41** | 0.09 | -0.40 | **-0.57** | **0.62** | 0.04 | 0.32 |
| $WASI_{fw}$ | 0.35 | -0.26 | **-0.42** | 0.35 | 0.38 | 0.25 | 0.21 | -0.27 | 0.04 | -0.35 | -0.31 | **0.56** | -0.18 | 0.23 |
| $WASI_{benz}$ | 0.38 | -0.27 | **-0.50** | **0.79** | **0.78** | **0.69** | **0.61** | **-0.76** | 0.13 | -0.38 | **-0.47** | **0.58** | 0.04 | **0.63** |
| $WASI_{etoh}$ | 0.15 | -0.15 | -0.07 | 0.36 | 0.35 | **0.42** | 0.11 | -0.31 | -0.30 | **-0.56** | -0.37 | 0.38 | **0.42** | **0.42** |

[a]sw, slow wetting; fw, fast wetting without pre-treatment; benz, pre-treatment with benzene; etoh, pre-treatment with ethanol.

[b]HC, humic carbon; HF1-C, humic fraction with apparent molecular weight > 100 kDa; HF2-C, humic fraction with apparent molecular weight of 100-10 kDa; HF3-C, humic fraction with apparent molecular weight < 10 kDa.

[c]CA, apparent contact angle.

A general overview of the factors influencing the wet aggregate stability was provided by PCA. Three factors were extracted (eigenvalue > 1) accounting for 76.2% of variance (factor loading > 0.7) (Table 2.6). The first accounted for 48.4% and was correlated with $WASI_{benz}$, the SOC, humic fractions (HF1-C and HF3-C) and contact angle. The second accounted for 15.7% and was correlated with $WASI_{fw}$, $WASI_{sw}$ and C5-0.1. The third had strong correlations with C0.1-0.0074 and Pore-Cor saturated hydraulic conductivity (PERM) (12.1% of variance).

**Table 2.6** - Factor loadings (varimax normalised) calculated for selected soil parameters.

| Soil parameters[a] | Factor 1 | Factor 2 | Factor 3 |
|---|---|---|---|
| $WASI_{sw}$ | 0.31 | **0.84** | 0.14 |
| $WASI_{fw}$ | 0.15 | **0.87** | -0.09 |
| $WASI_{benz}$ | **0.72** | 0.59 | 0.05 |
| $WASI_{etoh}$ | 0.31 | 0.39 | 0.55 |
| SOC | **0.89** | 0.29 | 0.10 |
| HF1-C | **0.91** | 0.12 | 0.10 |
| HF3-C | **-0.94** | -0.15 | 0.00 |
| C30-5 | -0.09 | -0.60 | -0.48 |
| C5-0.1 | 0.24 | **0.72** | 0.42 |
| C0.1-0.0074 | 0.05 | -0.16 | **0.93** |
| CA | **0.77** | 0.12 | 0.32 |
| PERM | -0.08 | -0.33 | -0.64 |
| Expl. variance (%) | 48.4 | 15.7 | 12.1 |

[a]WASI, wet aggregate stability index (suffices sw, slow wetting; fw, fast wetting without pre-treatment; benz, pre-treatment with benzene; etoh, pre-treatment with ethanol); SOC, soil organic carbon; HF1-C, humic fraction with apparent molecular weight > 100 kDa; HF3-C, humic fraction with apparent molecular weight < 10 kDa; C30-5, mesopores; C5-01, micropores; C0.1-0.0074, cryptopores; CA, apparent contact angle; PERM, Pore-Cor saturated hydraulic conductivity.

The scatter of the first two factors indicates that $WASI_{sw}$ and $WASI_{fw}$ were associated with the structural parameters (Figure 2.4) and $WASI_{benz}$ was closer to SOC, HF1-C and contact angle. Among the stability indices, only $WASI_{etoh}$ was not clearly related to the factors since it was positioned in proximity to the origin.

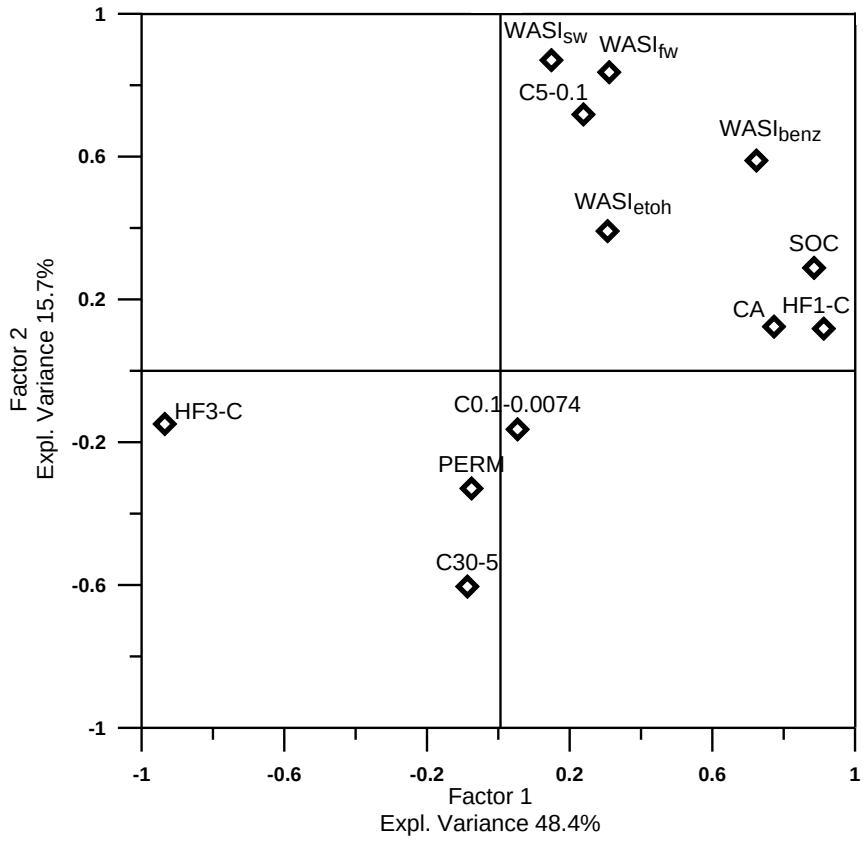


**Figure 2.4** - Variables projected in the plane determined by the first two principal axes. WASI, wet aggregate stability index (subscripts sw, slow wetting; fw, fast wetting without pre-treatment; benz, pre-treatment with benzene; etoh, pre-treatment with ethanol); SOC, soil organic carbon; HF1-C, humic fraction with apparent molecular weight > 100 kDa; HF3-C, humic fraction with apparent molecular weight < 10 kDa; C30-5, mesopores; C5-01, micropores; C0.1-0.0074, cryptopores.

## Pore-Cor simulations on wetting dynamics

The wetting dynamics changed according to the aggregate structure and contact angle (Table 2.7). If a contact angle of 0° is considered, the fastest wetting was in $NPK_2$+r (final fractional wetting of 0.271), while the slowest was in organic treatments ($L_2$+r and $F_2$).

**Table 2.7** - Fractional wetting results at different time steps modelled with Pore-Cor in eight selected unit cells and characterised by different fertilisations.

| Treatments[a] | Simulated porosity (%) | CA[b] (°) | Fractional wetting at different time steps (s) | | | | |
|---|---|---|---|---|---|---|---|
| | | | 0.9 | 9 | 90 | 180 | 900 |
| $F_2$ | 38.33 | 0 | 0.026 | 0.053 | 0.084 | 0.096 | 0.126 |
| | | 75.84 | 0.017 | 0.0036 | 0.067 | 0.076 | 0.087 |
| $L_2$+r | 38.42 | 0 | 0.033 | 0.046 | 0.071 | 0.085 | 0.120 |
| | | 75.85 | 0.025 | 0.037 | 0.055 | 0.062 | 0.076 |
| $F_1NPK_1$ | 37.61 | 0 | 0.039 | 0.072 | 0.123 | 0.149 | 0.194 |
| | | 75.3 | 0.032 | 0.048 | 0.088 | 0.106 | 0.141 |
| $L_1NPK_1$+r | 37 | 0 | 0.033 | 0.058 | 0.096 | 0.111 | 0.139 |
| | | 75.29 | 0.023 | 0.042 | 0.069 | 0.082 | 0.107 |
| $NPK_2$ | 34.33 | 0 | 0.072 | 0.102 | 0.156 | 0.169 | 0.200 |
| | | 75.13 | 0.049 | 0.083 | 0.130 | 0.144 | 0.162 |
| $NPK_2$+r | 38.77 | 0 | 0.055 | 0.124 | 0.198 | 0.225 | 0.271 |
| | | 72.53 | 0.035 | 0.124 | 0.152 | 0.177 | 0.227 |
| O | 36.25 | 0 | 0.058 | 0.102 | 0.158 | 0.171 | 0.213 |
| | | 72.50 | 0.044 | 0.079 | 0.132 | 0.146 | 0.174 |
| O+r | 35.5 | 0 | 0.063 | 0.105 | 0.170 | 0.190 | 0.257 |
| | | 72.12 | 0.047 | 0.084 | 0.136 | 0.154 | 0.194 |

[a]F, farmyard manure; L, liquid manure; NPK, inorganic fertilisation; O, control (no fertilisation); r, residue incorporation. Subscripts 1 and 2 refer to low and high input fertilisation.
[b]CA, apparent contact angle.

As an example, in the extreme treatments, $NPK_2$+r, O, $F_2$, after only 0.9 s fractional wetting was 0.055, 0.058 and 0.026 respectively. After 90 s, values increased to 0.198, 0.158 and 0.084. The final wetting porosity (900 s) was 0.271, 0.213 and 0.126 (Figure 2.5). The introduction of the contact angle into the equation [2.3] affected the degree of wetting, slowing down the wetting front velocity (Table 2.7). In $F_2$ and O the final wetting was reduced by 30% and 25% versus only 16% in $NPK_2$+r (Figure 2.5). As a final result the final fractional wetting ranged from 0.076 to 0.141 in organic and mixed treatments and from 0.162 to 0.227 in mineral and control treatments. Significant correlations were observed between final pore wetting and $WASI_{benz}$ and SOC content (Figure 2.6).

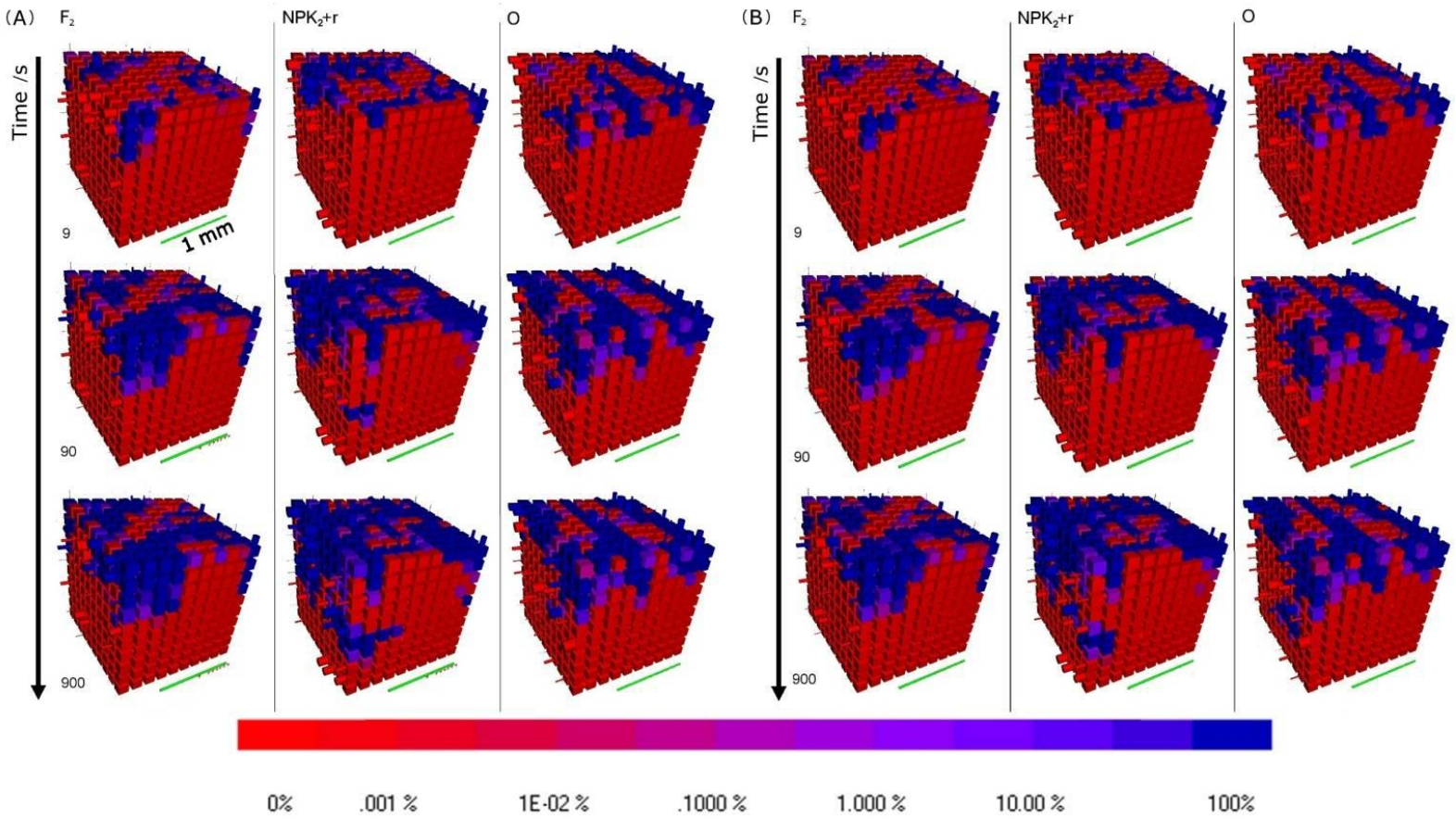


**Figure 2.5** - Fast dynamic wetting at 9, 90 and 900 s in $F_2$, $NPK_2$+r and O, with 0° (A) and measured apparent contact angle by capillary rise method (B). Colours represent the degree of wetting within pores and throats.

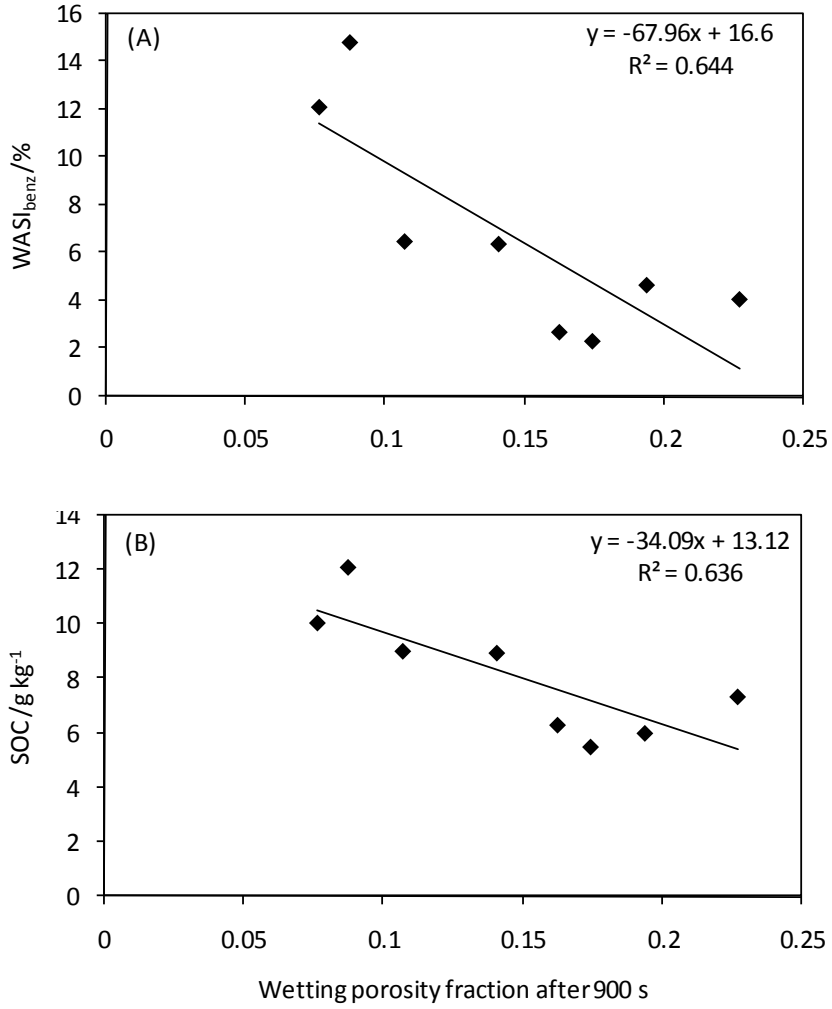


**Figure 2.6** - Correlations between wetting porosity fraction after 900 s and (A) SOC (g $kg^{-1}$) and (B) $WASI_{benz}$. Experimental apparent contact angle was used to simulate fast wetting. Correlations are significant at $p < 0.05$.

## Thermal and spectroscopic features of HS

Thermal behaviour of aggregate HS was characterised by two strong exothermic reactions (Exo1 and Exo2). Exo1 was mainly attributed to the decarboxylation reaction of acidic groups, proteins, carbohydrates and fatty acid decomposition (Schulten and Leinweber, 1996); the second one (Exo2) was related to the breakdown of aromatic structures and cleavage of the C–C bond (Francioso et al., 2009). Thermal behaviour of HS differed as a consequence of fertilisation practices: in soil treated with farmyard manure ($F_2$) and mixed fertilisers the mass loss associated with Exo1, related to carboxylic groups and

carbohydrates, decreased and the Exo2, related to aromatic compounds, increased (Table 2.8).

**Table 2.8** - Mass loss (%) in exothermic reactions, integrated IR peaks area and $^{1}$H NMR integrated regions area of humic substances from a soil consecutively treated with mineral and organic fertilisers over 40 years.

| Treatments[a] | TG-DTA[b] | | DRIFT, Area of peaks[c] | | | | | | | $^{1}$H NMR (%) | | |
|---|---|---|---|---|---|---|---|---|---|---|---|---|
| | Exo1 | Exo2 | $CH_3$ | $CH_2$ | Ester | Amides I, COOH | $COO^-$ | Amides II | Aromatics | Aromatics | Sugar-like, protein-like | Aliphatics |
| $F_2$ | 46.77 | 40.63 | 1.99 | 2.29 | 39.37 | 35.54 | 20.17 | 15.44 | 1.75 | 18.00 | 52.90 | 29.20 |
| $L_2$+r | 54.22 | 45.45 | 1.18 | 2.34 | 37.86 | 31.74 | 17.11 | 4.55 | 7.28 | 17.80 | 50.40 | 31.80 |
| $F_1NPK_1$ | 51.37 | 45.25 | 2.55 | 3.12 | 42.95 | 45.11 | 15.90 | 15.65 | 17.58 | 15.20 | 50.70 | 34.20 |
| $L_1NPK_1$+r | 52.84 | 47.16 | 0.77 | 2.83 | 28.34 | 52.66 | 13.76 | 7.09 | 1.26 | 15.90 | 55.20 | 28.90 |
| $NPK_2$ | 53.21 | 39.82 | 0.65 | 1.51 | 14.91 | 35.83 | 7.77 | 18.88 | 3.55 | 9.40 | 62.00 | 28.70 |
| $NPK_2$+r | 54.19 | 45.70 | 3.21 | 2.68 | 13.64 | 15.66 | 7.53 | 5.92 | 4.15 | 18.80 | 49.50 | 31.70 |
| O | 57.08 | 38.38 | 0.30 | 0.73 | 8.70 | 25.72 | 3.93 | 23.94 | nd | 10.80 | 58.40 | 30.90 |
| O+r | 59.91 | 39.43 | 6.09 | 0.11 | 15.90 | 68.65 | 1.94 | 23.36 | nd | 12.10 | 57.20 | 31.00 |

[a]F, farmyard manure; L, liquid manure; NPK, inorganic fertilisation; O, control (no fertilisation); r, residue incorporation. Subscripts 1 and 2 refer to low and high input fertilisation.

[b]Exo1, exothermic reactions at ca. 300 °C; Exo2, exothermic reactions at ca. 490 °C.

[c]Absolute values of peaks area; nd = not detected.

The integrated area of the peaks calculated in FT-IR spectra (Table 2.8) tended to increase with respect to the control (O). For instance, the hydrophobic groups such as methylene, ester and aromatic were more abundant following farmyard and liquid manure treatments and the abundance of $CH_3$ groups high when residues of O+r were present. The considerable concentrations of esters and aromatic compounds were probably derived from non-degraded lignin of crop residues. Hydrophilic groups, such as amides in protein-like structures, did not seem to follow a regular trend in relation to different treatments, as observed in thermal analysis. This discrepancy may arise from the poor resolution of aromatic and amide adsorption bands. By contrast, the carboxylate groups progressively increased in abundance in all treatments except O+r.

The proportion of aromatic-H increased in relation to fertilisation types, but no considerable change was observed in aliphatic-H (Table 2.8). The changes in proportion of H in sugar-like and protein-like structures were higher in mineral ($NPK_2$) and non-fertilised (O and O+r) treatments than in organic fertilisation. These observations, derived from NMR data, are in agreement with those of the thermal analysis.

Thermal and spectroscopic features were significantly related to the SOC and humic substances (Table 2.9). In particular, SOC, HC and higher molecular weight fractions showed positive correlations with $CH_2$, ester and COO- groups (DRIFT), aromatic-H structures (NMR) and a negative correlation with Exo1 (FT-IR). HF1-C and HF2-C contents were negatively correlated with H in sugar-like and protein-like structures. Conversely HF3-C content was negatively correlated with $CH_2$ ester and COO- groups and aromatic-H structures and positively with Exo1 and sugar-like and protein-like structures. With respect to aggregate stability, only $WASI_{benz}$ was correlated with spectroscopic features and in particular adsorption by esters ($r = 0.80$), COO- ($r = 0.85$) and aromatic-H structures ($r = 0.68$).

**Table 2.9** - Correlation matrix of organic carbon, humic fractions and functional groups (values in bold are significantly different at $p < 0.05$).

| Soil parameters[a] | TG-DTA | | DRIFT | | | | | | | $^1$H NMR | | |
|---|---|---|---|---|---|---|---|---|---|---|---|---|
| | Exo1 | Exo2 | $CH_3$ | $CH_2$ | Ester | Amides I, COOH | $COO^-$ | Amides II | Aromatics | Aromatics | Sugar-like, protein-like | Lipids, Waxes |
| SOC | **-0.82** | 0.44 | -0.16 | 0.66 | **0.88** | -0.06 | **0.96** | -0.54 | 0.28 | **0.75** | -0.60 | -0.02 |
| HC | **-0.81** | 0.49 | -0.16 | **0.67** | **0.84** | -0.04 | **0.94** | -0.58 | 0.21 | **0.78** | -0.60 | -0.07 |
| HF1-C | **-0.79** | 0.59 | -0.09 | **0.78** | **0.90** | -0.05 | **0.93** | -0.58 | 0.44 | **0.82** | **-0.74** | 0.19 |
| HF2-C | **-0.69** | 0.53 | 0.00 | **0.75** | **0.83** | -0.25 | **0.81** | -0.54 | **0.74** | **0.71** | **-0.77** | 0.48 |
| HF3-C | **0.79** | -0.59 | 0.06 | **-0.81** | **-0.91** | 0.14 | **-0.92** | 0.59 | -0.60 | **-0.81** | **0.79** | -0.34 |
| $WASI_{sw}$ | -0.33 | 0.03 | 0.03 | 0.06 | 0.55 | 0.16 | 0.56 | -0.17 | -0.20 | 0.52 | -0.37 | -0.11 |
| $WASI_{fw}$ | 0.04 | 0.23 | 0.06 | 0.04 | 0.44 | 0.02 | 0.39 | -0.38 | -0.02 | 0.54 | -0.53 | 0.22 |
| $WASI_{benz}$ | -0.65 | 0.23 | -0.05 | 0.39 | **0.80** | 0.00 | **0.85** | -0.41 | 0.12 | **0.68** | -0.53 | -0.05 |
| $WASI_{etoh}$ | -0.28 | -0.25 | 0.01 | -0.13 | 0.53 | 0.36 | 0.44 | 0.27 | -0.08 | 0.13 | -0.08 | -0.05 |
| CA | **-0.77** | 0.41 | -0.48 | **0.67** | **0.88** | -0.17 | **0.95** | -0.46 | 0.54 | 0.47 | -0.43 | 0.13 |

[a]SOC, soil organic carbon; HC, humic carbon; HF1-C, humic fraction with apparent molecular weight > 100 kDa; HF2-C, humic fraction with apparent molecular weight of 100-10 kDa; HF3-C, humic fraction with apparent molecular weight < 10 kDa; WASI, wet aggregate stability index (subscripts sw, slow wetting; fw, fast wetting without pre-treatment; benz, pre-treatment with benzene; etoh, pre-treatment with ethanol); CA, apparent contact angle.

## *Discussion*

Organic fertilisation was the main factor to stabilise soil structure. In particular farmyard manure was the most effective agent in the stabilisation of soil structure in terms of $WASI_{sw}$, $WASI_{etoh}$ and $WASI_{benz}$, but $L_2$+r mostly influenced $WASI_{fw}$. $WASI_{etoh}$ was less affected by organic fertilisation, probably due to it testing the wet mechanical cohesion of soil particles independently of slaking. As a consequence, our experimental results suggest that organic compounds, rich in humic substances, form a water-repellent coating outside the aggregates in addition to the humus-clay complexes. The positive correlation between $WASI_{benz}$ with SOC content, HF1-C content and contact angle establishes the significant contribution that SOM and HS make to the stability of soil aggregates. Benzene enhances soil aggregate hydrophobicity in $F_2$ ($WASI_{benz} > WASI_{fw}$), as well as the slaking in the other treatments ($WASI_{benz} < WASI_{fw}$). If the aggregate SOM content is low, then pre-treatment with benzene decreases WASI, whereas if it is medium to high, WASI may be only slightly modified or increased (Baver, 1972). The relatively high level of SOC content in $F_2$ in comparison with the other treatments (< 10 g $kg^{-1}$), together with its larger high molecular weight humic acid fraction, suggests that the increase in WASI arises from a coating of benzene on SOC.

The contact angles demonstrated that all soils were affected by a sub-critical level of hydrophobicity. Nevertheless, the differences among treatments reflected a significant influence of hydrophobicity on aggregate stability. HF1-C and HF2-C contained more hydrophobic compounds than HF3-C, as reported in Table 2.9. Indeed, higher molecular weight humic fractions were correlated with functional groups ($CH_2$, ester and COO-groups) that increased the contact angle. HF3-C content was positively correlated with Exo1 (polysaccharides and polypeptides), usually associated with the most recent microbial activity. The strong correlation existing between the hydrophilic carboxylate groups and HF1-C and HF2-C content seems in contrast with the hydrophobic properties of humic compounds. However Bachmann et al. (2008) suggested that with a low SOC/mineral ratio (e.g. < 10 g $kg^{-1}$) hydrophilic groups such as carboxylate can be directly involved in the formation of bonds with the mineral surface that orient the hydrophobic chains outside the aggregates to form a water-repellent coating.

Our results on PCA indicated a second mechanism of aggregate stabilisation which was related to pore structure. In the plane determined by the first two principal components $WASIf_w$ and $WASI_{sw}$ were clearly associated with soil structural parameters (e.g. porosity, saturated hydraulic conductivity), instead $WASI_{benz}$ was located in a middle position since affected also by SOC-related parameters. The position of $WASI_{etoh}$ near the origin clearly indicates that SOC content was not significantly involved in other mechanisms of aggregate stability (e.g. via chemical bonds).

Fast dynamic wetting simulations provided a simplified representation of the effect of pore size distribution on the wetting dynamics and consequently on the soil slaking. Most likely the infiltration rate was overestimated since Pore-Cor did not consider the effects of the pneumatic potential generated at the wetting front due to trapped air and change of pore size distribution due to slaking, pore clogging and swelling (Zaher et al., 2005). Moreover, it was not possible to get information on small-scale architecture of the pore space and the distribution/position of hydrophobic components inside the matrix and implement them on Pore-Cor (Ramirez-Flores et al., 2008). However even with these limitations the model allowed resolution of the contribution of hydrophobicity from that of pore structure.

Simulations indicated that in treatments with high SOC input (i.e. $F_2$ and $L_2$+r) the pore structure could be the main factor affecting the wetting, reducing the simulated final pore wetting by 2/3 with respect to the control (O with a contact angle of °0). Hydrophobicity contributed the remaining 1/3 reduction. By contrast, in mineral treatments, pore structure was either not a factor ($NPK_2$) or increased the final pore wetting in simulated cells ($NPK_2$+r). In these cases hydrophobicity was the leading mechanism able to decrease the fast wetting with respect to the control. Ramirez-Flores et al. (2008) observed that hydrophobicity is higher when measured in powdered samples than in aggregated soils. As a consequence our modelling simulation may have overestimated the effect of hydrophobicity.

Our simulated results are consistent with the work of Hafida et al. (2007), who observed that contact angle played a minor role in the overall mechanisms causing structural instability of a clay-loam soil treated with organic amendants (e.g. deinking secondary sludge mix) at rates comparable to our $F_2$ and $L_2$+r. These authors pointed out that the

mechanism of hydrophobicity could have been overestimated in past studies since it could have been confused with other mechanisms (e.g. pore occlusion).

As the small dimensions of aggregates were not amenable to measurement of their rapid wetting it was not possible to test the predictions of the model. In any case the significant correlation observed between the final pore wetting and $WASI_{benz}$, which was the most sensitive index of SOC content, can be considered an evidence of the model's capability to represent the physical mechanisms of structural stability associated with aggregate wetting and stability. The extreme variability of simulated saturated hydraulic conductivity necessarily arises from the failure of the present simulations of the pore network structure to match the complexity of that in soil. This failure may be remedied by enhancing the model with improved resolution between macro- and microporosity as reported by Laudone et al. (2011).

Experimental data and simulations indicate the retarding effect of SOM on the entry of water into the soil aggregates as a consequence of an increase in hydrophobicity and a modification in the pore size distribution involving a shift from micro- and mesopores towards ultramicropores, the extent of which is influenced by the level of SOM.

## *Conclusions*

Our study confirmed the enhanced stability of soil arising from organic amendants. Both the quality and quantity of SOM, present following long-term treatments with fertiliser, confer beneficial physical and chemical properties improving aggregate stability. SOM determined the shift of pore network towards small pores, as shown by its positive correlation with ultramicropores and negative correlation with meso- and micropores. They impede the wetting of aggregates with water and prevent a rapid increase in pressure inside pores from which air is unable to easily escape. This is enhanced by the hydrophobic nature of HS (arising from the presence of alkyl, ester and aromatic compounds associated with its high molecular weight fraction). The association of carboxylates with HF in agricultural soils of low SOC/mineral ratio indicates that water-repellent coatings may arise from orientation and distribution of such molecules in aggregates of soils of this type. Modelling of fast wetting dynamics, however, suggests that the contribution that hydrophobicity makes to aggregate stability, especially to soils treated with high SOC input, may not be the most significant factor.

## *References*


Abiven, S., Menasseri, S., Chenu, C., 2009. The effects of organic inputs over time on soil aggregate stability - A literature analysis. Soil Biol. Biochem. 41, 1-12.

Bachmann, J., Guggenberger, G., Baumgartl, T., Ellerbrock, R.H., Urbanek, E., Goebel, M.O. et al. 2008. Physical carbon-sequestration mechanisms under special consideration of soil wettability. J. Plant Nutr. Soil Sci., 171, 14-26.

Bartoli, F., Dousset, S., 2011. Impact of organic inputs on wettability characteristics and structural stability in silty vineyard topsoil. Eur. J. Soil Sci., 62, 183-194.

Baver, L.D., 1972. Physical properties of soils. In: Soils of the humid tropics, pp. 50-62. National Academy of Sciences, Washington D.C.

Bocchi, S., Confalonieri, R., Frigeni, S., Morari, F., Patruno, A., 2008. Wet Aggregate Stability Index: precision assessment of Tiulin method through an inter-laboratory test. Agrochimica 52, 71-82.

Bodurtha, P.A., Matthews, G.P., Kettle, J.P., Roy, I.M., 2005. Influence of anisotropy on the dynamic wetting and permeation of paper coatings. J. Colloid Interf. Sci., 283, 171-189.

Cameron, K.C., Buchan, G.D., 2006. Porosity and pore-size distribution. In: Encyclopedia of Soil Science (ed. R. Lal), pp. 1350–1353. CRC Press, Boca Raton, Florida.

Chenu, C., Le Bissonnais, Y.,Arrouays, D., 2000. Organic matter influence on clay wettability and soil aggregate stability. Soil Sci. Soc. Am. J. 64, 1479-1486.

De Bano, P.S., 1981. Water repellent soils: a state-of-the-art. US Department of Agriculture. Pacific Southwest Forest and Range Experiment Station, Berkeley, California.

Dell'Agnola, G. and Ferrari, G., 1971. Molecular sizes and functional groups of humic substances extracted by 0.1 M pyrophosphate from soil. J. Soil Sci. 22, 342-349.

Diaz-Zorita, M., Perfect, E., Grove, J.H., 2002. Disruptive methods for assessing soil structure. Soil Till. Res. 64, 3-22.

Douglas, J.T., Goss, M.J., 1982. Stability and organic matter content of surface soil aggregates under different methods of cultivation and in grassland. Soil Till. Res. 2, 155-175.

Echeverría, J.C., Morera, M.T., Mazkiarán, C., Garrido, J.J., 1999. Characterization of the porous structure of soils: adsorption of nitrogen (77 K) and carbon dioxide (273 K), and mercury porosimetry. Eur. J. Soil Sci. 50, 497-503.

FAO-UNESCO, 1990. Soil map of the world. Revised Legend. FAO, Rome.

Francioso, O., Montecchio, D., Gioacchini, P., Cavani, L., Ciavatta, C., Trubetskoj, O. et al. 2009. Structural differences of Chernozem soil humic acids SEC-PAGE fractions revealed by thermal (TG-DTA) and spectroscopic (DRIFT) analyses. Geoderma 152, 264-268.

Giardini, L., 2004. On going trial. In: Giardini, L. (Eds.), Productivity and Sustainability of different Cropping Systems. 40 years of experiments in Veneto region (Italy), Patron, Bologna, pp. 73-98.

Gribble, C.M., Matthews, G.P., Laudone, G.M., Turner, A., Ridgway, C.J., Schoelkopf, J., Gane, P.A.C., 2011. Porometry, porosimetry, image analysis and void network modelling in the study of the pore-level properties of filters. Chem. Eng. Sci. 66, 3701-3709.

Hafida, Z., Caron, J., Angers, D.A., 2007. Pore occlusion by sugars and lipids as a possible mechanism of aggregate stability in amended soils. Soil Sci. Soc. Am. J. 71, 1831-1839.

Henin, S., Monnier, G., Combeau, A., 1958. Méthode pour l'étude de la stabilité structurale des sols. Annales Agronomiques 9, 73-92.

Johnson, A., Roy, I.M., Matthews, G.P., Patel, D., 2003. An improved simulation of void structure, water retention and hydraulic conductivity in soil with the Pore-Cor three-dimensional network. Eur. J. Soil Sci. 54, 477-489.

Kaiser, H.F., 1974. An index of factorial simplicity. Psychometrika 39, 31-36.

Laudone, G.M., Matthews, G.P., Bird, N.R.A., Whalley, W.R., Cardenas, L.M., Gregory, A.S. 2011. A model to predict the effects of soil structure on denitrification and N2O emission. J. Hydrol. 409, 283-290.

Le Bissonnais, Y., 1996. Aggregate stability and assessment of soil crustability and erodibility: I. Theory and methodology. Eur. J. Soil Sci. 47, 425-437.

Lugato, E., Simonetti, G., Morari, F., Nardi, S., Berti, A., Giardini, L., 2010. Distribution of organic and humic carbon in wet-sieved aggregates of different soils under long-term fertilization experiment. Geoderma 157, 80-85.

Martin, M., Celi, L., Bonifacio, E., Nardi, S., Barberis, E., 2006. Characteristics of soil organic matter in a limnic histosol of the alpine morainic system. Soil Sci. 171, 527–540.

Matthews, G.P., Canonville C.F., Moss, A.K., 2006. Use of a void network model to correlate porosity, mercury porosimetry, thin section, absolute permeability, and NMR relaxation time data for sandstone rocks. Phys. Rev. E 73, 031307-1-9.

Matthews, G.P., Laudone, G.M., Gregory, A.S., Bird, N.R., Matthews, A.G. de G., Whalley, W.R., 2010. Measurement and simulation of the effect of compaction on the pore structure and saturated hydraulic conductivity of grassland and arable soil. Water Resour. Res. 46, W05501-1-13.

Montecchio, D., Francioso, O., Carletti, P., Pizzeghello, D., Chersich, S., Previtali, F. et al. 2006. Thermal analysis (TG-DTA) and drift spectroscopy applied to investigate the evolution of humic acids in forest soil at different vegetation stages. J. Therm. Anal. Calorim. 83, 393-399.

Nardi, S., Morari, F., Berti, A., Tosoni, M., Giardini, L., 2004. Soil organic matter properties after 40 years of different use of organic and mineral fertilisers. Eur. J. Agron. 21, 357-367.

Papadopoulos, A., Bird, N.R., Whitmore, A.P., Mooney, S.J., 2009. Investigating the effects of organic and conventional management on soil aggregate stability using X-ray computed tomography. Eur. J. Soil Sci. 60, 360-368.

Piccolo, A., Mbagwu, J.S.C., 1990. Effects of different organic waste amendments on soil microaggregate stability and molecular sizes of humic substances. Plant Soil 123, 27-37.

Piccolo, A., Mbagwu, J.S.C., 1999. Role of hydrophobic components of soil organic matter in soil aggregate stability. Soil Sci. Soc. Am. J. 63, 1801-1810.

Ramirez-Flores, J.C., Woche, S.K., Bachmann, J., Goebel, M.O., Hallett, P.D., 2008. Comparing capillary rise contact angles of soil aggregates and homogenised soil. Geoderma 146, 336-343.

Schulten, H.R. and Leinweber, P., 1996. Characterization of humic and soil particles by analytical pyrolysis and computer modeling. J. Anal. Appl. Pyrol. 38, 1-53.

Sibbesen, E., Skjoth, F., Rubaek, G.H., 2000. Tillage caused dispersion of phosphorus and soil in four 16-year old field experiments. Soil Till. Res. 54, 91-100.

Siebold, A., Walliser, A., Nardin, M., Opplinger, M., Schultz, J., 1997. Capillary rise for thermodynamic characterization of solid particle surface. J. Colloid Interf. Sci. 186, 60-70.

Six, J., Bossuyt, H., Degryze, S., Denef, K., 2004. A history of research on the link between (micro)aggregates, soil biota, and soil organic matter dynamics. Soil Till. Res. 79, 7-31.

Statsoft Inc., 2004. STATISTICA, Version 7, www.statsoft.com. 29/06/2011.

Zaher, H., Caron, J., Ouaki, B., 2005. Modeling aggregate internal pressure evolution following immersion to quantify mechanisms of structural stability. Soil Sci. Soc. Am. J. 69, 1-12.

# Chapter III

# Coupling X-ray microtomography and mercury intrusion porosimetry to quantify aggregate structures of a Cambisol under different fertilisation treatments

## *Introduction*

Problems for agriculture of land degradation (e.g. surface crusting, erosion and compaction) are due to soil structure degradation and lots of research have shown a relationship between loss of soil fertility and management practices (e.g. Pagliai et al., 2004; Williams and Petticrew, 2009). Soil structure affects root growth, liquid and gas permeability (Horn et al., 1994), the soil biological activity (Nunan et al., 2006) as well as the aggregate formation. Soil aggregation is influenced by soil organic carbon content (Tisdall and Oades, 1982), which is usually recognised as one of the main indicator of soil fertility as it improves structure stability (Abiven et al., 2009). A complex feedback links the soil structure and the organic carbon content that acts as a binding agent promoting aggregation. In turn, the soil matrix affects the organic carbon availability according to its spatial location: organic carbon residing in small pores tends to be more protected than that residing in larger pores (Lugato et al., 2009). For this reason soil structure and its evolution are widely monitored to assess the effect of agronomic practices on the soil environment (Diaz-Zorita et al., 2002; Bronick and Lal, 2005).

Several studies focussed on pore network at micro- (< 50 μm) and macropore (> 50 μm ) scale to quantify soil structure characteristics. Both water retention (Holtham et al., 2007, Schjonning et al., 2005) and mercury intrusion curves (Lugato et al., 2009) are traditional techniques to estimate pore size distribution in soils (mercury intrusion porosimetry can reveal pores up to nanoscale level). The classical method of analysing mercury intrusion pressure-volume curves is based on the model of parallel cylindrical non-intersecting pores of differing radii (Gregg and Sing, 1982). Lawrence (1978) showed that sample damage is unlikely to occur despite the high pressure and hence pore distribution curves are fairly comparable. However, these techniques have some important drawbacks: they cannot provide an estimation of the pore shape and total porosity is calculated as the sum of accessible pores from the intrusion of the liquid (mercury or water) so that unconnected pores are not detected. Pores are always detected below 900 μm but this does not reflect the real pore size distribution since the liquid reveals the diameter of the throat entrance instead of the true pore diameter (Cnudde et al., 2009). Pore size distribution curves have been successfully parameterised with different models (e.g. network models, fractal dimensions) to estimate different

parameters such as pore connectivity, tortuosity, hydraulic properties, etc.( Bartoli et al., 1999; Johnson et al., 2003; Boulin et al., 2008). More advanced methods of pore morphology characterisation are based on thin sectioning and image analysis ( Ringrose-Voase, 1996; Hubert et al., 2007). However these techniques are time consuming and usually performed on few images.

X-ray computer assisted microtomography (micro-CT), combined with image processing techniques, has recently been put forward as a non-destructive technique to study the soil structure as it allows the quantification of pore size distribution and total porosity (Hainsworth and Aylmore, 1983). It can reveal both individual pores and pore shape ( Mooney et al., 2006; Tippkoetter et al., 2009) depending on the spatial resolution of the instrument, but only analyses of small samples can provide detailed information on high resolution images (Mees et al., 2003). Micro-CT has been used to investigate the soil surface structure in undisturbed columns affected by simulated rainfall (Lee et al., 2008) and sodium content (Jassogne et al., 2007), while Mooney et al. (2006) and Sander et al. (2008) analysed undisturbed soil cores to highlight the importance of root growth in the structure and its effect on macroporosity. Deurer et al. (2009) and Papadopoulos et al. (2009) studied the effects of organic fertilisers on macrostructure and showed that organic matter influenced pore connectivity and soil stability.

In order to better characterise the soil porosity a combination of techniques is required (Klobes et al., 1997; Cnudde et al., 2009), although only a few authors combined mercury intrusion porosimetry and image analysis to study soil structure (e.g. Pagliai et al., 2004). It is therefore essential to compare the pore measurements that are determined from tomographic images and mercury intrusion porosimetry to understand the advantages and disadvantages of the two techniques. By studying aggregates of soil amended with different types and amounts of fertilisation, we: a) compared mercury intrusion porosimetry (MIP) and X-ray computer assisted microtomography (micro-CT) for quantifying total porosity, pore size distribution and porous network characteristics. A network model was also applied to the distribution curves, of both MIP and micro-CT, as a tool to compare the different techniques, and b) combined these techniques to evaluate whether different fertilisation practices affect porosity and pore morphology of the soil aggregates.

## *Materials and methods*

### Description of long-term experiment and soil sampling

A long-term experiment was established in 1962 at the experimental farm of the University of Padova (Legnaro, Veneto Region, NE Italy) (Giardini, 2004). It is the longest running rotation experiment in Italy. Details of the experiment have been already reported in Nardi et al. (2004). Briefly: the top soil is a fluvi-calcaric cambisol (CMcf), silty or sandy loam (FAO-UNESCO, 1990), with a mean pH of 8.11 (Table 3.1). The trial considers eight treatments with maize as main crop. These allow the comparison between fertilisations with only organic ($F_2$ = farmyard manure, 60 t $ha^{-1}$ $y^{-1}$, 20% d.m.; $L_2$ = liquid manure, 120 t $ha^{-1}$ $y^{-1}$, 10% d.m.), only mineral ($NPK_2$ = high mineral input, 300 kg N $ha^{-1}$ $y^{-1}$, 66 kg P $ha^{-1}$ $y^{-1}$, 348 kg K $ha^{-1}$ $y^{-1}$) or mixed inputs ($F_1NPK_1$ = farmyard manure, 30 t $ha^{-1}$ $y^{-1}$, 20% d.m. + mineral input, 150 kg N $ha^{-1}$ $y^{-1}$, 33 kg P $ha^{-1}$ $y^{-1}$, 174 kg K $ha^{-1}$ $y^{-1}$; $L_1NPK_1$ = liquid manure, 60 t $ha^{-1}$ $y^{-1}$, 20% d.m. + mineral input, 150 kg N $ha^{-1}$ $y^{-1}$, 33 kg P $ha^{-1}$ $y^{-1}$, 174 kg K $ha^{-1}$ $y^{-1}$) and no fertilisation (O). Half of the treatments also include crop residue incorporation (r).

**Table 3.1** - Main physical and chemical properties of the top soil (0-20cm) (soil without fertilisation input).

| | Mean | (s.e.)[a] |
|---|---|---|
| Sand (%) | 33.62 | (0.82) |
| Silt (%) | 61.39 | (0.76) |
| Clay (%) | 4.99 | (0.11) |
| Organic Carbon (g $kg^{-1}$) | 12.69 | (0.61) |
| Humic Carbon (g $kg^{-1}$) | 5.93 | (0.39) |
| pH | 8.11 | (0.06) |
| EC[b] 1:2.5 (mS $cm^{-1}$) | 0.42 | (0.04) |
| CEC[c] (meq 100 $g^{-1}$) | 17.36 | (0.68) |

[a] Standard error.
[b] Electrical conductivity.
[c] Cation exchange capacity.

The experimental layout is a randomised block with three replicates, on plots of 7.8 × 6 m. Sampling was done in 2005 at the end of maize growing season. Soil samples were collected in the first 15 cm layer from five different points in the central area of 16 $m^2$ area of the plot to avoid soil movement effects (Sibbesen et al., 2000) and bulked to obtain a sample of about 1 kg. In order to perform comparable chemical and physical analyses, samples were broken up manually, air-dried and sieved at 5-6 mm. About 50 g of sample aggregates were collected randomly for analysis.

## Texture and chemical analysis

Soil texture was determined by means of laser diffractometry, using a Malvern Mastersizer 2000 (Malvern Instruments, Malvern, England). Diffracted light was measured by 52 sensors and accumulated in 100 size fraction bins. Particle-size distributions, i.e. clay (< 2 µm), silt (2-50 µm) and sand (50-2000 µm) were expressed in volume units. Before analysis, soils were dispersed for 24 h in a 5% v/v sodium hexametaphosphate solution to enhance the dispersion of clay particles (Dane and Topp, 2002).

Aggregates were analysed for organic carbon (g OC $kg^{-1}$ dry soil) by dichromate oxidation (Walkley and Black, 1934) and humic carbon (HC). Humic substances were extracted from the air-dried samples with 0.5 M NaOH (1:10 w/v) in a Dubnoff bath at 50 °C for 16 h and separated from the suspended material by centrifuging at 15000 rpm for 15 min. Here, the term humic substances is the fraction soluble in bases and comprehensive of humic and fulvic acids. Humic extracts (50 ml) were transferred into 18,000 mol. wt cut-off dialysis Visking tubing (Medicell Ltd, London, UK) and dialysed against double-distilled water. The water was changed daily until the liquid outside the dialysis tube was colourless. The retained solution was then desalted by ion exchange on Amberlite IR 120 $H^+$ (Stevenson, 1994) and analysed for HC by dichromate oxidation.

## Mercury intrusion porosimetry

Accessible porosity and pore size distribution were measured within the diameter range of 100-0.0074 µm with Thermo Finnigan Pascal 140 (100-3.8 µm) and Thermo Finnigan Pascal 240 (15-0.0074 µm). The pore radius into which Hg was intruded was calculated as a function of pressure using the Young-Laplace equation:

$$r = \frac{2\gamma \cos\theta}{P} \qquad [3.1]$$

assuming cylindrical pores, where $r$ is the pore radius, $P$ is the pressure, $\gamma$ is the Hg surface tension (0.47 N $m^{-1}$) and $\theta$ is the contact angle between Hg and soil (140°). Pores were labelled with a classification adapted from Cameron and Buchan (2006) as macropores (100-75 µm), mesopores (75-30 µm), micropores (30-6.25 µm), ultramicropores (6.25-0.1 µm) and cryptopores (0.1-0.0074 µm). The micropore and ultramicropore ranges in the Cameron and Buchan (2006) classification were modified to take into account the micro-CT scan pixel size (6.25 µm).

## X-ray microtomography

One aggregate per plot (randomly selected) was scanned using a Skyscan 1172 X-ray microtomography (Skyscan, Belgium). The detector was a 12-bit 4008 × 2670 pixels CCD and the scanner was set at 70 kV and 112 µA. Projections were collected during a 360° sample rotation at 0.2° angular incremental step. Beam hardening artefacts were minimised during data acquisition with a 0.5 mm Al filter. Projections were reconstructed using the cone-beam reconstruction software from Skyscan to obtain a stack of at least 760 2D slices in 16-bit depth. 16-bit images were later converted into 8-bit depth. Isotropic voxels had a resolution of 6.25 µm in all the three directions.

## Digital image processing and analysis

A region of interest of 270 × 270 pixels was manually selected within each stack to represent the largest pixel area fully occupied by the aggregates. To avoid edge effects, only 256 contiguous slices from each stack were used for analysis (Mooney et al., 2006; Hallett et al., 2009). The reconstructed volume produced a 3D visualisation of about 1.7 × 1.7 × 1.6 mm. Using public domain software ImageJ (Vs. 1.44, National Institute of Health, http://rsb.info.nih.gov/ij) stack slices were subjected to histogram normalisation and were then interactively segmented. Segmentation was performed using a unique threshold level throughout the whole volume data. Greyscale level of soil samples slightly differed because of variations in image attenuation intensity. Manual thresholding was therefore employed since different automatic threshold algorithms

created segmentation bias (Mooney et al., 2006; Papadopoulos et al., 2009). A one-pixel mathematical morphology operator closing (Serra, 1982) was applied to the binary images to fill misclassified pixels inside the pores (Mooney et al., 2006) as well as to maintain pore connections.

## 3D porosity and degree of anisotropy

3D porosity was defined as the total number of pore voxels, within the volume of interest, divided by the total number of voxels of the volume. 3D degree of anisotropy (DA) was calculated according to the mean intercept length (MIL) method (Harrigan and Mann, 1984). It was calculated globally within each volume of interest and was used for quantifying if the pores were directionally dependent. MIL is found by sending, from the centre of the volume, several vectors in all directions throughout the segmented volume. Each vector is divided by the number of times that it intercepted the boundary between foreground (pores) and background (soil matrix). An ellipsoid is fitted to the MIL and a material anisotropy tensor is constructed. Finally the resulting eigenvalues give the ellipsoid axes and the eigenvectors give the ellipsoid orientation. DA was calculated as:

$$DA = 1 - \frac{L_s}{L_l} \qquad [3.2]$$

where $L_s$ and $L_l$ are the shortest and longest ellipsoid axes respectively. DA varies between 0 (perfect isotropic structure) and 1 (anistropic structure) and was calculated using the free software package Quant3D (Ketcham and Ryan, 2004).

## 2D pore characterisation

2D pore size distribution was obtained by classifying, in each slice, the hydraulic diameter of each disconnected pore ($D_h = 4A/P_p$), where $A$ is the pore area and $P_p$ the pore perimeter. Pores were classified according to Cameron and Buchan (2006).

The shape of each pore (S) was estimated by the shape factor (Pagliai et al., 2004; Tippkoetter et al., 2009):

$$S = \frac{P_p^2}{4\pi A} \quad [3.3]$$

Shape factor takes a minimum value of 1 for a perfect round pore and increases with a longer or more irregular pore. According to Bouma et al. (1977) pores were classified as regular ($S \leq 2$), irregular ($2 < S \leq 5$) and elongated ($S > 5$). Shape factor was not estimated for pores with less than 50 pixels because their shape was insufficiently resolved for the analysis (Ringrose-Voase and Bullock, 1984).

The 2D connectivity ($2D_{conn}$) index (Hallaire et al., 1997; Prado et al., 2009) was estimated for each slice, from the following equation:

$$2D_{conn} = 1 - \frac{N_p}{N_u} \quad [3.4]$$

where $N_p$ is the number of pores within each slice and $N_u$ is the number of ultimate eroded objects. $N_u$ was computed by consecutive morphological erosion of the pores and corresponds to the number of convex components in porosity (Serra, 1982). $2D_{conn}$ varies from 0 to 1 as the pores change from isolated to highly interconnected. 2D parameters were not determined for pores touching the borders of the region of interest.

## Pore-Cor modelling

The Pore-Cor network model (Matthews et al., 2010) was used to analyse pore distribution curves of both MIP and micro-CT. The model generates simple stochastic representations of soil structure and quantifies model parameters that are real properties of the simulated soil sample. The pore structure is represented by cubes that simulate pores, surrounded by cylindrical throats. The unit cell of the model comprises 1000 pores in a 10 × 10 × 10 array, connected by up to 3000 throats. Each simulated curve can be thought of as being the function of five parameters: throat skew (the asymmetry of the throat distribution), throat spread (defined as twice the standard deviation of the beta distribution), pore skew (which compensates for the fact that the regular positional spacing of the features in the network, irrespective of size, often makes it difficult to achieve the correct experimental porosity), connectivity (the average number of

connected throats per pore) and correlation level (setting level of local autocorrelation of throats and pores). A Boltzman-annealed simplex is used to adjust model parameters so that the simulated pore distribution curves closely match the experimental ones. Ten fits were conducted per replication, corresponding to different stochastic generation numbers. The average values of the five parameters were used for the comparison.

## Statistical analysis

Soil data were analysed with one-way ANOVA and the Duncan's test was used to differentiate the means. A stepwise multiple regression analysis ($Y = \beta_0 + \beta_1X_1 + \beta_2X_2 +\ldots+ \beta_kX_k$) with backward selection was also conducted in order to identify the strongest physical and chemical predictors of aggregate morphometric features detected by MIP and micro-CT (total porosity, pore size distribution, pore shape). Statistical analyses were performed with STATISTICA 7.0 (StatSoft Inc., 2004).

## *Results and Discussion*

### Comparison between MIP and micro-CT

Total porosity detected with mercury intrusion porosimetry (MIP), on average 40.21%, was very different from that measured by micro-CT, on average 9.66% (Table 3.2). Porosity of the overlapping pore range (from 6.25 to 100 μm) showed similar results with the two techniques, on average 9.7% and 10.32% for MIP and micro-CT respectively.

**Table 3.2 -** Porosity calculated with mercury intrusion porosimetry (MIP) and micro-CT. Data refer both to total porosity and porosity of the overlapping range whose pores, detected with both techniques, ranged between 6.25 and 100 μm.

| Treatments | Total 3D porosity | | Porosity of overlapping range | |
|---|---|---|---|---|
| | MIP (s.e.)[a] | Micro-CT (s.e.) | MIP (s.e.) | Micro-CT (s.e.) |
| $F_2$ | 41.52 (1.31) | 8.55 (1.27) | 9.12 (0.49) | 8.54 (1.27) |
| $L_2$+r | 39.38 (0.31) | 10.96 (3.34) | 10.57 (1.13) | 10.92 (3.30) |
| $F_1NPK_1$ | 37.60 (3.14) | 10.73 (0.87) | 8.71 (1.00) | 10.71 (0.86) |
| $L_1NPK_1$+r | 43.94 (3.29) | 6.57 (1.17) | 11.07 (2.95) | 6.57 (1.17) |
| $NPK_2$ | 38.65 (1.23) | 12.38 (3.54) | 6.73 (0.86) | 12.35 (3.54) |
| $NPK_2$+r | 44.32 (4.89) | 12.22 (4.23) | 14.01 (1.06) | 12.21 (4.23) |
| O | 37.33 (0.52) | 12.54 (1.81) | 7.94 (1.88) | 12.53 (1.81) |
| O+r | 38.97 (1.03) | 8.76 (2.65) | 9.17 (1.00) | 8.74 (2.64) |
| Mean | 40.21 (0.90) | 10.34 (0.89) | 9.66 (0.62) | 10.32 (0.88) |

[a] Standard error.

Significant differences were found between pore classes in MIP and micro-CT ($p \leq 0.05$) (Table 3.3). Ultramicroporosity was the main class calculated by MIP (28.7%), followed by micropores (7.0%) and meso- and cryptopores, 2.3% and 1.9% respectively. Conversely micro-CT pore size distribution was represented mainly by micropores (8.4%) and to a lesser extent by mesopores (1.8%), macropores (0.05%) and ultramacropores (0.02%). It follows that MIP was an adequate technique to detect almost the entire range of porosity in small aggregates (5-6 mm), while micro-CT was useful only for meso- and macroporosity.

**Table 3.3** - Pore size distribution calculated by mercury intrusion porosimetry (MIP) and micro-CT. Values differ significantly when followed by different letters ($p \leq 0.05$).

| Pore size distribution (μm) | Porosity (%) | | Pore size changes |
|---|---|---|---|
| | MIP | micro-CT | |
| > 100 | - | 0.016 c | |
| 100-75 | 0.36 d | 0.046 c | +3.3% |
| 75-30 | 2.28 c | 1.80 b | +6.1% |
| 30-6.25 | 7.03 b | 8.47 a | -9.4% |
| 6.25-0.1 | 28.66 a | - | |
| 0.1-0.0074 | 1.89 c | - | |

D'acqui et al. (1993), comparing the porosity of a silty clay soil taken from wheel-traffic and seed-line areas, found that the pore size distribution curves were bimodal in both MIP and image analysis. They showed that modal sizes were shifted from 0.7-0.8 μm and 10-15 μm in MIP to 1-2 μm and 30-50 μm in image analysis respectively. Lange et al. (1994) observed similar underestimation of coarser pores and overestimation of finer pores by MIP in comparison to image analysis in different cement-based materials. By contrast our analysis evidenced that only microporosity (30-6.25 μm) determined by MIP was lower (-9.4%) than microporosity calculated with micro-CT, whereas meso- and macroporosity of MIP were higher (+6.1% and +3.3% respectively) when compared to those determined by micro-CT (Table 3.3).

Most likely the intrusion of mercury into micropores (30-6.25 μm) was controlled by smaller pores (6.25-0.1 μm and 0.1-0.074 μm) that acted as throats. In fact MIP, which is subjected to the "ink bottle effect", measures part of the large pores in the specimen only by intruding mercury through smaller bottle necks, therefore the technique systematically misrepresents their size (Lange et al., 1994). It follows that the intrusion of mercury into the pores depends on their connectivity and access to the external surfaces (Farber et al., 2003; Cnudde et al., 2009). These morphological features were not revealed by micro-CT since their dimension was smaller than the instrumental resolution limit.

These results are in agreement with the relationship observed between 2D connectivity ($2D_{conn}$) and pore size distribution by image analysis (Figure 3.1). A negative correlation was found between micropores and 2D connectivity ($R^2$ = 0.67), while the correlation was positive between meso- and macropore classes and connectivity ($R^2$ = 0.68 and 0.30 respectively). At first glance these results seemed to indicate that only meso- and macropores were well connected, while micropores were mainly isolated. However most likely the low degree of connectivity in 30-6.25 µm would be related to the low resolution of the micro-CT which prevented detecting pores < 6.25 µm.

Parameters calculated by Pore-Cor (Figure 3.2) differed between the two techniques since they evaluated the pore size distribution and total porosity differently (Johnson et al., 2003). Throat skew (the throat distribution skewed around the geometric mean size) was on average -4.11 and -6.80 in MIP and micro-CT respectively. Although the range of porosity differed between the two techniques, the negative values indicated distributions shifted towards smaller pores. Pore skew (scaling factor that bulks up the sizes of the pores to achieve the experimental porosity) was dramatically higher in MIP (on average 2380) than in micro-CT (on average 9.89).

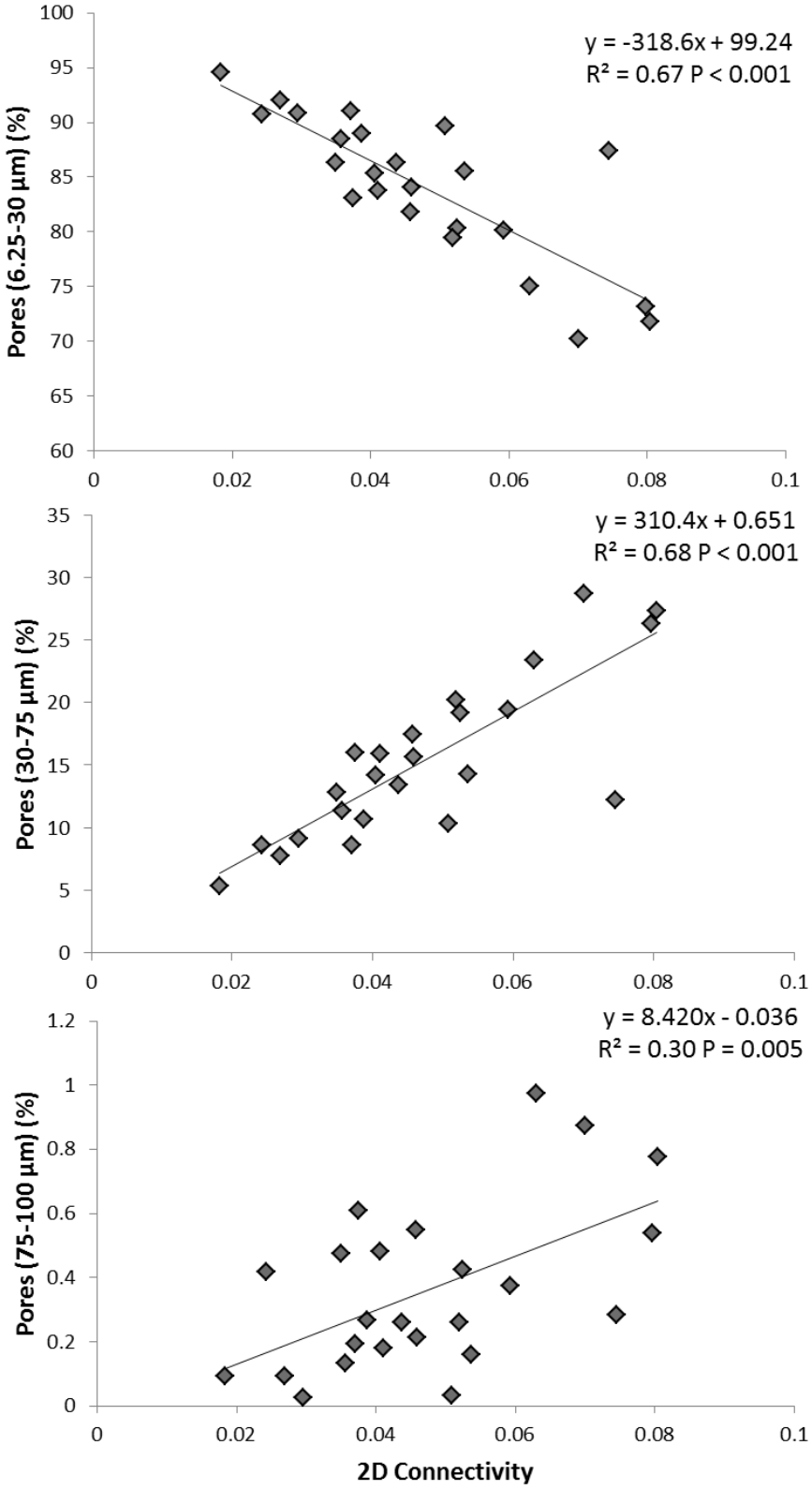


**Figure 3.1** - Correlations between 2D connectivity and pore size classes detected by micro-CT.

This can be explained by considering that total porosity detected by MIP was higher than micro-CT and mainly characterised by smaller throats. The network model is unable to pack these small features sufficiently close together to achieve the correct porosity and it can only obtain the experimental porosity by bulking up the pores using the pore skew parameter (Matthews et al., 2010). Pore-Cor connectivity (the mean number of throats among pores) was similar in the two techniques, with mean values of 3.76 and 3.86 for MIP and micro-CT respectively. In agreement with other authors who applied Pore-Cor on soil samples ( Johnson et al., 2003; Holtham et al., 2007), connectivity was poorly sensitive to changes in soil structure and did not evidence significant differences between samples. Correlation level (i.e. the short-range size autocorrelation of the throats and pores within the soil structure) was significantly different between the two measurement techniques (Figure 3.2).

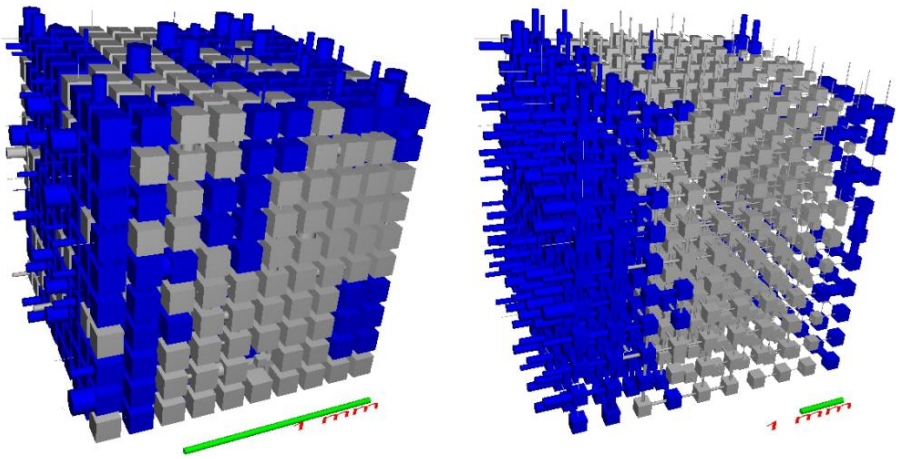

**Figure 3.2** - Representations of soil structure modelled with Pore-Cor from MIP (left) and micro-CT (right) pore distribution curves and characterised by mixed fertilisation ($F_1NPK_1$). Water (blue) drained vertically displaced by air (grey), occupying 50% of the entire pore volume.

Results showed a higher local size correlation level between the sizes of pores and throats in micro-CT (on average 0.66) than MIP (on average 0.22). The lower value in MIP indicated that throats and pores of small size were connected to throats and pores of larger size generating more complex structures. These results are in agreement with previous considerations on pore size spatial distribution: MIP measurements suggested

that micropores (30-6.25 µm) were connected by smaller throats (6.25-0.1 µm and 0.1-0.074 µm). By contrast the higher correlation level in micro-CT emphasised that pores of homogenous size were clustered in local structures. Most likely this is a model artefact because the micro-CT resolution limit provides a wrong estimation of the micropore connections. Throat size distribution was bimodal when calculated on MIP curves (throat spread of 0.78) as indicated by the value higher than 0.55 (Matthews et al., 2010). By contrast, throat spread was on average 0.49 for micro-CT, underlying a unimodal distribution. The low resolution of micro-CT still explains this significant difference as MIP detected at least 70% more porosity than micro-CT.

## Effects of treatments on soil properties

## OC and HC

A progressive and consistent increase in OC was observed with animal manure amendants (Table 3.4). OC ranged from 8.9 g $kg^{-1}$ in the control (O) to 15.9 and 17.1 g $kg^{-1}$ in liquid ($L_2$+r) and farmyard manure ($F_2$) respectively.

**Table 3.4** - Total soil organic and humic carbon in the different soil treatments. Values differ significantly when followed by different letters ($p \leq 0.05$).

| Treatments | Organic carbon (g $kg^{-1}$) | Humic carbon (g $kg^{-1}$) |
|---|---|---|
| $F_2$ | 17.06 a | 7.60 ab |
| $L_2$+r | 15.91 ab | 8.11 a |
| $F_1NPK_1$ | 13.48 c | 6.93 ab |
| $L_1NPK_1$+r | 14.07 bc | 6.77 ab |
| $NPK_2$ | 9.47 e | 4.12 c |
| $NPK_2$+r | 11.86 cd | 4.64 c |
| O | 8.88 e | 3.69 c |
| O+r | 10.79 de | 5.55 bc |

Intermediate values were observed in the mixed treatments ($F_1NPK_1$ and $L_1NPK_1$+r). As was observed by Freibauer et al. (2004), crop residues incorporation significantly raised

the level of OC in the mineral treatment and control (+21% in O+r vs. O and +25% in $NPK_2$+r vs. $NPK_2$). Similarly to OC, a significant accumulation of HC was estimated for organic and mixed treatments (Table 3.4). The percentage of HC increased by 98% on average with respect to the control. These findings are also supported by Ferrari et al. (2011).

## Soil porosity

Total porosity calculated by MIP varied between a minimum of 37.3% in the control (O) and a maximum of 44.3% in $NPK_2$+r (inorganic fertilisation + residues). By contrast, the porosity investigated by micro-CT (pores larger than 6.25 µm) varied from 6.6% to 12.5% in farmyard manure ($F_2$) and O respectively. Wide variability was observed within the treatments with both techniques (i.e. $NPK_2$+r) (Table 3.2) and no significant differences were observed as a consequence of fertilisation inputs, even in terms of pore size distribution.

However the unit cells simulated by Pore-Cor highlighted structural differences depending on the treatments. Particularly $F_2$ and $L_2$+r increased the complexity of the structures as they were characterised ($p \leq 0.05$) by a lower correlation level (0.40) and a stronger bimodality (throat spread = 0.66) than the other treatments (Figure 3.3).

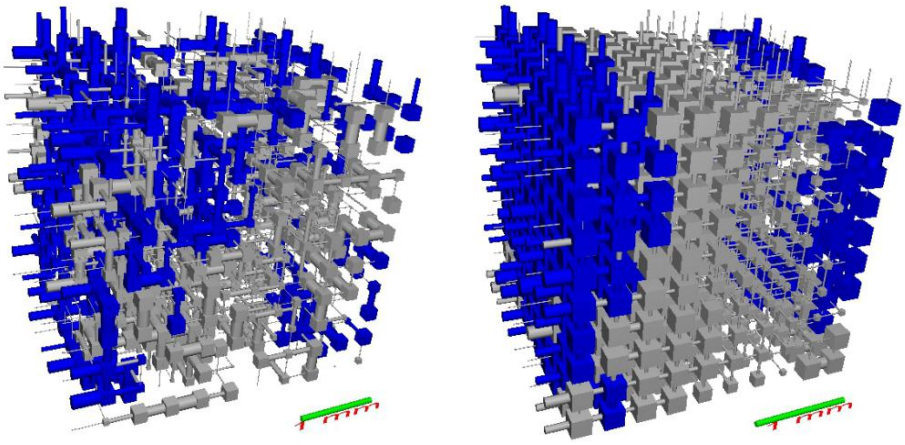

**Figure 3.3** - Representations of soil structure modelled with Pore-Cor from micro-CT pore distribution curves and characterised by farmyard manure (left) and no fertilisation (right). Water (blue) drained vertically displaced by air (grey), occupying 50% of the entire pore volume.

It follows that the randomly connected pores of different sizes typified the soils with organic amendants whereas the others had mostly local auto-correlated structures. Significant correlations were found by multiple linear regressions between porosity and texture and chemical properties (Table 3.5).

**Table 3.5** - Multiple linear regression analysis for soil morphometric features. y = a + b × sand (%) + c × clay (%) + d × OC (g $kg^{-1}$) + e × HC (g $kg^{-1}$). Standardised regression coefficients are reported.

| Morphometric features | Regression coefficients | | | | | Multiple R |
|---|---|---|---|---|---|---|
| | Intercept | Sand (%) | Clay (%) | OC (g $kg^{-1}$) | HC (g $kg^{-1}$) | |
| MIP | a | b | c | d | e | |
| 100-75 µm | -0.34 | 0.51* | - | - | - | 0.51 |
| 75-30 µm | -0.28 | 0.45* | - | - | - | 0.45 |
| 30-6.25 µm | -2.94 | 0.50* | - | - | - | 0.50 |
| 0.1-0.0074 µm | -2.51 | - | 0.55* | - | 0.46* | 0.52 |
| micro-CT | | | | | | |
| 3D porosity | 32.87* | - | -0.40[a] | - | -0.48* | 0.47 |
| 75-30 µm | 9.11* | - | -0.40[a] | -0.55* | - | 0.50 |
| 2D connectivity | 0.14* | - | -0.43* | - | -0.55* | 0.53 |

* $p \leq 0.05$.
[a] $p \leq 0.08$.

Micropores (standard regression coefficient b = 0.50), mesopores (b = 0.45) and macropores (b = 0.51) detected by MIP were positively correlated with sand ($p \leq 0.05$), while cryptoporosity was positively correlated with both clay (c = 0.55) and HC content (e = 0.46). Image analysis on micro-CT scan showed a negative correlation between total porosity, clay and HC content (multiple R = 0.47), while mesopores were mostly affected by OC (d = -0.55) and to a lesser extent by clay (b = -0.40). Lastly clay (b = 0.55) and HC (e = 0.46) were negative significant predictors of 2D connectivity (multiple R = 0.53). It follows that HC was a stronger indicator of pore characteristics than OC. These results are consistent with recent studies ( Strong et al., 2004; Lugato et al., 2009) since positive correlations were observed between organic materials and pores < 1.2 µm whilst negative correlations were observed between organic inputs and pores >

15 µm. By contrast Pagliai et al. (2004), studying the effect of organic materials on the soil with image analysis, found that organic treatments significantly increased the macroporosity (> 50 µm). These discrepancies were probably affected by the different size of undisturbed samples. Indeed in Pagliai et al. (2004), image analysis was carried out in undisturbed samples and the frame length was about 30 mm. Instead our X-ray microtomography and image analyses, for consistency with MIP, were conducted on small aggregates of 5-6 mm.

Pore shape was weakly affected by different treatments (Figure 3.4). Regular pores were more frequent in mineral treatments than in organic ($F_2$) or the control (O). They represented 32% of total pores on average. Irregular pores were dominants in all soil samples (on average 58%) without significant differences between treatments. Elongated pores had an opposite distribution with respect to regular pores, with a higher percentage in farmyard and liquid manure fertilisations ($F_2$ = 11% and $L_2$+r = 10%) and in the control (O = 17%). They represented 10% of total pores on average. Pore shape was equally distributed within each pore size class, reflecting the mean distribution observed between treatments (data not shown). Contrasting effects of management practices were found by Pagliai et al. (2004): they characterised the pore morphology in soils treated with different fertilisations and found a significantly high percentage of elongated pores in amended treatments. Accordingly, Papadopoulos et al. (2009), studying the effects of organic and conventional treatments on pore morphology, found that the pores of aggregates fertilised with organic input were mainly cracked and elongated.

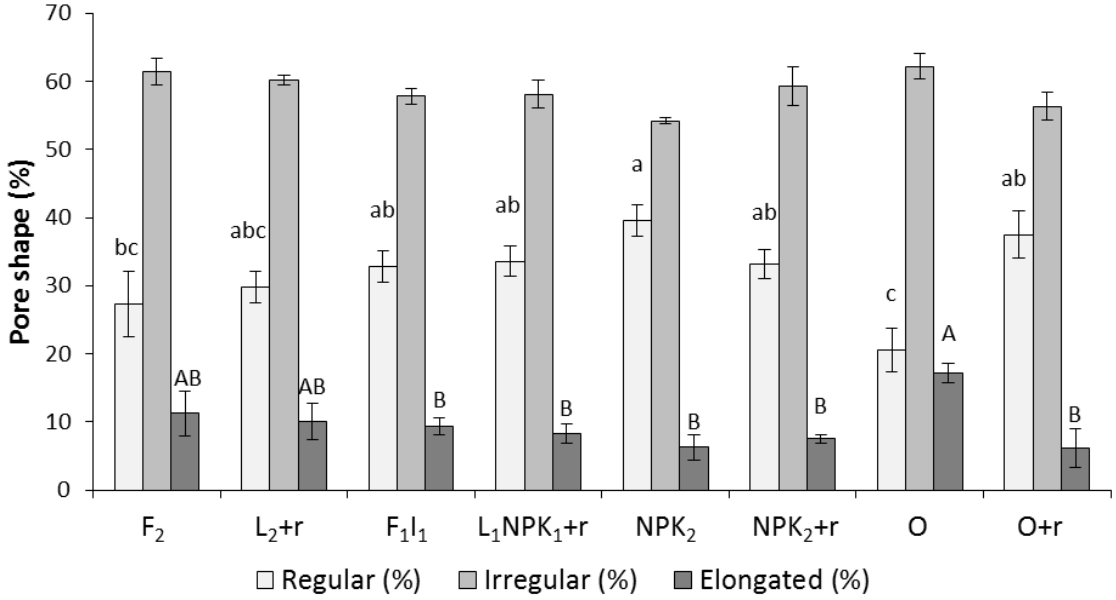


**Figure 3.4** - Pore shape distribution in different soil treatments. Columns differ significantly when labelled with different letters ($p \leq 0.05$). Error bars indicate standard errors. F, farmyard manure; L, liquid manure; NPK, inorganic fertilisation; O, control (no fertilisation); r, residue incorporation. Subscripts 1 and 2 refer to low and high input fertilisation.

The degree of anisotropy did not vary between treatments. It was only 0.15 on average (Figure 3.5) evidencing the lack of a prevailing direction of the pore network. 2D parameters can therefore be considered representative of the 3D matrix since the soil can be considered an isotropic medium (Prado et al., 2009).

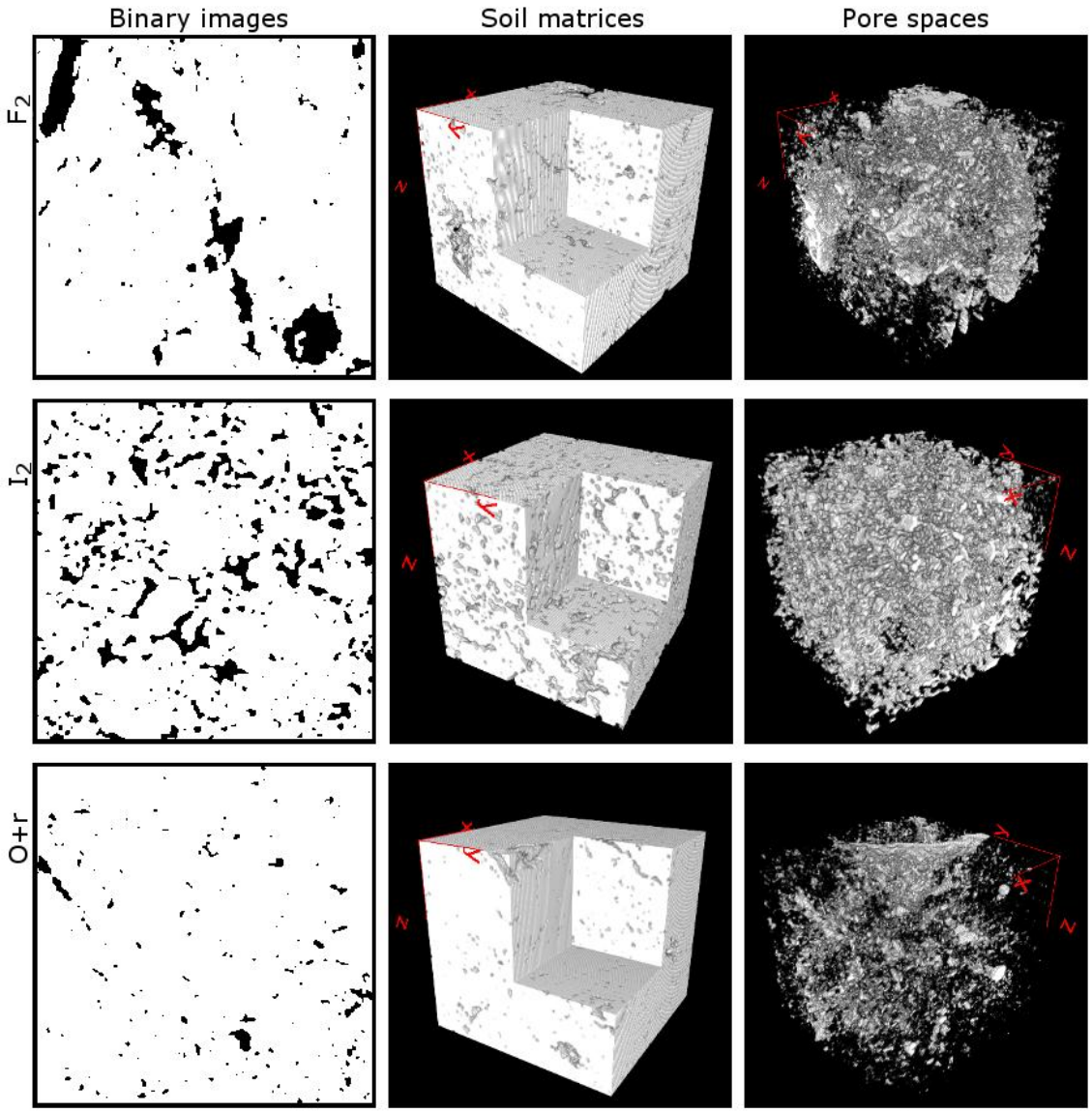


**Figure 3.5** - Examples of soil samples illustrating the selected region of interest (pores are dark objects in the binary images) and 3D representations of soil matrix and pore space. 256 binary images (1.675 × 1.675 cm) were superimposed to create a stack (1.675 × 1.675 × 1.600 cm). Total porosity here was: $F_2$ (farmyard manure) = 11.1%, $NPK_2$ (inorganic fertilisation) = 15.2%, O+r (only residue incorporation) = 3.5%. Degree of anisotropy was: $F_2$ = 0.15, $NPK_2$ = 0.10; O+r = 0.06.

## *Conclusions*

Our results suggest a need to couple mercury intrusion porosimetry (MIP) and micro-CT for pore structure analysis. MIP confirmed its potential as it allowed ultramicro- and cryptoporosity to be detected, which were prevailing in our soil. Resolution limit of micro-CT showed its inapplicability to pores smaller than a few microns. Instead micro-CT allowed pore morphology characterisation and showed that pores were affected by fertilisation practices. Furthermore micro-CT provides a quantitative measure of pore size distribution that is more reliable than MIP since it is not affected by the "ink bottle" effect. The comparison of pore size distribution obtained with the two techniques improved the study of pore network features such as the degree of connection between the different pore classes. Pore-Cor model proved to be an effective tool to improve knowledge of the soil porosity, allowing complex network structures to be described.

Such a high detail of analyses was particularly useful in the study of the relationships between soil organic carbon and porosity and the effects of organic fertilisers. Indeed we proved that soil organic carbon and organic fertilisations can influence the soil structure both in terms of pore morphology and network organisation.

In the near future improvement of micro-CT scan resolution will allow a wider range of pores to be investigated, but at present the combination of MIP and micro-CT is still fundamental for a thorough evaluation of soil structure.

## *References*


Abiven, S., Menasseri, S., Chenu, C., 2009. The effects of organic inputs over time on soil aggregate stability - A literature analysis. Soil Biol. Biochem. 41, 1-12.

Bartoli, F., Bird, N.R.A., Gomendy, V., Vivier, H., Niquet, S., 1999. The relation between silty soil structures and their mercury porosimetry curve counterparts: fractals and percolation. Eur. J. Soil Sci. 50, 9-22.

Boulin, P.F., Angulo-Jaramillo, R., Daian, J.F., Talandier, J., Berne, P., 2008. Pore gas connectivity analysis in Callovo-Oxfordian argillite. Appl. Clay. Sci. 42, 276-283.

Bouma, J.J., Boersma, A., Jager, O., Schoonderbeek, A., 1977. The Function of Different Types of Macropores During Saturated Flow through Four Swelling Soil Horizons1. Soil Sci. Soc. Am. J. 41, 945.

Bronick, C.J., Lal, R., 2005. Soil structure and management: a review. Geoderma 124, 3-22.

Cameron, K.C., Buchan, G.D., 2006. Porosity and pore size distribution. In: Lal, R. (Eds.), Encyclopedia of soil science. CRC Press, Boca Raton, FL, pp. 1350-1353.

Cnudde, V., Cwirzen, A., Masschaele, B., Jacobs, P.J.S., 2009. Porosity and microstructure characterization of building stones and concretes. Eng. Geol. 103, 76-83.

D'acqui, L.P., Bruand, A., Pagliai, M., 1993. Study of soil porosity with mercury porosimetry and image analysis on backscattered electron scanning images (BESI). Application to tilled “crusting soils” in Zimbabwe. Dev. Soil Sci. 22, 581-590.

Dane, J.H. and Topp, G.C. (Eds.), 2002. Methods of Soil Analysis, Part 4-Physical Methods. Soil Sci. Soc. Am. Book Series 5. Soil Sci. Soc. Am., Madison, WI.

Deurer, M., Grinev, D., Young, I., Clothier, B.E., Müller, K., 2009. The impact of soil carbon management on soil macropore structure: a comparison of two apple orchard systems in New Zealand. Eur. J. Soil Sci. 60, 945-955.

Diaz-Zorita, M., Perfect, E., Grove, J.H., 2002. Disruptive methods for assessing soil structure. Soil Till. Res. 64, 3-22.

FAO-UNESCO, 1990. Soil map of the world. Revised Legend. FAO, Rome.

Farber, L., Tardos, G., Michaels, J.N., 2003. Use of X-ray tomography to study the porosity and morphology of granules. Powder Tech. 132, 57-63.

Ferrari, E., Francioso, O., Nardi, S., Saladini, M., Dal Ferro, N., Morari, F., 2011. DRIFT and HR MAS NMR characterization of humic substances from a soil treated with different organic and mineral fertilizers. J. Mol. Struct. 998, 216-224.

Freibauer, A., Rounsevell, M.D.A., Smith, P., Verhagen, J., 2004. Carbon sequestration in the agricultural soils of Europe. Geoderma 122, 1-23.

Giardini, L., 2004. On going trial. In: Giardini, L. (Eds.), Productivity and Sustainability of different Cropping Systems. 40 years of experiments in Veneto region (Italy), Patron, Bologna, pp. 73-98.

Gregg, S.J., Sing, K.S.W., 1982. Adsorption, surface and porosity. Academic Press, London.

Hainsworth, J.M., Aylmore, L.A.G., 1983. The use of computer assisted tomography to determine spatial distribution of soil water content. Aust. J. Soil Res. 21, 435-443.

Hallaire, V., Curmi, P., Widiatmaka, 1997. Morphologie de la porosité et circulations préférentielles en saturé. Etude et Gestion des Sols 4, 115-126.

Hallett, P.D., Feeney, D.S., Bengough, A.G., Rillig, M.C., Scrimgeour, C.M., Young, I.M., 2009. Disentangling the impact of AM fungi versus roots on soil structure and water transport. Plant Soil 314, 183-196.

Harrigan, T., Mann, R., 1984. Characterization of microstructural anisotropy in orthotropic materials using a second rank tensor. J. Mater. Sci. 19, 761-767.

Holtham, D.A.L., Matthews, G.P., Scholefield, D.S., 2007. Measurement and simulation of void structure and hydraulic changes caused by root-induced soil structuring under white clover compared to ryegrass. Geoderma 142, 142-151.

Horn, R., Taubner, H., Wuttke, M., Baumgartl, T., 1994. Soil physical properties related to soil structure. Soil Till. Res. 30, 187-216.

Hubert, F., Hallaire, V., Sardini, P., Caner, L., Heddadj, D., 2007. Pore morphology changes under tillage and no-tillage practices. Geoderma 142, 226-236.

Jassogne, L.T.P., McNeill, A.M., Chittleborough, D.J., 2007. 3D-visualization and analysis of macro-and mesoporosity of the upper horizons of a sodic, texture-contrast soil. Eur. J. Soil Sci. 58, 589-598.

Johnson, A., Roy, I.M., Matthews, G.P., Patel, D., 2003. An improved simulation of void structure, water retention and hydraulic conductivity in soil with the Pore-Cor three-dimensional network. Eur. J. Soil Sci. 54, 477-489.

Ketcham, R.A., Ryan, T.M., 2004. Quantification and visualization of anisotropy in trabecular bone. J. Microsc. 213, 158-171.

Klobes, P., Riesemeier, H., Meyer, K., Goebbels, J., Hellmuth, K.H., 1997. Rock porosity determination by combination of X-ray computerized tomography with mercury porosimetry. Fresenius J. Anal. Chem. 357, 543-547.

Lange, D.A., Jennings, H.M., Shah, S.P., 1994. Image-Analysis Techniques for Characterization of Pore Structure of Cement-Based Materials. Cem. Concr. Res. 24, 841-853.

Lawrence, G.P., 1978. Stability of soil pores during mercury intrusion porosimetry. J. Soil Sci. 29, 299-304.

Lee, S.S., Gantzer, C.J., Thompson, A.L., Anderson, S.H., Ketcham, R.A., 2008. Using high-resolution computed tomography analysis to characterize soil-surface seals. Soil Sci. Soc. Am. J. 72, 1478-1485.

Lugato, E., Morari, F., Nardi, S., Berti, A., Giardini, L., 2009. Relationship between aggregate pore size distribution and organic-humic carbon in contrasting soils. Soil Till. Res. 103, 153-157.

Matthews, G.P., Laudone, G.M., Gregory, A.S., Bird, N.R.A., Matthews, A.G.G., Whalley, W.R., 2010. Measurement and simulation of the effect of compaction on the pore structure and saturated hydraulic conductivity of grassland and arable soil. Water Resour. Res. 46, W05501-1-13.

Mees, F., Swennen, R., Geet, M.V., Jacobs, P., 2003. Applications of X-ray computed tomography in the geosciences. Geological Society, London, Special Publications. 215, 1-6.

Mooney, S.J., Morris, C., Berry, P.M., 2006. Visualization and quantification of the effects of cereal root lodging on three-dimensional soil macrostructure using X-ray computed tomography. Soil Sci. 171, 706-718.

Nardi, S., Morari, F., Berti, A., Tosoni, M., Giardini, L., 2004. Soil organic matter properties after 40 years of different use of organic and mineral fertilisers. Eur. J. Agron. 21, 357-367.

Nunan, N., Ritz, K., Rivers, M., Feeney, D.S., Young, I.M., 2006. Investigating microbial micro-habitat structure using X-ray computed tomography. Geoderma 133, 398-407.

Pagliai, M., Vignozzi, N., Pellegrini, S., 2004. Soil structure and the effect of management practices. Soil Till. Res. 79, 131-143.

Papadopoulos, A., Bird, N.R.A., Whitmore, A.P., Mooney, S.J., 2009. Investigating the effects of organic and conventional management on soil aggregate stability using X-ray computed tomography. Eur. J. Soil Sci. 60, 360-368.

Prado, B., Duwig, C., Marquez, J., Delmas, P., Morales, P., James, J., Etchevers, J., 2009. Image processing-based study of soil porosity and its effect on water movement through Andosol intact columns. Agric. Water Manag. 96, 1377-1386.

Ringrose-Voase, A.J., Bullock, P., 1984. The automatic recognition and measurement of soil pore types by image analysis and computer programs. J. Soil Sci. 35, 673-684.

Ringrose-Voase, A.J., 1996. Measurement of soil macropore geometry by image analysis of sections through impregnated soil. Plant Soil 183, 27-47.

Sander, T., Gerke, H.H., Rogasik, H., 2008. Assessment of Chinese paddy-soil structure using X-ray computed tomography. Geoderma 145, 303-314.

Schjonning, P., Iversen, B.V., Munkholm, L.J., Labouriau, R., Jacobsen, O.H., 2005. Pore characteristics and hydraulic properties of a sandy loam supplied for a century with either animal manure or mineral fertilizers. Soil Use Manage. 21, 265-275.

Serra, J., 1982. Image analysis and mathematical morphology. Academic Press, London.

Sibbesen, E., Skjoth, F., Rubaek, G.H., 2000. Tillage caused dispersion of phosphorus and soil in four 16-year old field experiments. Soil Till. Res. 54, 91-100.

StatSoft, Inc., 2004. STATISTICA, Version 7, www.statsoft.com. 29/06/2011

Stevenson, F J, 1994. Humus Chemistry: Genesis, Composition, Reactions. John Wiley, New York.

Strong, D.T., De Wever, H., Merckx, R., Recous, S., 2004. Spatial location of carbon decomposition in the soil pore system. Eur. J. Soil Sci. 55, 739-750.

Tippkoetter, R., Eickhorst, T., Taubner, H., Gredner, B., Rademaker, G., 2009. Detection of soil water in macropores of undisturbed soil using microfocus X-ray tube computerized tomography (mu CT). Soil Till. Res. 105, 12-20.

Tisdall, J.M., Oades, J.M., 1982. Organic matter and water-stable aggregates in soils. J. Soil Sci. 33,141-163.

Walkley, A. and Black, I.A., 1934. An examination of the Degtjareff method for determining soil organic matter, and a proposed modification of the chromic acid titration method. Soil Sci. 37, 29-38.

Williams, N.D., Petticrew, E.L., 2009, Aggregate stability in organically and conventionally farmed soils. Soil Use Manage. 25, 284-292.

# Chapter IV

# Three-dimensional visualisation and quantification of macropores in undisturbed soils under long-term fertilisation experiment

## *Introduction*

The close relationship existing between soil organic carbon (SOC) and porosity is considered a key issue to evaluate soil quality (Six et al., 2004). Moreover, intensive agriculture can cause soil structure degradation due to a reduction in organic matter (Bronick and Lal, 2005). Several studies focussed on SOC dynamics and the relationship with small soil aggregates, which are usually considered as surrogates of the soil matrix complexity, neglecting the soil macropores outside aggregates. In fact aggregate-SOC interactions have been included in basic conceptual models that describe SOC protection. In turn, SOC compounds have been evaluated as effective binding agents that form bridges between negatively charged clay platelets (Six, 2000). For example, Tisdall and Oades (1982) presented a conceptual model for aggregate hierarchy that described how primary mineral particles are bound together with biological compounds (bacteria, fungi, plant debris) into microaggregates. Transient binding agents would then favour the formation of macroaggregates. As a result the SOC content and its chemical compounds are of primary importance for network porosity as they affect the soil structure. The relationship between organic carbon, pore size distribution and morphology were assessed in small incubated, newly formed and field aggregates to which fresh residue was added (De Gryze et al., 2006). In addition, Papadopoulos et al. (2009) compared stable and unstable aggregates from organically and conventionally treated soils to determine the role of management in aggregate stability.

Macropores of intact soil cores (usually considered > 50 μm), their size distribution and derived parameters such as tortuosity and connectivity, which are not detectable at aggregate scale, have a pivotal role for characterising soil structure since they influence gas diffusion (Deurer et al., 2009), water flow and transport of solutes (Jarvis, 2007; Luo et al., 2008; Rezanezhad et al., 2010,). Nevertheless less attention has been given to the influence of SOC on the macropore network, even if it is assumed that the ramified pore structure can be affected by organic compounds. Deurer et al. (2009), studying the effects of long-term OC addition in apple orchards using X-ray microtomography (micro-CT), reported that organic management affected the soil structure that had significantly greater macroporosity than with conventional management. They also evidenced a larger simulated gas diffusion in the organic managed soil, which would

favour lower N2O emissions due to more and better connected macropores. For Schlüter et al. (2011) the higher OC content and nutrient supply trigger an enhanced biological activity including root growth with implications for macropore-space reallocation. They also showed that pore connectivity was a suitable indicator for the quality of soil structure since it was influenced by SOC content.

X-ray micro-CT can easily detect three-dimensional macroporosity, unlike traditional models of pressure-volume curves (water retention and mercury intrusion porosimetry) that can only reveal pores of a few hundred micrometres. The advent of soil thin sectioning methods allowed the quantification of soil macropores, although precise interpretations of the 3D pore network from 2D thin-sections? are essentially impossible (Stoops, 2003).

A three-dimensional and non-destructive approach is therefore useful to better quantify the soil macroporosity and clarify the role of different agriculture strategies on soil structure. In particular, long-term field experiments that manage addition of SOC, such as farmyard manure or compost, are an excellent chance to study soils under controlled conditions in order to enhance the soil physical quality (Morari et al., 2006).

In a long-term experiment established in the 1960s we studied the effects of organic and mineral fertilisations on the structure of undisturbed soil cores. We analysed in 3D a) total macroporosity (> 40 µm), b) pore size distribution and c) porous network characteristics and their relationship with OC content.

## *Materials and methods*

### Experimental design

A long-term experiment was established in 1962 at the experimental farm of the University of Padova (Legnaro, Veneto Region, NE Italy) (Giardini, 2004). It is the oldest running rotation experiment in Italy. The soil is a fluvi-calcaric cambisol (CMcf), silty or sandy loam (FAO-UNESCO, 1990) with a mean pH of 8.11 (Table 4.1). Details of the experiment have already been reported in Nardi et al. (2004).

**Table 4.1 -** Main physical and chemical properties of the top soil (0-20cm) (soil without fertilisation input).

| Soil parameters | Soil Treatments | | | | | | | |
|---|---|---|---|---|---|---|---|---|
| | $F_2$ | (s.e.) | $L_2$+r | (s.e.) | $NPK_2$ | (s.e.) | O | (s.e.) |
| Sand (%) | 34.30 | 3.81 | 36.48 | 1.39 | 30.90 | 1.42 | 33.40 | 4.63 |
| Silt (%) | 61.01 | 3.48 | 59.20 | 1.35 | 63.56 | 1.51 | 61.44 | 4.48 |
| Clay (%) | 4.70 | 0.34 | 5.34 | 0.16 | 5.54 | 0.20 | 5.16 | 0.15 |
| pH | 7.28 | 0.18 | 7.29 | 0.15 | 6.79 | 0.22 | 7.08 | 0.03 |
| EC[b] 1:2.5 (mS $cm^{-1}$) | 0.35 | 0.12 | 0.43 | 0.16 | 0.61 | 0.13 | 0.22 | 0.01 |
| CEC[c] (meq $100g^{-1}$) | 19.26 | 1.64 | 16.55 | 0.92 | 17.04 | 1.11 | 22.55 | 2.47 |
| Organic Carbon (g $kg^{-1}$) | 17.06 | 0.57 | 15.91 | 0.40 | 9.47 | 1.00 | 8.88 | 0.46 |
| Humic Carbon (g $kg^{-1}$) | 7.60 | 0.72 | 8.11 | 1.18 | 4.12 | 0.57 | 3.69 | 0.19 |

[a] Standard error.
[b] Electrical conductivity.
[c] Cation exchange capacity.

The trial considers eight treatments with maize as main crop. In this work we considered only four treatments characterised by different fertilisations with only organic ($F_2$ = farmyard manure, 60 t $ha^{-1}$ $y^{-1}$, 20% d.m.; $L_2$ = liquid manure, 120 t $ha^{-1}$ $y^{-1}$, 10% d.m.), only mineral ($NPK_2$ = high mineral input, 300 kg N $ha^{-1}$ $y^{-1}$, 66 kg P $ha^{-1}$ $y^{-1}$, 348 kg K $ha^{-1}$ $y^{-1}$) and no fertilisation (O). Liquid manure input also includes crop residue incorporation (r). The experimental layout is a randomised block with three replicates, on plots of 7.8 × 6 m. A total of 12 undisturbed soil cores (5 cm diameter, 6 cm length)

were collected in August 2010 from the topsoil (5 to 20 cm depth) in polymethylmethacrylate (PMMA) cylinders using a manual hydraulic core sampler. The cores were stored at 5 °C until analysis.

## X-ray microtomography and reconstruction

Scanning was done at the "RX Solutions" facility sited in Grenoble (www.rxsolutions.fr). The X-ray generator was multi-energy and different spot size (Hamamatsu), with a voltage range of 40-150 kV and intensity of 0-500 µA. The beam open angle was 43°. The detector dimensions were 1920 × 1536 pixels. All samples were scanned with the same technical parameters that were calibrated as a function of sample size, composition and distance from the X-ray beam generator. Setting parameters were 100 kV, 300 µA and projections were collected during a 360° sample rotation at 0.3° angle incremental step. Each projection was the mean of 10 and scan frequency was 7 images $s^{-1}$. Projections were reconstructed using the dedicated software DigiCT 1.1 (Digisens, France) to obtain a stack of about 1000 2D slices in 32-bit depth. 32-bit images were later converted into 8-bit depth. Final voxel resolution was 40 µm in all three directions.

## Digital image processing and analysis

The digital image processing and analysis was conducted with the public domain image processing ImageJ (Vs. 1.45, National Institute of Health, http://rsb.info.nih.gov/ij) and CTAn software, provided by Skyscan (Belgium). A three-dimensional image dataset of each column was cropped to a region of interest of 750 × 750 pixels (30 × 30 mm) and a depth of 32 mm, which consisted of a continuous stack of 800 slices. By cropping the images and reducing the stack artefacts caused by edge effects and beam hardening were avoided (Mooney et al., 2006; Deurer et al., 2009). Slices were segmented using a global-threshold value based on the histogram greyscale that was determined by the maximum entropy threshold algorithm. The threshold value was selected where the inter-class entropy was maximised (Jassogne et al., 2007; Luo et al., 2010). A one-pixel mathematical morphology operator closing (Serra, 1982) was successively applied to the binary images to fill misclassified pixels inside the pores (Mooney et al., 2006) as well as to maintain pore connections. Only pores represented by more than three pixels were

used for structure analysis since smaller objects are not sufficient to describe pore parameters (Papadopoulos et al., 2009).

## Total macropore structure

3D degree of anisotropy (*DA*) was calculated according to the mean intercept length (MIL) method (Harrigan and Mann, 1984). It was calculated globally within each stack and used for quantifying if the pores were directionally dependent. MIL is found by sending, from the centre of the volume, several vectors in all directions throughout the segmented volume. Each vector is divided by the number of times that it intercepts the boundary between foreground (pores) and background (soil matrix). An ellipsoid is fitted to the MIL and a material anisotropy tensor is constructed. Finally the resulting eigenvalues give the ellipsoid axes and the eigenvectors give the ellipsoid orientation. DA was calculated as:

$$DA = 1 - \frac{L_s}{L_l} \qquad [4.1]$$

where $L_s$ and $L_l$ are the shortest and longest ellipsoid axes respectively. DA varies between 0 (perfect isotropic structure) and 1 (anisotropic structure).

The three dimensional connectivity of macropores was quantified with the volumetric Euler-Poincaré characteristic (for simplicity here called ”Euler number”). Euler number ($E_V$) is defined as follows (Vogel, 2000):

$$E_V = \frac{I - C}{V} \qquad [4.2]$$

Where $I$ is the number of clusters that are not interconnected, $C$ the number of redundant connections and $V$ the volume represented by the image stack. $E_V$ is positive when the number of isolated pores that are not connected to each other exceeds the number of multiple connections between pores ($I > C$) and vice versa. As a result the greater the value of the Euler number, the smaller is the connectivity of the pore system. The biggest connected pore within each stack was also labelled in order to calculate the

bigger connected pore/total porosity volume ratio and to better evaluate the macropore connectivity. Indeed we assumed that the total porosity composed mostly by one big macropore network could be considered an index of connectivity more than different disconnected pores.

Finally three dimensional mass fractal dimension (FD) was calculated with the box counting method by covering the image stack with cubic boxes of side $\varepsilon$ and recording the number of boxes ($N(\varepsilon)$) intersecting the pores within the stack. The characteristic of a geometrical fractal is its fractal dimension (FD), which can be determined by measuring the length of the structure over a range of measurement scales. As the structure becomes more complex the fractal dimension increases. Therefore the fractal dimension can be seen as a quantitative measure of the tortuosity or complexity of a geometrical shape.

The number of boxes ($N(\varepsilon)$) varies with box size ($\varepsilon$) according to:

$$N(\varepsilon) = \left(\frac{1}{\varepsilon}\right)^{FD} \qquad [4.3]$$

The fractal dimension can be estimated from the slope of $\log(1/\varepsilon)$ against $\log(N(\varepsilon))$. Fractal dimension was computed using the ImageJ plugin Fractal Count (Ersoy et al., 2008) (available at: http://www.pvv.org/~perchrh/imagej).

## Total macroporosity and pore size distribution

3D total macroporosity was defined as the total number of pore voxels, within the volume of interest, divided by the total number of voxels in the volume. A three-dimensional pore size distribution of the total macroporosity was calculated from each binarised stack drawing a sphere inside the 3D pore space that touched the bordering soil matrix and measuring the sphere diameter (Figure 4.1). The method first identifies the medial axes of all structures and then the sphere-fitting is done for all the voxels lying along this axis (Cnudde et al., 2009; Pajor et al., 2010). Pores were classified according to a logarithmic scale (Mooney et al., 2006; Papadopoulos et al., 2009).

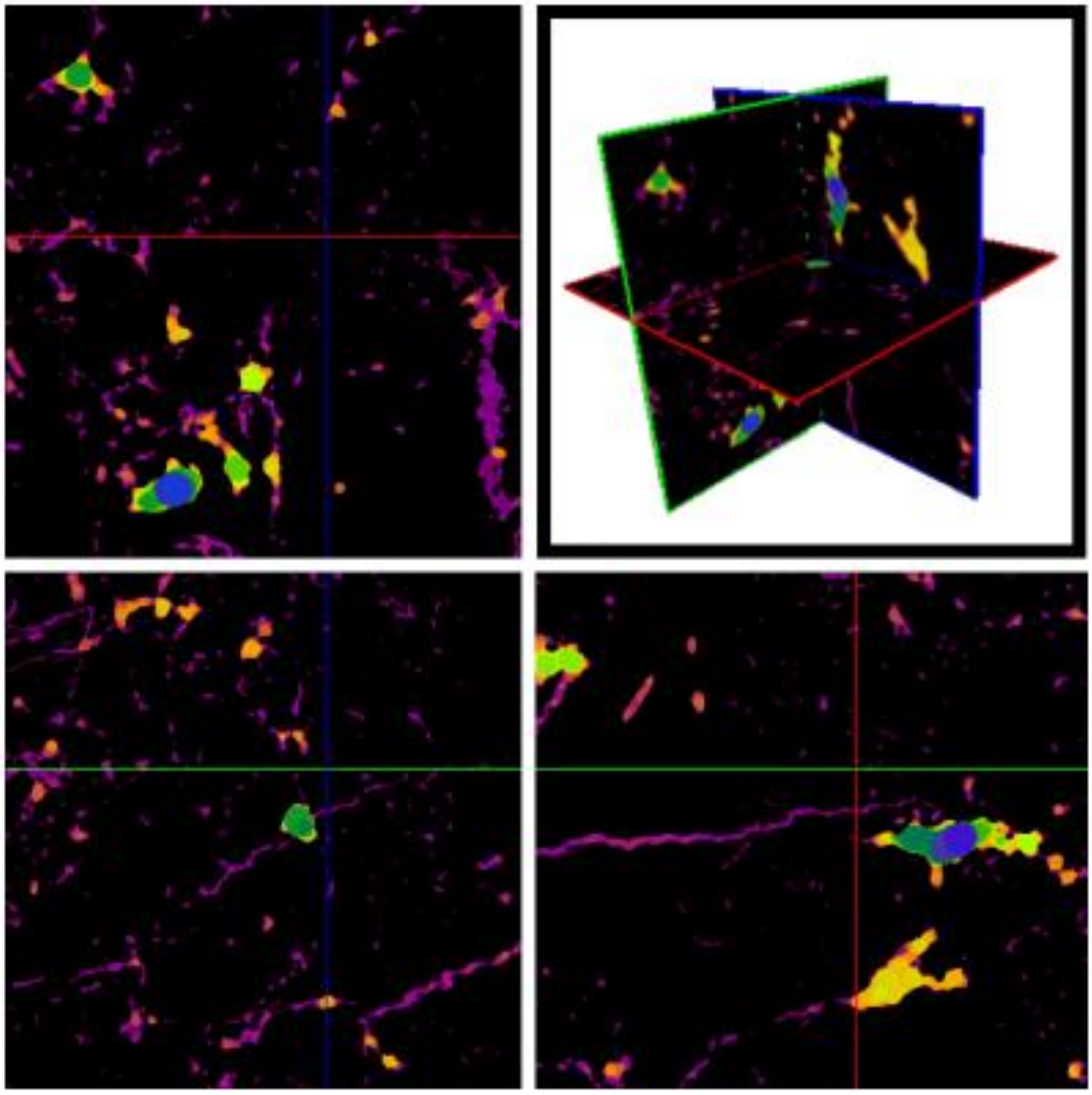

**Figure 4.1** - 2D representation of pore sphere-fitting with disks in order to determine the maximum inscribed sphere diameter. Image stack is 750 × 750 × 800 pixels.

## Statistical analysis

Soil pore size distribution (> 40 µm) and morphological parameters were analysed with one-way ANOVA and Duncan's test was used to differentiate the means. Correlations between variables were determined using Spearman's coefficient, utilising the total macroporosity, pore sizes, organic (OC) and humic carbon (HC). To clarify the structure of these interdependences, we performed a joint principal component analysis (PCA) on 6 standardised variables: fractal dimension (FD), total macroporosity, pore size classes ≤

0.08 mm and 0.56-1.00 mm, HC and Euler number ($E_V$). Variables were selected according to Kaiser's measure of sampling adequacy (MSA). The overall MSA was 0.68 indicating that PCA was suitable (Kaiser, 1974). Rotated orthogonal components (varimax method of rotation) were extracted and the relative scores were determined. Only principal components with eigenvalues > 1 were considered for the discussion. Statistical analyses were performed with STATISTICA 7.0 (StatSoft Inc., 2004).

## *Results and discussion*

### Total macropore structure

Significant differences of volumetric Euler number ($E_V$) were observed between treatments (Figure 4.2), with a minimum of 0.080 and a maximum of 2.32 in $F_2$ and O respectively. The $E_V$ was always positive and indicated that the number of isolated pores exceeded the number of multiple connections within the whole soil sample. Organic fertilisations ($F_2$ and $L_2$+r) increased the 3D connectivity of the macroporosity with respect to $NPK_2$ and O. Nevertheless it should be noted that limitations in structure analysis could lead to a connectivity underestimation because the image resolution and segmentation could mask small connections, overestimating isolated pores.

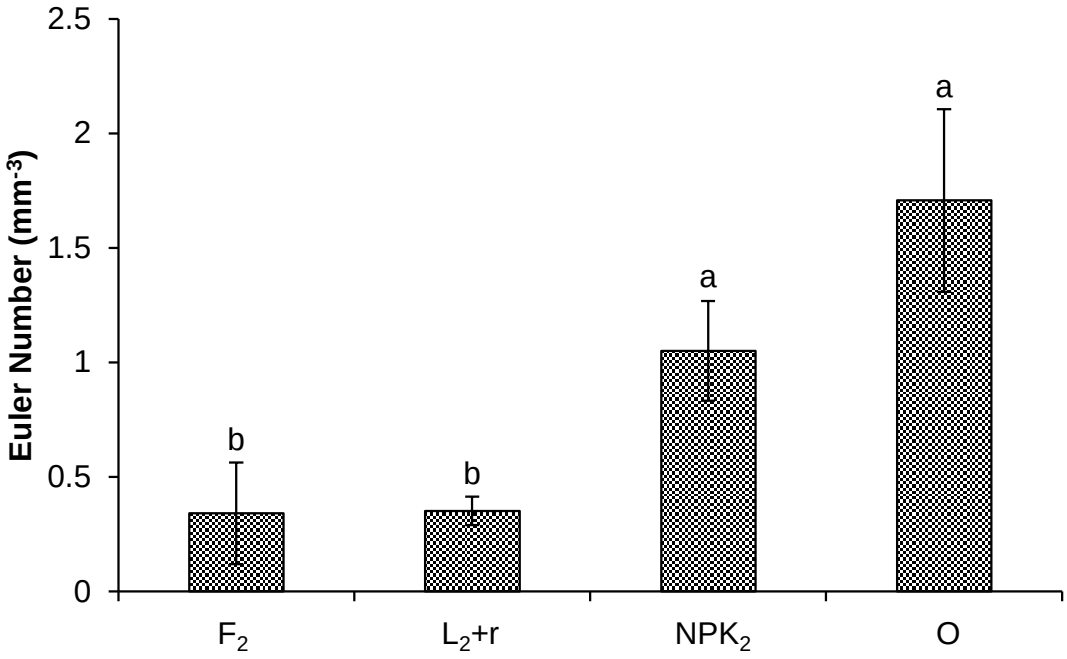


**Figure 4.2** - Euler number in soils treated with organic and mineral fertilisations.

However any bias in the $E_V$ estimation should be similar in all soils and thus a comparison is still possible (Schlüter et al., 2011). It is also worth highlighting that the biggest connected pore/total macroporosity volume ratio (Table 4.2) was at least 0.47. As a consequence the volume of the biggest highly connnected pore network was

representative of almost half the total macroporosity and this supported the fact that all soil samples were characterised by a high degree of connectivity (Figure 4.3).

**Table 4.2** - Properties of soil pore networks in the different treatments.

| Soil parameters | Soil Treatments | | | | | | | |
|---|---|---|---|---|---|---|---|---|
| | $F_2$ (s.e.)[a] | | $L_2$+r (s.e.) | | $NPK_2$ (s.e.) | | O (s.e.) | |
| Total macroporosity (%) | 7.26 | (2.17) | 8.89 | (5.26) | 6.14 | (0.84) | 4.35 | (0.85) |
| Min. pore radius (mm) | 0.04 | - | 0.04 | - | 0.04 | - | 0.04 | - |
| Max. pore radius (mm) | 2.12 | (0.33) | 2.07 | (1.12) | 0.96 | (0.11) | 0.69 | (0.06) |
| Mean pore radius (mm) | 417.25 | (54.89) | 753.85 | (495.48) | 237.03 | (26.03) | 164.33 | (0.52) |
| Biggest pore/Tot. porosity ($mm^3\,mm^{-3}$)[b] | 0.83 | (0.069) | 0.65 | (0.24) | 0.79 | (0.05) | 0.47 | (0.19) |
| Degree of anisotropy | 0.30 | (0.01) | 0.41 | (0.08) | 0.31 | (0.04) | 0.27 | (0.02) |
| Fractal dimension | 2.525 | (0.091) | 2.425 | (0.140) | 2.581 | (0.019) | 2.600 | (0.050) |

[a]Standard error.
[b]Biggest connected pore/total macroporosity ratio.

These results were consistent with recent studies of Schlüter et al. (2011), which reported that the pore network of fertilised soils could retain or re-establish a better connected macropore space. Moreover, Deurer et al. (2009) found a higher connectivity (low $E_V$) in an organic orchard system than in a conventional one. By contrast Eden et al. (2011), modelling the gas diffusion of inter-aggregate pore space, did not find significant treatment effects on pore-connectivity, although there was a tendency for more water blockage in soils dressed with mineral fertilisers as compared with those receiving organic manure.

The degree of anisotropy (DA) varied between a minimum of 0.27 in O to a maximum of 0.41 in $L_2$+r (Table 4.2). No significant differences were observed between treatments, suggesting that soils had an overall similar orientation in the three dimensions. According to equation [4.1] the ratio between the shortest and longest ellipsoid axes was always higher than 0.5, emphasising the presence of a slight orientation of the pore network (Figure 4.3).

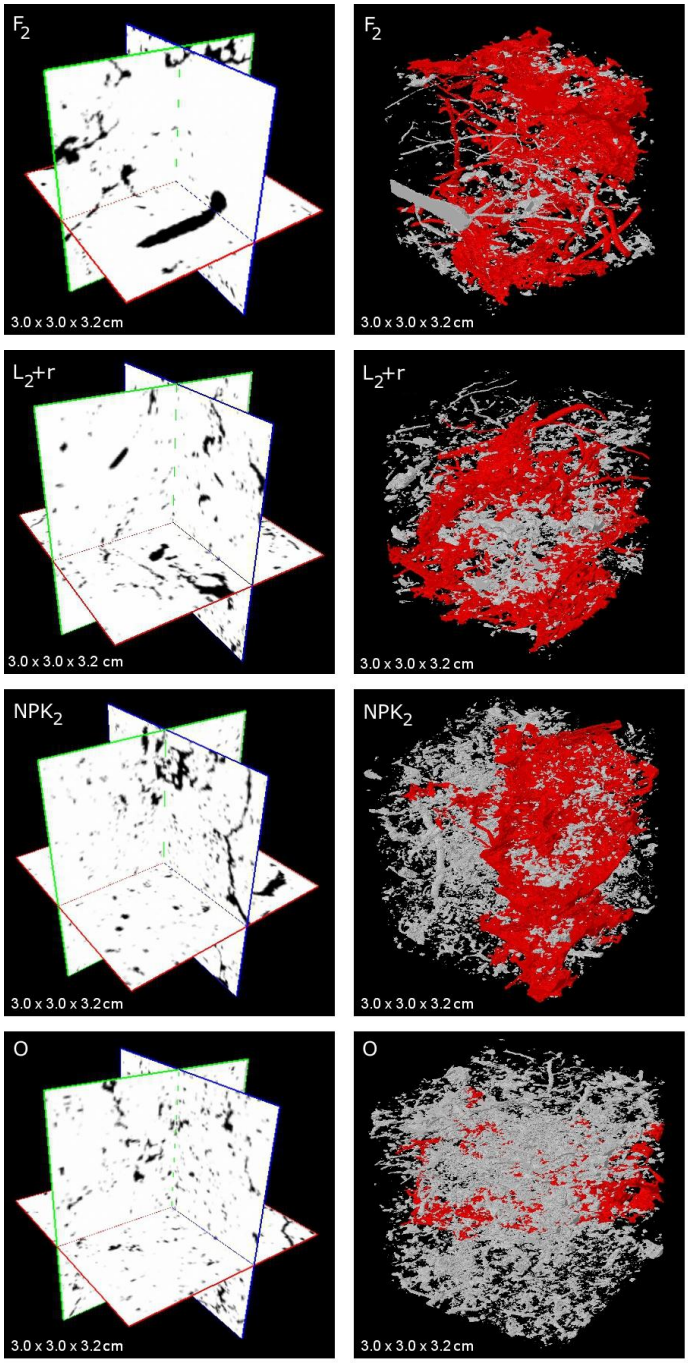


**Figure 4.3** - Three-dimensional representations of pore network. Left side images show the intersection of three different 2D images along the x, y, z planes. Dark objects represent the pores inside the soil matrix (white). Right side images show the total pore network. Red porosity evidences the biggest highly connected pore network, while the grey porosity is what remains of the pores. $F_2$, farmyard manure; $L_2$+r, liquid manure + residues; $NPK_2$, mineral fertilisation; O, control.

Results obtained in the same soils, but at aggregate scale (Dal Ferro et al., 2012a; *in press*), showed lower values of DA than those of soil cores and on average equal to 0.14. This suggests that macropores are more oriented than micropores as a consequence of cracks (Deeks et al., 1999), root growth (Dowuona et al., 2009), soil fauna (Bastardie et al., 2003) and water movement.

There was only a slight difference in the 3D fractal dimension between soil treatments (Table 4.2), with a minimum in $L_2$+r (2.425) and a maximum in O (2.600). The coefficient of determination ($R^2$) for 3D fractal dimension was always > 0.985 (data not shown). Therefore all soils, in the pore size range analysed here, were characterised by a pore self-similarity which rose by the ratio of increasing detail with increasing scale. By contrast these results provided no evidence that pore tortuosity and complexity differed. Our data were supported by De Gryze et al. (2006), who studied the effect of organic residues on porosity and pore morphology of artificial and native field aggregates. They found a small variation in fractal dimension that was less noticeable as pore morphology changed.

By contrast they observed a curvilinear relationship between fractal dimension and total porosity. Finally they concluded that the observed differences in average mass fractal dimension could be mostly attributed to differences in porosity rather than in pore morphology due to a methodological issue (i.e. image resolution). Perret et al. (2003) described a logarithmic trend plotting the total macroporosity and fractal dimension and their results of total macropores seemed to have a consequential effect on the mass fractal dimensions obtained from both the 2D and 3D approach. Similarly our data showed a logarithmic distribution of 3D fractal dimension with total macroporosity (Figure 4.4) and most likely pore morphology had a limited impact on the fractal calculation due to resolution limitation.

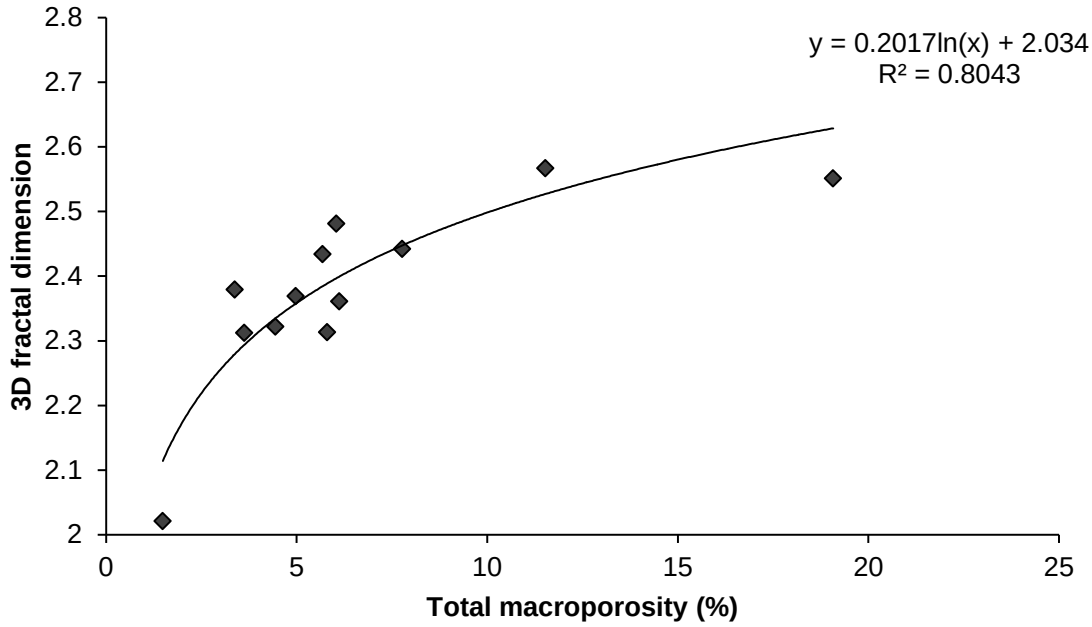


**Figure 4.4** - 3D fractal dimension versus total macroporosity of undisturbed soil samples.

## Total macroporosity and pore size distribution

A comparison between the cultivation plots did not demonstrate significant differences in total macroporosity, although higher values were observed in organic amended soils (Table 4.2). $L_2$+r (liquid manure + residues) showed the greater total macroporosity (on average 8.89%), followed by $F_2$ (farmyard manure) (on average 7.26%) and successively by the mineral treated soil ($NPK_2$) and the control (O), with 6.14% and 4.35% respectively. $L_2$+r was also characterised by the highest variability since the maximum and minimum macroporosity values were 19.1% and 1.5%. Similar results were observed by Pagliai et al. (2004) who studied the effect of organic fertilisations on soil macroporosity (50-1000 µm) and found the highest percentage of macropores in soil treated with livestock manure and the lowest one in the control. They suggested that the decrease in the control plot could be due to the lack of organic matter addition and its progressive mineralisation.

The type of treatments affected macroporosity only in the classes ≤ 0.08 mm and 0.08-0.16 mm (Figure 4.5), with a significantly higher value in the control ($p \leq 0.05$) with respect to the organic fertilisations. $NPK_2$ showed intermediate values and differed from O and

$L_2$+r in the class ≤ 0.08 mm ($p \leq 0.05$). Organic soils, which had significantly fewer macropores ≤ 0.16 mm, had higher macroporosities than the mineral and control soils at bigger pore size classes (> 0.56 mm). It follows that the bigger pores had been developed at the expense of the smaller ones since the total macroporosity was much the same.

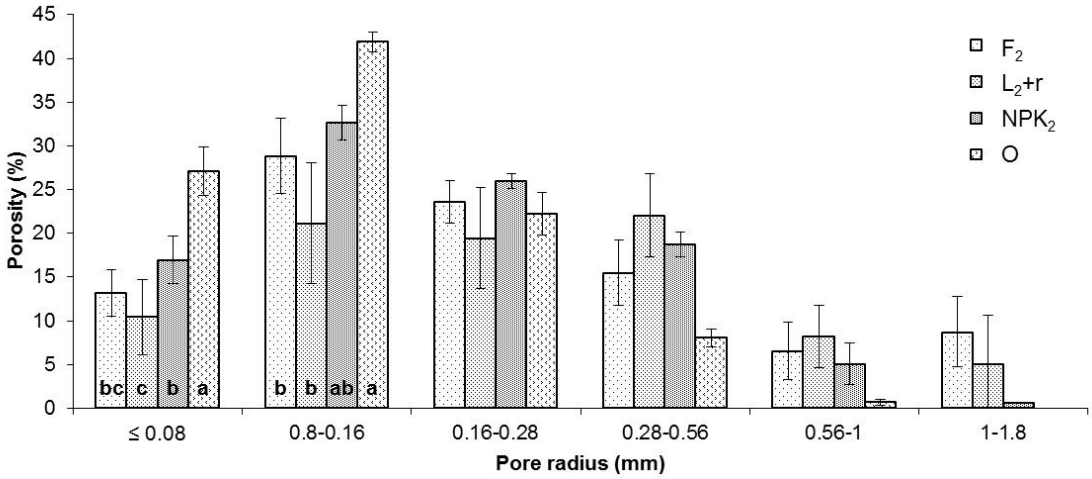


**Figure 4.5 -** Pore size distribution.

In addition the maximum pore diameter (Table 4.2) tended to be larger in farmyard manure $F_2$ (2.12 mm), followed by $L_2$+r (2.07 mm) and finally $NPK_2$ and O (0.96 mm and 0.69 mm respectively). Comparable results were observed by Schlüter et al. (2011) who studied mixed and non-fertilised soils in a long-term experiment. They underlined that porosity changed in the two soils as a consequence of the different OC content. Similarly, we compared the pore size distribution with data of organic (OC) and humic (HC) carbon (Table 4.3): the results suggested that the OC management of our soils, which led to more SOC in $F_2$ and $L_2$+r, had implications on pore-space reallocation. A negative correlation was found between organic carbon and humic carbon content with the small macropore classes (≤ 0.08 mm and 0.08-0.16 mm) while a positive one emerged between HC and the macropore class 0.56-1.00 mm, suggesting the importance of highly stable organic compounds for soil structure.

**Table 4.3** - Correlation matrix of soil porosity, pore size distribution, organic (OC) and humic carbon (HC). Values in bold are significantly different at $p \leq 0.05$.

| | ≤ 0.08 | 0.08-0.16 | 0.16-0.28 | 0.28-0.56 | 0.56-1.00 | Tot. macroporosity | OC | HC |
|---|---|---|---|---|---|---|---|---|
| ≤ 0.08 | *1.00* | | | | | | | |
| 0.08-0.16 | **0.88** | *1.00* | | | | | | |
| 0.16-0.28 | 0.23 | **0.60** | *1.00* | | | | | |
| 0.28-0.56 | -0.48 | -0.42 | 0.30 | *1.00* | | | | |
| 0.56-1.00 | **-0.88** | **-0.85** | -0.34 | 0.39 | *1.00* | | | |
| Tot. macroporosity | **-0.62** | **-0.63** | -0.55 | -0.22 | **0.64** | *1.00* | | |
| OC | **-0.68** | **-0.66** | -0.25 | 0.36 | 0.50 | 0.33 | *1.00* | |
| HC | **-0.79** | **-0.83** | -0.53 | 0.24 | **0.68** | 0.55 | **0.88** | *1.00* |

A general overview of the parameters characterising the 3D soil structure was provided by PCA. Two factors were extracted (eigenvalue > 1) explaining 87.5% of total variance (factor loading > 0.7) (Table 4.4). The first factor explained 63.7% of variance and was correlated with HC, Euler number, ≤ 0.08 and 0.56-1.00 mm macropore classes. The second explained 23.8% and was associated with fractal dimension and total macroporosity.

**Table 4.4** - Factor loadings (varimax normalised) calculated for selected soil parameters.

| Soil parameters[a] | Factor 1 | Factor 2 |
|---|---|---|
| FD | -0.07 | **0.98** |
| HC (%) | **0.88** | 0.11 |
| ≤ 0.08 mm | **-0.96** | -0.20 |
| 0.56-1.00 mm | **0.82** | 0.36 |
| Total macroporosity (%) | 0.50 | **0.82** |
| $E_V$ | **-0.91** | 0.05 |
| Expl. variance (%) | 63.70 | 23.80 |

[a]FD, fractal dimension; HC, humic carbon; $E_V$, Euler number.

The plot of the two factors (Figure 4.6) highlighted that humic carbon was associated with both macropore size distribution and structural parameters. Therefore long-term application of organic amendants could affect the pore distribution and their global spatial location. HC is in proximity to the 0.56-1.00 mm macropore class and in the opposite position with respect to the small macropores ≤ 0.08 mm. By contrast the position of the Euler number ($E_V$) on the left hand side of the graph underlined that pores were mainly connected when soils had high HC content. Vice versa, total macroporosity and fractal dimension were neither affected by organic input nor associated with $E_V$, suggesting that the total macropore complexity would be independent of the pore connections and dimensions.

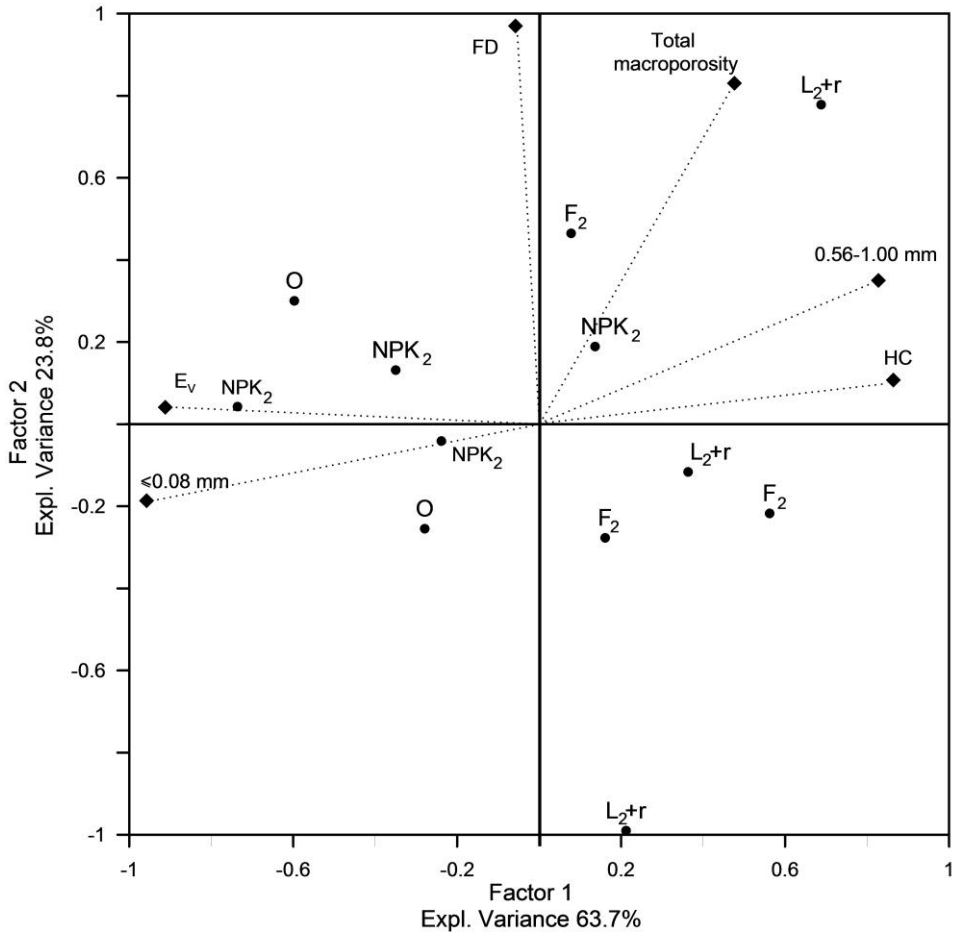


**Figure 4.6** - Variables projected in the plane determined by the two principal axes. $E_V$, Euler number; HC, humic carbon (%); FD, fractal dimension.

The position of the soil cases charted in the PCA graph emphasised the importance of the first factor since the soil management was associated with HC, $E_V$ and macropore sizes (Figure 4.6), while total macroporosity and FD were not affected by organic treatments. Indeed organic treated soils were all clustered on the right hand side of the graph despite a high variability of total macroporosity in $L_2$+r. Conversely, mineral treated soils and the control were mainly clustered on the left hand side.

A comparison on the relationship between organic compounds and pore size distribution of the same soils, but at aggregate scale, highlighted that OC and HC content were important factors for pore size changes at both micro- and macropore scale. Dal Ferro et al. (2012b; *submitted*), studying the long-term effect of organic and mineral fertilisers on soil aggregates, observed that organic compounds played a key role on structural features, increasing the ultramicropores (5-0.1 µm) and decreasing the meso- and macropores (30-5 and 75-30 µm respectively) at the aggregate scale. They also reported non-significant effects of organic compounds on ultramacropores (100-75 µm), cryptopores (0.1-0.0074 µm) and total macroporosity. These structural changes were mediated by OC content and high molecular weight humic fractions, usually associated to soil fertility as they improve soil structure (Nardi et al., 2004). Recent research in long-term experiments that correlated organic compounds and pore size distribution showed comparable results: Lugato et al. (2009), studying the effect of a long-term addition of organic and mineral fertilisers on contrasting soils, argued that organic compounds had positive effects on pores < 5 µm and conversely a negative effect on the pore size class 100-75 µm. Also Chakraborty et al. (2010) found fewer macropores in soils treated with mixed fertilisations with respect to the control.

By contrast this work on undisturbed soil cores, which concentrated only on macropororosity, showed a shift towards bigger macropores and similarly no effects on total porosity. As already reported by other studies (Pagliai et al., 2004), the contribution of long-term application of OC (and its evolution into the more recalcitrant HC) to macropore network changes was significant and it improved the soil structure.

## Conclusions

The three-dimensional structure of undisturbed soil cores was affected by the long-term management practices. There was a clear relationship between improvement of soil structure and organic fertilisers as a result of farmyard and liquid manure inputs. We used different indices to evaluate the soil structure and observed positive effects of both quantity (OC) and quality (HC) of organic compounds on the soil pore network, which can be summarised as: a) increase in big macropores at the expense of small ones and b) improvement of pore connectivity as a result of low volumetric Euler number. Such a high degree of connectivity was also supported by the very high representativeness of the bigger pore/total porosity ratio. These parameters proved to be suitable indices for the quality of soil structure. Vice versa, 3D fractal dimension was not a sensitive index for pore morphology changes since differences in total porosity could mask the alterations in morphology.

X-ray microtomography, by means of morphological analyses on the pore network, played a pivotal role as it highlighted subtle structural changes between treatments at macropore scale, although the pixel resolution was restricted to 40 µm. The comparison of our results with others on the same soils, but on soil aggregates, proved that SOC content and its humic compounds have a dual significant influence on pore network as they improve the soil structure at both micro- and macropore scale. Further improvements of micro-CT scan resolution will allow the investigation of undisturbed soil samples in a wide range of porosity.

## *References*


Bastardie, F., Capowiez, Y., de Dreuzy, J.R., Cluzeau, D., 2003. X-ray tomographic and hydraulic characterization of burrowing by three earthworm species in repacked soil cores. Appl. Soil Ecol. 24, 3-16.

Bronick, C.J., Lal, R., 2005. Soil structure and management: a review. Geoderma 124, 3-22.

Chakraborty, D., Garg, R.N., Tomar, R.K., Dwivedi, B.S., Aggarwal, P., Singh, R., Behera, U.K., Thangasamy, A., Singh, D., 2010. Soil physical quality as influenced by long-term application of fertilizers and manure under maize-wheat system. Soil Sci. 175, 128-136.

Cnudde, V., Cwirzen, A., Masschaele, B., Jacobs, P.J.S., 2009. Porosity and microstructure characterization of building stones and concretes. Eng. Geol. 103, 76-83.

Dal Ferro, N., Delmas, P., Duwig, C., Simonetti, G., Morari, F., 2012a. Coupling X-ray microtomography and mercury intrusion porosimetry to quantify aggregate structures of a Cambisol under different fertilisation treatments. Soil Till Res. DOI:10.1016/j.still.2011.12.001.

Dal Ferro, N., Berti, A., Francioso, O., Ferrari, E., Matthews, G.P., Morari, F., 2012b. Investigating the effects of wettability and pore size distribution on aggregate stability: the role of soil organic matter and the humic fraction. Eur. J. Soil Sci. *submitted*.

De Gryze, S., Jassogne, L., Six, J., Bossuyt, H., Wevers, M., Merckx, R., 2006. Pore structure changes during decomposition of fresh residue: X-ray tomography analyses. Geoderma 134, 82-96.

Deeks, L.K., Williams, A.G., Dowd, J.F., Scholefield, D., 1999. Quantification of pore size distribution and the movement of solutes through isolated soil blocks. Geoderma 90, 65-86.

Deurer, M., Grinev, D., Young, I., Clothier, B.E., Müller, K., 2009. The impact of soil carbon management on soil macropore structure: a comparison of two apple orchard systems in New Zealand. Eur. J. Soil Sci. 60, 945-955.

Dowuona, G.N.N., Taina, I.A., Heck, R.J., 2009. Porosity Analysis of Two Acrisols by X-Ray Computed Microtomography. Soil Sci. 174, 583-593.

Eden, M., Schjonning, P., Moldrup, P., De Jonge, L.W., 2011. Compaction and rotovation effects on soil pore characteristics of a loamy sand soil with contrasting organic matter content. Soil Use Manage. 27, 340-349.

Ersoy, O., Aydar, E., Gourgaud, A., Bayhan, H., 2008. Quantitative analysis on volcanic ash surfaces: Application of extended depth-of-field (focus) algorithm for light and scanning electron microscopy and 3D reconstruction. Micron 39, 128-136.

FAO-UNESCO, 1990. Soil map of the world. Revised Legend. FAO, Rome.

Giardini, L., 2004. On going trial. In: Giardini, L. (Eds.), Productivity and Sustainability of different Cropping Systems. 40 years of experiments in Veneto region (Italy), Patron, Bologna, pp. 73-98.

Harrigan, T., Mann, R., 1984. Characterization of microstructural anisotropy in orthotropic materials using a second rank tensor. J. Mater. Sci. 19, 761-767.

Jarvis, N.J., 2007. A review of non-equilibrium water flow and solute transport in soil macropores: principles, controlling factors and consequences for water quality. Eur. J. Soil Sci. 58, 523-546.

Jassogne, L.T.P., McNeill, A.M., Chittleborough, D.J., 2007. 3D-visualization and analysis of macro-and meso-porosity of the upper horizons of a sodic, texture-contrast soil. Eur. J. Soil Sci. 58, 589-598.

Kaiser, H.F., 1974. An index of factorial simplicity. Psychometrika 39, 31-36.

Lugato, E., Morari, F., Nardi, S., Berti, A., Giardini, L., 2009. Relationship between aggregate pore size distribution and organic-humic carbon in contrasting soils. Soil Till. Res. 103, 153-157.

Luo, L., Lin, H., Halleck, P., 2008. Quantifying soil structure and preferential flow in intact soil using x-ray computed tomography. Soil Sci. Soc. Am. J. 72, 1058-1069.

Luo, L., Lin, H., Li, S., 2010. Quantification of 3-D soil macropore networks in different soil types and land uses using computed tomography. J. Hydrol. 393, 53-64.

Mooney, S.J., Morris, C., Berry, P.M., 2006. Visualization and quantification of the effects of cereal root lodging on three-dimensional soil macrostructure using X-ray computed tomography. Soil Sci. 171, 706.

Morari, F., Lugato, E., Berti, A., Giardini, L., 2006. Long-term effects of recommended management practices on soil carbon changes and sequestration in north-eastern Italy. Soil Use Manage. 22, 71-81.

Nardi, S., Morari, F., Berti, A., Tosoni, M., Giardini, L., 2004. Soil organic matter properties after 40 years of different use of organic and mineral fertilisers. Eur. J. Agron. 21, 357-367.

Pagliai, M., Vignozzi, N., Pellegrini, S., 2004. Soil structure and the effect of management practices. Soil Till. Res. 79, 131-143.

Pajor, R., Falconer, R., Hapca, S., Otten, W., 2010. Modelling and quantifying the effect of heterogeneity in soil physical conditions on fungal growth. Biogeosciences 7, 3731-3740.

Papadopoulos, A., Bird, N.R.A., Whitmore, A.P., Mooney, S.J., 2009. Investigating the effects of organic and conventional management on soil aggregate stability using X-ray computed tomography. Eur. J. Soil Sci. 60, 360-368.

Perret, J.S., Prasher, S.O., Kacimov, A.R., 2003. Mass fractal dimension of soil macropores using computed tomography: from the box-counting to the cube-counting algorithm. Eur. J. Soil Sci. 54, 569-579.

Rezanezhad, F., Quinton, W.L., Price, J.S., Elliot, T.R., Elrick, D., Shook, K.R., 2010. Influence of pore size and geometry on peat unsaturated hydraulic conductivity computed from 3D computed tomography image analysis. Hydrol. Process. 24, 2983-2994.

Schlüter, S., Weller, U., Vogel, H.J., 2011. Soil-structure development including seasonal dynamics in a long-term fertilization experiment. J. Plant Nutr. Soil Sci. 174, 395-403.

Serra, J., 1982. Image analysis and mathematical morphology. Academic Press, London.

Six, J., 2000. Soil structure and organic matter: I. Distribution of aggregate-size classes and aggregate-associated carbon. Soil Sci. Soc. Am. J. 64, 681-689.

Six, J., Bossuyt, H., De Gryze, S., Denef, K., 2004. A history of research on the link between (micro)aggregates, soil biota, and soil organic matter dynamics. Soil Till. Res. 79, 7-31.

StatSoft, Inc., 2004. STATISTICA, Version 7, www.statsoft.com. 29/06/2011

Stoops, G, 2003. Guidelines for analysis and description of soil and regolith thin sections. SSSA, Inc. Madison, WI.

Tisdall, J.M., Oades, J.M., 1982. Organic matter and water-stable aggregates in soils. J. Soil Sci. 33, 141-163.

Vogel, H.J., 2000. A numerical experiment on pore size, pore connectivity, water retention, permeability, and solute transport using network models. Eur. J. Soil Sci. 51, 99-105.

# Chapter V

# General conclusions

## *Conclusions*

Soil architecture is the result of a complex interplay between structure-forming and structure-decaying events including natural processes and management practices. This study showed that the long-term fertilisation treatments played a key role by modifying the soil structure. The results confirmed that organic amendants (i.e. farmyard and liquid manure) induced the most relevant beneficial effects on soil structure, both in soil aggregates (few mm) and undisturbed samples (5 cm diameter, 6 cm length), avoiding soil degradation. The quantification of the shape, size, continuity, orientation and irregularity of pores allows the prediction of changes that may be expected following soil structural modifications induced by management practices.

At aggregate scale, SOC and its humic fraction diminished aggregate breakdown by means of two main mechanisms: first it increased the hydrophobicity, as demonstrated by the significant correlations with experimental data of $WASI_{benz}$ (wet aggregate stability index with pre-treatment of benzene) and contact angle. The massive presence of high molecular weight humic fractions (HF1-C), characterised by a high degree of recalcitrance, enhanced the soil water repellency due to the presence of hydrophobic molecules (e.g. aromatic-H structures, esters, alkyls etc.), detected by spectroscopic analysis, and mostly associated with complex humic molecules. Conversely HF3-C, i.e. the most labile humic fraction that has not reached the molecular complexity and chemical characteristics of mature humus, was mostly associated with sugar-like and protein-like structures (DTA and NMR analysis), usually associated with the most recent microbial activity. Second, aggregate wetting was reduced since SOC shifted micropores (5-30 µm) and mesopores (30-75 µm) towards ultramicro-pores (0.1-5 µm). As a consequence the entry of water into the aggregate, which would cause a build-up of internal air pressure, was slowed and this reduced slaking. These results were supported by simulations of fast wetting, even if the model provided a simplified representation of the complex interactions between water movement, soil matrix and air pressure inside the aggregate. By contrast the chemical bonds had a minor role, probably masked by a more consistent effect of the water-repellent coating outside the aggregates. Indeed the carboxylates might be involved in the formation of bonds with the mineral surface that

oriented the hydrophobic chains outside the aggregates to form a water-repellent coating.

The quantification of pore structure of undisturbed samples (5 cm diameter, 6 cm length) showed that organic compounds also affected the macroporosity. Pore size distribution and connectivity, measured by means of X-ray microtomography, were suitable indicators of the quality of soil structure. In fact the high SOC content and its degree of humification (represented by the humic carbon content) had positive effects on pore connectivity and macroporosity, symptoms of well-structured and non-compacted pores. 3D fractal analysis showed that soils were all characterised by a pore self-similarity which arose through the ratio of increasing detail with increasing scale, although these results did not provide evidence that pore tortuosity and complexity were different. These weak differences in 3D fractal dimension could be mostly attributed to differences in porosity and much less to pore morphology due to a methodological issue (i.e. image resolution).

The study of these complex interactions between soil structure and organic amendants were possible thanks to advanced three-dimensional reconstructions, together with more traditional investigations of pore size distribution such as mercury intrusion porosimetry. Both the network model Pore-Cor, which generates stochastic representations of the soil pore network, and X-ray microtomography allowed subtle structural changes between differently fertilised soils to be quantified. More precisely, the micro-CT allows a three-dimensional morphological quantification, plus pore size distribution is more reliable than mercury intrusion porosimetry since it is not affected by the “ink bottle” effect. By contrast, the resolution limit of micro-CT showed its inapplicability to pores smaller than a few microns, while mercury intrusion porosimetry and the network models confirmed their potential as tools to analyse ultramicropores and cryptopores. They are particularly important in these samples as they represent, at aggregate scale, more than 20% of total porosity.

Lastly this work demonstrated a dual effect of the SOC content and its humic fraction on soil structure, in contrast with a lack of overall results reported in the literature. While the organic amendants, at aggregate scale, shifted micro- and mesopores towards ultramicroporosity, on the other hand soils treated with high input farmyard manure

increased the pores > 0.56 mm and had significantly fewer macropores ≤ 0.16 mm. The good agreement of the results on soil structure from three-dimensional reconstructions and classical physico-chemical measurements is promising for further investigations along these lines.

## *Acknowledgments*

I am particularly grateful to my supervisor, Prof. Francesco Morari, for the opportunity to undertake my PhD. I passed on his expertise, devotion and enthusiasm for research.

I want particularly thank Dr Celine Duwig and the LTHE staff for their support during my stay in Grenoble, and Prof. Patrice Delmas and the Department of Computer Science staff for their support during my stay in Auckland. They helped me a lot with their knowledge and experience to make this work.

I am thankful to prof. Luigi Giardini, "visionary creator" of the long-term experiment, Prof. Antonio Berti, University of Padova, for his help and support, Dr Gianluca Simonetti, University of Padova, for texture and mercury porosimetry analysis, Prof. Gilberto Artioli and Dr Matteo Parisatto, University of Padova, for X-ray micro-CT analysis, Dr Ornella Francioso, University of Bologna, and Dr Erika Ferrari, University of Modena and ReggioEmilia, for chemical analysis, Prof. Peter Matthews, University of Plymouth, for helping me in modelling interpretations.